Universidade Federal do Rio Grande do Sul – UFRGS

Instituto de Pesquisas Hidráulicas – IPH

Programa de Pós-Graduação em Recursos Hídricos e Saneamento Ambiental - PPGRHSA

Danrlei de Menezes

SIMULAÇÃO FÍSICA DO TRANSPORTE DE ÁGUA E SEDIMENTOS EM CANAIS COM LEITO DE GRANULOMETRIA EXTENSA

Porto Alegre, 28 de novembro de 2025.

Danrlei de Menezes

SIMULAÇÃO FÍSICA DO TRANSPORTE DE ÁGUA E SEDIMENTOS EM CANAIS COM LEITO DE GRANULOMETRIA EXTENSA

Tese apresentada ao Programa de Pós-graduação em Recursos Hídricos e Saneamento Ambiental, do Instituto de Pesquisas Hidráulicas, da Universidade Federal do Rio Grande do Sul, como requisito parcial à obtenção do grau de doutor.

Orientadora: Prof. Ana Luiza de Oliveira Borges

Porto Alegre, 28 de novembro de 2025.

CIP - Catalogação na Publicação

de Menezes, Danrlei
SIMULAÇÃO FÍSICA DO TRANSPORTE DE ÁGUA E SEDIMENTOS EM CANAIS COM LEITO DE GRANULOMETRIA EXTENSA / Danrlei de Menezes. -- 2025.
211 f.
Orientadora: Ana Luiza de Oliveira Borges.

Tese (Doutorado) -- Universidade Federal do Rio Grande do Sul, Instituto de Pesquisas Hidráulicas, Programa de Pós-Graduação em Recursos Hídricos e Saneamento Ambiental, Porto Alegre, BR-RS, 2025.

1. Modelagem física. 2. Rugosidade do leito. 3. Resistência ao fluxo. 4. Fundo móvel. 5. Perfis de velocidade. I. Luiza de Oliveira Borges, Ana, orient. II. Título.

Elaborada pelo Sistema de Geração Automática de Ficha Catalográfica da UFRGS com os dados fornecidos pelo(a) autor(a).

Danrlei de Menezes

SIMULAÇÃO FÍSICA DO TRANSPORTE DE ÁGUA E SEDIMENTOS EM CANAIS COM LEITO DE GRANULOMETRIA EXTENSA

Tese apresentada ao Programa de Pós-graduação em Recursos Hídricos e Saneamento Ambiental, do Instituto de Pesquisas Hidráulicas, da Universidade Federal do Rio Grande do Sul, como requisito parcial à obtenção do grau de doutor.

Banca Examinadora:

_____
Prof.º Drª Nilza Maria dos Reis Castro (UFRGS)

_____
Drª Carolina Boffo (UFRGS)

_____
Prof. Drº Jean Paolo Gomes Minella (UFSM)

Porto Alegre, 28 de novembro de 2025.

Dedico esta tese aos meus pais, Mara e Nelso, cujo incentivo constante ao estudo e cuja convicção no poder transformador da educação foram fundamentais para que eu pudesse trilhar este caminho.

AGRADECIMENTOS

Inicio estes agradecimentos destacando o papel essencial dos meus pais, Mara e Nelso. O incentivo constante aos estudos e a confiança que sempre depositaram em mim foram fundamentais para que eu pudesse desenvolver toda a minha trajetória acadêmica e, consequentemente, concluir esta tese. Meu profundo agradecimento a vocês. Agradeço também à minha irmã, cujo apoio foi sempre presente, e aos meus sobrinhos, Kézia e Kaick, que renovaram minha motivação e tornaram minhas idas à Paraíso mais leves e significativas ao longo desta jornada.

À minha orientadora, professora Ana, expresso minha sincera gratidão. Obrigado por acreditar em mim e na relevância desta pesquisa. Seu exemplo de profissionalismo, dedicação e humanidade foi determinante para minha formação.

À minha psicóloga, Genara, pelo cuidado, empatia e suporte emocional ao longo desta jornada, que foram essenciais para manter minha perseverança nesta trajetória.

Aos colegas e amigos do NECOD, agradeço pelos inúmeros momentos de convivência, tanto no pavilhão fluvial quanto nas conversas informais no café. A colaboração, o apoio técnico e intelectual, e a amizade construída foram fundamentais para o desenvolvimento deste trabalho. Agradeço, em especial, aos técnicos Cristian e Felipe, pelo auxílio direto nas atividades que envolviam o canal experimental.

Aos amigos que o IPH me proporcionou, deixo meu agradecimento coletivo. São muitas pessoas que, de diferentes maneiras, desempenharam papel importante durante o mestrado e o doutorado, tornando essa trajetória mais leve e significativa.

Estendo meu agradecimento aos amigos de Porto Alegre, que me acolheram e me fizeram sentir pertencente a este lugar, ouvindo (inúmeras vezes) as angústias e conquistas deste processo. Agradeço também aos amigos de Paraíso, que compreenderam minhas ausências e, ainda assim, mantiveram o vínculo firme e afetuoso, como se o tempo jamais tivesse passado. A duas pessoas em especial, Tais e Fernanda, deixo um agradecimento singular: obrigado pelo apoio incondicional, pela escuta e pelos momentos inesquecíveis que tornaram este percurso mais humano. Realizamos um sonho juntos!

Agradeço aos membros da banca, à Carolina e aos professores Jean e Nilza, pela disponibilidade e contribuição na avaliação desta tese.

Agradeço ao Laboratoire d'Hydraulique Environnementale (LHE) da EPFL, na Suíça, pela oportunidade de vivenciar de perto a modelagem física de rios de montanha. Agradeço também aos meus amigos que fiz durante o período: Fernando e Kenny, que foram fundamentais durante o período de doutorado sanduíche.

Agradeço à CAPES/PROEX pelo apoio financeiro durante o doutorado e à CAPES/Print pela bolsa que viabilizou o estágio no exterior.

Por fim, agradeço ao NECOD, ao IPH e à UFRGS, universidade pública e de excelência, que proporcionaram o ambiente acadêmico necessário tanto para minha formação quanto para o desenvolvimento desta pesquisa.

A todos que, de alguma forma, contribuíram para esta trajetória, deixo meu sincero muito obrigado.

A complexidade dos escoamentos fluviais resulta, sobretudo, do tipo de interações entre a água e os sedimentos que faz com que estes escoamentos sejam autores da sua própria geometria, simultaneamente escultores e matéria esculpida, num processo interativo constantemente renovado.

Luis Veiga da Cunha (1997)

APRESENTAÇÃO

Esta tese foi desenvolvida no Programa de Pós-Graduação em Engenharia de Recursos Hídricos e Saneamento Ambiental do Instituto de Pesquisas Hidráulicas (IPH) da Universidade Federal do Rio Grande do Sul (UFRGS) sob a orientação da professora Ana Luiza de Oliveira Borges (IPH-UFRGS). A pesquisa foi financiada com bolsa de Doutorado pela Coordenação de Aperfeiçoamento de Pessoal de Nível Superior – Brasil (CAPES) (Código de Financiamento 001) no período de setembro de 2021 a agosto de 2025, com período de Doutorado Sanduíche na École Polytechnique Fédérale de Lausanne (EPFL) sob orientação do professor Christophe Ancey, financiado com bolsa de estudos concedida pelo Programa de Internacionalização Institucional – PRINT/UFRGS nº. 002/2023-PROPG, entre outubro de 2023 e março de 2024.

As principais publicações referentes a esta tese estão listadas a seguir:

Menezes, D. D., & Borges, A. L. O. (2023). Conformação morfológica de equilíbrio em simulação física de rios com leito de granulometria extensa. *Simpósio Brasileiro de Recursos Hídricos (25.: 2023: Aracaju). Anais. Porto Alegre: ABRHidro, 2023*.

Menezes, D. D., & Borges, A. L. O. (2024). Simulação física do transporte de água e sedimentos em rios de leito de cascalho: uma perspectiva em escala de canal. *Simpósio Nacional de Mecânica dos Fluidos e Hidráulica (2.: 2024: Curitiba); Encontro Nacional de Engenharia de Sedimentos (16.: 2024: Curitiba). Anais. Porto Alegre: ABRHidro, 2024*.

Menezes, D. D., & Borges, A. L. O. (2025). Exploring morphological equilibrium and flow resistance in gravel-bed rivers: insights from channel-scale experimental analysis. *RBRH*, *30*, e2.

Menezes, D., & Borges, A. L. O. (2025). Bed roughness in gravel-bed rivers: channel-scale responses to flow and sediment dynamics. Advances in Water Resources.

Menezes, D. D., & Borges, A. L. D. O. Hydrodynamic effects of bed roughness on velocity profiles in gravel-bed rivers: an experimental approach. A ser submetido para a *Journal of Geophysical Research: Earth Surface*.

RESUMO

SIMULAÇÃO FÍSICA DO TRANSPORTE DE ÁGUA E SEDIMENTOS EM CANAIS COM LEITO DE GRANULOMETRIA EXTENSA

No Brasil, a compreensão da dinâmica do escoamento e transporte de sedimentos em rios de granulometria extensa ainda é pouco explorada. Esses rios possuem material grosseiro no leito, o que afeta a geometria da seção transversal do canal, a trajetória do escoamento e a resistência ao fluxo. Dessa forma, nessa Tese, o objetivo foi estudar a influência da rugosidade do leito no padrão de escoamento e no regime de transporte de sedimentos em rios de granulometria extensa por meio da simulação física. Para alcançar esse objetivo, foram utilizados dados medidos em um rio de leito de cascalho do Sul do Brasil para constituir um canal experimental de 10 m de comprimento, 0,4 m de altura e 0,56 m de largura. O material do leito é de areia e cascalho muito fino (D_{50} = 3,19 mm), representando um rio natural de leito de cascalho (D_{50} = 63,9 mm) em escala reduzida (1:20). O trabalho foi dividido em três estudos complementares: o primeiro estudo concentrou-se na definição e calibração do aparato experimental, com ênfase na geração de um leito móvel capaz de reproduzir, em escala reduzida, os padrões morfológicos e hidrodinâmicos observados em campo. O segundo estudo abordou o comportamento da resistência ao escoamento em função da submersão relativa e da dinâmica sedimentar. O terceiro estudo analisou os perfis de velocidade em diferentes condições hidráulicas, a fim de compreender seus efeitos sob a rugosidade de fundo de um canal com leito de granulometria extensa. De modo geral, os resultados evidenciaram a importância do equilíbrio morfológico inicial e do preenchimento dos vazios entre os grãos maiores por sedimentos finos, elementos decisivos para a obtenção de resultados representativos da realidade natural. Além disso, observou-se que a resistência hidráulica decresce com o aumento da submersão relativa, enquanto condições de baixa vazão e pouca profundidade resultam em maiores valores de rugosidade, associados à microtopografia do leito e à formação de camadas de armadura. Destaca-se também que as equações empíricas disponíveis na literatura subestimaram a resistência sob condições de alta rugosidade relativa, indicando a necessidade de formulações mais específicas para rios tropicais e subtropicais, cujas características hidrológicas diferem substancialmente de ambientes temperados e alpinos. Os resultados também mostraram que sob condições rasas (baixos valores de h/D_{84}), a resistência é dominada por arrasto de forma e rugosidade, enquanto para maiores profundidades (alto h/D_{84}), o coeficiente ks tende à estabilização como múltiplo do tamanho dos grãos. Os resultados reforçam a importância da submersão relativa no controle da resistência hidráulica em canais de leito de cascalho. De forma integrada, os resultados obtidos demonstram que a modelagem física baseada em dados de campo constitui uma estratégia eficaz para o avanço do entendimento dos processos hidrossedimentológicos em rios de granulometria extensa. O modelo físico reproduziu com fidelidade as condições hidráulicas e morfológicas de um rio natural, permitindo estimar parâmetros de resistência ao escoamento. As conclusões fortalecem a compreensão da rugosidade de fundo e da interação entre fluxo e sedimentos em rios de leito de cascalho, representando um avanço no contexto brasileiro.

Palavras – chave: Modelagem física; Rugosidade do leito; Resistência ao fluxo; Fundo móvel; Perfis de velocidade.

ABSTRACT

PHYSICAL SIMULATION OF WATER AND SEDIMENT TRANSPORT IN GRAVEL-BED CHANNELS

In Brazil, the understanding of flow dynamics and sediment transport in rivers with coarse-grained beds remains limited. These rivers contain coarse material on the bed, which affects the cross-sectional geometry, flow trajectory, and flow resistance. Therefore, this Thesis aims to investigate the influence of bed roughness on flow patterns and sediment transport regimes in coarse-grained rivers through physical modeling. To achieve this objective, field data from a gravel-bed river in southern Brazil were used to construct an experimental flume 10 m long, 0.4 m high, and 0.56 m wide. The bed material, composed of sand and very fine gravel (D_{50} = 3.19 mm), represents a natural gravel-bed river (D_{50} = 63.9 mm) at a 1:20 scale. The research was divided into three complementary studies. The first focused on defining and calibrating the experimental setup, emphasizing the generation of a mobile bed capable of reproducing, at reduced scale, the morphological and hydrodynamic patterns observed in the field. The second investigated flow resistance behavior as a function of relative submergence and sediment dynamics. The third analyzed velocity profiles under different hydraulic conditions to understand their effects on bed roughness in a coarse-grained channel. Overall, the results highlighted the importance of the initial morphological equilibrium and interstitial filling by fine sediments, which are essential for obtaining realistic and representative results. Hydraulic resistance was found to decrease with increasing relative submergence, while low-flow and shallow conditions led to higher roughness values associated with bed microtopography and the formation of armor layers. Empirical equations available in the literature underestimated flow resistance under high relative roughness conditions, indicating the need for more specific formulations for tropical and subtropical rivers, whose hydrological characteristics differ substantially from those in temperate and alpine environments. The results also showed that under shallow flow conditions (low h/D84 values), resistance is dominated by form drag and roughness–flow interactions, whereas for deeper flows (high h/D84 values), the roughness height (ks) tends to stabilize as a multiple of grain size. These findings reinforce the role of relative submergence as a key control on flow resistance in gravel-bed channels. Overall, the results demonstrate that physical modeling based on field data is an effective strategy to advance the understanding of hydro-sedimentary processes in coarse-grained rivers. The developed physical model successfully reproduced the hydraulic and morphological conditions of a natural river, providing valuable insights for estimating flow resistance parameters. The conclusions contribute to the characterization of the processes governing bed roughness and flow–sediment interactions in gravel-bed rivers, representing a novel contribution within the Brazilian context. Furthermore, the findings have potential applications in river restoration studies, flood management, and hydraulic engineering projects, where understanding the effects of bed roughness and morphology is crucial for performance and sustainability.

Keywords: Physical modeling; Bed roughness; Flow resistance; Mobile bed; Velocity profiles.

LISTA DE FIGURAS

Figura 2-1 - Interação entre o fluxo do rio e a morfologia em rios de leito de cascalho 29
Figura 2-2 - Mobilidade dos sedimentos: a) o efeito do peso da partícula; b) o efeito de ocultação; c) o efeito de rolamento. Fonte: Adaptado de Southard (2006). 38

Figure 3-1 - Schematic representation of the experimental channel: a) cross and b) longitudinal view 54
Figure 3-2 - Grain size distribution curve of the material for the channel's movable bed 56
Figure 3-3 - (a) Pitot tube coupled with piezometer; (b) Measurement setup, (c) Pitot tube 58
Figure 3-4 - Movable bed channel: (a) schematic showing evaluated cross-sections and respective velocity measurement points; (b) pre-test photos (inclined and ruled plane) and post-test photos (change in texture and creation of preferential pathways). 59
Figure 3-5 - Correction term (*x*) in the formula proposed by Einstein (1950) 60
Figure 3-6 - Flow and transported sediment until stabilization of the mobile bed channel 63
Figure 3-7 - Behavior of transported characteristic diameters throughout the morphological configuration phase 64
Figure 3-8 - Changes in the channel bed (between 40 and 170 cm of the MB) during the initial bed configuration tests (greener color indicates positive elevation, while browner colour indicates negative elevation) 67
Figure 3-9 - Longitudinal profile at positions 15, 30, and 45cm (from right to left) 68
Figure 3-10 - Variation of bed diameters throughout the experiment 69
Figure 3-11 - Velocity profiles obtained for verticals (V14, V30, and V45) at sections (ST-120 and ST-160) for the conducted tests (E1, E2, E3, E4, and E5) 71
Figure 3-12 - Velocity profiles for each vertical at ST-120 and ST-160 cm 72
Figure 3-13 - Behavior of ks and U across the tests for the two velocity profile measurement sections 73
Figure 3-14 - Bathymetry of transverse sections (a) at 120 cm (ST-120) and (b) at 160 cm (ST-160) at the end of each test, along with the water depth measured during the test 74
Figure 3-15 - Channel bed throughout the tests (greener color indicates positive elevation, and browner color indicates negative elevation) 75
Figure 3-16 - Oscillation factor (OF) of the bed elevation in transverse measurement sections of the channel 76
Figure 3-17 - Behavior of resistance variables throughout the tests: C (Chezy coefficient), F (Darcy–Weisbach coefficient), and n (Manning coefficient). 77
Figure 3-18 - Relationship between Re and Fr versus U/u* 78
Figure 3-19 - Comparison between the dimensionless variables proposed by Rickenmann and Recking (2011) 80

Figure 4-1 - Schematic representation of the experimental channel: a) cross and b) longitudinal view 95

Figure 4-2 - Grain size distribution curve of the material for the channel's movable bed 97
Figure 4-3 - Sediment inlet grain size distribution 100
Figure 4-4 - Flow rate and sediment introduced into the channel during the experiments (Phases I and II) 101
Figure 4-5 - Channel bed survey after Phase I experiments, both conducted with Q = 366 L/min and Qs = 0.7 g/s. All values shown in the figure are in millimeters 103
Figure 4-6 - Behavior of a) water depth (h), b) wetted perimeter (Pm); c) wetted area (Am), d) hydraulic radius (Rh), and e) velocity (U) along the cross-sections – Phase I 105
Figure 4-7 - Oscillation factor and standard deviation of bed elevation fluctuations - Phase I 106
Figure 4-8 - Behavior of Manning's roughness coefficient (n) and Darcy-Weisbach friction factor (f) – Phase I 107
Figure 4-9 - Channel bed elevation survey after tests from Phase II experiments. All values shown in the figure are in millimeters 109
Figure 4-10 - Behavior of a) water depth (h), b) wetted perimeter (Pm); c) wetted area (Am), d) hydraulic radius (Rh), and e) velocity (U) along the cross-sections – Phase II 110
Figure 4-11 - Oscillation factor and standard deviation of bed elevation variations - Phase II 111
Figure 4-12 - Behavior of Manning's roughness coefficient (n) and Darcy-Weisbach friction factor (f) – Phase II 112
Figure 4-13 - Comparison between the initial sediment distribution (selected material) and the distribution of bed elevation fluctuations (here referred to as roughness coefficient - R) for ST-120 and ST-220 113
Figure 4-14 - Roughness values: arithmetic absolute, root mean square and bed roughness coefficients R_{84} and R_{50} obtained after each test 116
Figure 4-15 - Hydraulic radius and Manning's n over experiments for different sections 118
Figure 4-16 - Flow velocity and Darcy-Weisbach friction factor: flow resistance equations 119
Figure 4-17 - Relationship between $(8/f)^{1/2}$ and h/D_{84} for different equations 120
Figure 4-18 - Grain size distribution of the injected and transported sediment 122
Figure 4-19 - Relationship between θcr,i/θc,50 and Di/D50 for different equations from the literature 125
Figure 4-20 - Boundary shear stress and critical shear stress for a) R10, b) R16, c) R84, and d) R90 126
Figure 4-21 - Relationship between velocity and Manning's n for each cross-section in phase II data 128
Figure 4-22 - Relationship between velocity and Darcy-Weisbach friction factor for phase II data 129

Figure 5-1 - Illustration of Velocity Profile in gravel-bed rivers (not to Scale) according Smart (1999) 153

Figure 5-2 - Schematic representation of the experimental channel: a) cross and b) longitudinal view. 157
Figure 5-3 - Grain size distribution curve of the material for the channel's movable bed 158
Figure 5-4 - (a) Pitot tube coupled with piezometer; (b) Measurement setup, (c) Pitot tube 159
Figure 5-5 - Movable bed channel: (a) schematic showing evaluated cross-sections and respective velocity measurement points; (b) initial condition (inclined and ruled plane with detail of the initial thalweg at the center of the channel) and end of E10 (change in texture and creation of preferential pathways) 160
Figure 5-6 - Correction term (x) in the formula proposed by Einstein (1950)..... 161
Figure 5-7 - Sediment inlet: (a) equipment and (b) grain size distribution 164
Figure 5-8 - Flow rate and sediment introduced into the channel during the experiments (Phases I and II)..... 165
Figure 5-9 - Velocity profiles (V15, V30, and V45) measured at section 120 (ST-120) 166
Figure 5-10 - Behavior of the mean velocity (U) compared with shear stress (τ) and shear velocity (u*) for the measured velocity profiles 167
Figure 5-11 - ks for the analyzed sections (ST-120 and ST-160) 168
Figure 5-12 - Temporal variation of bed particle sizes during the experiments at ST-120 and ST-160 169
Figure 5-13 - Channel bed profile after each test for section ST-120 and ST-160. 170
Figure 5-14 - -Relationship between relative submergence (h/D84) and the roughness coefficient (ks)..... 171
Figure 5-15 - Relationship between particle diameter (D84 and D90) and the roughness coefficient (ks)..... 172
Figure 5-16 - Relationship between shear stress (τ) and relative roughness (h/ks) across different classes of ks/δ 173
Figure 5-17 - Relationship among the Manning (n), Darcy–Weisbach (f), and Chezy (C) coefficients..... 174
Figure 5-18 - Particle Reynolds number (Re) behavior versus Darcy–Weisbach friction factor (f) under different ks/δ conditions..... 175
Figure 5-19 - Relationship between $(8/f)^{1/2}$ and h/D_{84} for different equations..... 177
Figure 5-20 - Comparison between the dimensionless variables proposed by Rickenmann & Recking (2011)..... 178

Figura 6-1 – Relação entre τxh/ks para os dados do artigo III e artigo II. 188
Figura 6-2 - Relação entre τ e Ilocal=J para os dados do artigo III, artigo II e dados de campo 190
Figura 6-3 - Relação entre h/D84 e (8/f)1/2 191
Figura 8-1 - Localização do trecho do rio Forqueta. Fonte: Menezes (2021). 204
Figura 8-2 - Distribuição climática em relação ao relevo. Fonte: Rocha (2013). 206

Figura 8-3 - Medição da vazão: (a) em baixo nível d'água; e (b) alto nível d'água. Fonte: Menezes (2021) 207

Figura 8-4 - Perfil longitudinal do trecho em estudo do rio Forqueta (565 m). Fonte: Menezes (2021). 208
Figura 8-5 - Batimetria de seções do rio Forqueta. Fonte: Menezes (2021) 209

LISTA DE TABELAS

Tabela 2-1 - Equações utilizadas para cálculo da resistência ao fluxo 33
Tabela 2-2 - Submersão relativa do fluxo conforme categorizado por Bathurst (1985). 35
Tabela 2-3 – Equações utilizadas para estimativa de transporte de sedimentos de fundo em rios de granulometria extensa 42

Table 3-1 - Scale relationships between the model and the prototype 55
Table 3-2 - Equations used for the calculated variables 61
Table 3-3 - Flow and transported sediment rates before bed stabilization 63
Table 3-4 - Erosion vs. deposition balance through analysis of surfaces in Surfer 66
Table 3-5 - Characterization of flow rates and sediments for the conducted tests 70
Table 3-6 - Measured and calculated variables for the tests conducted in the channel .. 77

Table 4-1 - Scale relationships between the model and the prototype 96
Table 4-2 – Experiments design 99
Table 4-3 - Flow resistance equations 120
Table 4-4 - Sediment transport characteristics 123
Table 4-5 - Equations used to calculate critical stress 124

Table 5-1 - Flow relative submergence as categorized by Bathurst (1985) 155
Table 5-2 - Scale relationships between the model and the prototype 157
Table 5-3 - Equations used for the calculated variables 161
Table 5-4 - Experimental design 163
Table 5-5 - Flow resistance equations 175

Tabela 8-1 - Variáveis hidráulicas levantadas na primeira campanha (agosto/2020). Fonte: Menezes (2021). 210

LISTA DE SÍMBOLOS

Símbolo	Descrição	Unidade dimensional
a	Constante	-
A	Valor adimensional de ajuste da equação	-
b	Expoente relacionado ao arrastamento	-
B	Constante	-
C	Coeficiente de Chèzy	$L^{1/2}/T$
C_d	Coeficiente de descarga	-
D_{10}	Diâmetro da partícula correspondente a porcentagem acumulada de 10%	L
D_{16}	Diâmetro da partícula correspondente a porcentagem acumulada de 16%	L
D_{50}	Diâmetro da partícula correspondente a porcentagem acumulada de 50%	L
D_{84}	Diâmetro da partícula correspondente a porcentagem acumulada de 84%	L
D_{90}	Diâmetro da partícula correspondente a porcentagem acumulada de 90%	L
D_i	Diâmetro de grão característico	L
D_m	Diâmetro médio dos grãos	L
f	Fator de perda de Darcy–Weisbach	-
f_1	Parâmetro de ajuste	-
f_2	Coeficiente de perda (fricção)	-
f_3	Parâmetro de ajuste	-
Fr	Número de Froude	-
g	Aceleração devido à gravidade	L/T^2
h	Profundidade média do escoamento	L
H	Altura da lâmina d'água no vertedor	L
h/D	Submergência relativa = Relação entre profundidade do escoamento e diâmetro do grão de fundo	-
I	Inclinação de fundo do canal	L/L
I_c	Inclinação do canal experimental	L/L
k_s	Rugosidade equivalente = Rugosidade do leito	L
J	Inclinação da linha de energia	L/L
L	Largura do canal	L
L_l	Largura da superfície gerada pelo laser na seção	L
L_{modelo}	Largura do canal (modelo)	L
$L_{natural}$	Largura do rio (protótipo)	L
n	Coeficiente de Manning	$T/L^{1/3}$
N_0	Valor adimensional de ajuste da equação	-
q	Vazão por unidade de largura	L^2/T
Q	Vazão	L^3/T

q^{**}	Adimensional de vazão da Equação de Rickenmann e Recking (2011)	-
Q_b	Transporte de sedimento de fundo	M^3/T
Q_{med}	Vazão média	L^3/T
R	Raio hidráulico da seção	L
r	Fator de escala geométrica	-
Re	Número de Reynolds	-
Re^*	Número de Reynolds do grão	-
U	Velocidade média do fluxo	L/T
u	Velocidade em uma determinada distância do fundo	L/T
U^{**}	Adimensional de velocidade da Equação de Rickenmann e Recking (2011)	-
X	Variável qualquer	-
x	Fator de correção da Equação de Einstein (1950)	-
X_{cr}	Variável qualquer crítica	-
x_m	Média dos N valores x_i observados	-
y	Distância do fundo	L
y_0	Altura onde ocorre interação entre água e fundo do canal	L
y_m	Média dos N valores y_i calculados	-
α	Constante empírica	-
α_2	Inclinação do piezômetro	°
β	Constante empírica	-
γ	Constante empírica	-
δ	Espessura da subcamada viscosa	L
Δh	Diferença entre a altura dinâmica e altura estática do piezômetro	L
ζ_i	Coeficiente de ocultação	-
θ	Ângulo de abertura do vertedor	°
θ_c	Parâmetro da Equação de Shields	-
κ	Constante de von Karman	-
μ_*	Velocidade de cisalhamento	L/T
ν	Viscosidade cinemática da água	L^2/T
ρ	Massa específica da água	M/L^3
ρ_s	Massa específica do sedimento	M/L^3
σ_z	Desvio padrão das elevações do leito	L
τ_*	Tensão de cisalhamento adimensional	M/LT^2
τ_c	Tensão de cisalhamento crítica	M/LT^2
τ_{r50}	Tensão de cisalhamento para o D_{50}	M/LT^2
τ_{ri}	Tensão de cisalhamento de referência	M/LT^2
Υ	Peso específico da água	M/L^2T^2
Υ_s	Peso específico do sedimento	M/L^2T^2
ψ	Número de Shields	-
ω	Potência de fluxo por unidade de largura	ML^2/T^3

M: massa; L: comprimento; T: tempo.

SUMÁRIO

1. INTRODUÇÃO 22

1.1 Caracterização do problema e justificativa 22

1.2 Questão de pesquisa 24

1.3 Objetivos 24

1.3.1 Objetivo geral 24

1.3.2 Objetivos específicos 24

1.4 Estrutura da Tese 24

2. REVISÃO BIBLIOGRÁFICA 27

2.1 Rios de granulometria extensa 27

2.2 Morfodinâmica de rios com leito de cascalho 28

2.3 Resistência hidráulica 30

2.3.1 Tipos de resistência ao fluxo 30

2.3.2 Equacionamento 31

2.3.3 Submergência relativa 34

2.4 Transporte de sedimentos 36

2.4.1 Condições iniciais 36

2.4.2 Leito de granulometria não uniforme 39

2.4.3 Equações utilizadas em leito de granulometria extensa 41

3. ARTIGO I: EXPLORING MORPHOLOGICAL EQUILIBRIUM AND FLOW RESISTANCE IN GRAVEL-BED RIVERS: INSIGHTS FROM CHANNEL-SCALE EXPERIMENTAL ANALYSIS 45

3.1 INTRODUCTION 48

3.1.1 Definition of morphological equilibrium conformation 48

3.1.2 Flow resistance in gravel-bed rivers 49

3.2 MATERIAL AND METHODS 53

3.2.1 Experimental setup 53

3.2.2 Similarity analysis 54

3.2.3 Inlet flow *55*
3.2.4 Characterization of the Movable Bed (MB) *56*
3.2.5 Measurement of channel bed deformations *56*
3.2.6 Collector box for transported material *57*
3.2.7 Measurement of velocities and water level *57*
3.2.8 Treatment of velocity profiles *59*
3.2.9 Experimental design *61*
3.3 RESULTS AND DISCUSSION 62
3.3.1 Evaluation of bed morphological configuration *63*
3.3.2 Evaluation of velocity profiles and flow resistance *70*
3.3.3 Evaluation of bed roughness *72*
3.4 CONCLUSIONS 80
3.5 REFERENCES 81
4. ARTIGO II: BED ROUGHNESS IN GRAVEL-BED RIVERS: CHANNEL-SCALE RESPONSES TO FLOW AND SEDIMENT DYNAMICS 86
4.1 INTRODUCTION 89
4.1.1 Roughness in gravel-bed rivers *89*
4.1.2 Sediment supply in gravel-bed rivers *90*
4.2 MATERIAL AND METHODS 94
4.2.1 Experimental setup *94*
4.2.2 Similarity Analysis *95*
4.2.3 Inlet Flow *96*
4.2.4 Characterization of the Movable Bed (MB) *96*
4.2.5 Measurement of channel bed deformations *97*
4.2.6 Collector box for transported material *98*
4.2.7 Experimental Design *99*
4.3 RESULTS AND DISCUSSION 101
4.3.1 Phase I: Bed conformation *101*
4.3.2 Phase II: suppression of sediment injection *107*
4.3.3 Flow resistance parameters *113*
4.3.4 Sediment transport analysis *121*

4.3.5 Relationship between characteristic variables *127*
4.4 CONCLUSIONS 129
4.5 FUTURE SCOPE 131
4.6 REFERENCES 132
4.1 APPENDIX A 137
4.2 APPENDIX B 139
4.3 APPENDIX C 141
4.4 APPENDIX D 145
5. ARTIGO III: HYDRODYNAMIC EFFECTS OF BED ROUGHNESS ON VELOCITY PROFILES IN GRAVEL-BED RIVERS: AN EXPERIMENTAL APPROACH 148
5.1 INTRODUCTION 151
5.1.1 Velocity profile *151*
5.1.2 Bed roughness *154*
5.2 MATERIAL AND METHODS 156
5.2.1 Experimental setup *156*
5.2.2 Measurement of profile velocities *158*
5.2.3 Treatment of velocity profiles *160*
5.2.4 Experimental Design *162*
5.3 RESULTS AND DISCUSSION 165
5.3.1 Velocity profile determination *165*
5.3.2 Channel Bed Roughness *167*
5.3.3 Flow Resistance *173*
*5.3.4 Relationships between dimensionless variables q** and U*** *177*
5.4 CONCLUSIONS 178
5.5 REFERENCES 180
5.6 APPENDIX A 183
5.7 APPENDIX B 186
6. CONCLUSÕES E PERSPECTIVAS 187
6.1 GENERALIZAÇÕES 187

6.2 PRINCIPAIS CONSIDERAÇÕES....192
6.3 RECOMENDAÇÕES PARA TRABALHOS FUTUROS....194
7. REFERÊNCIAS....196
8. APÊNDICE A....203
8.1 ÁREA DE ESTUDO (PROTÓTIPO)....203
8.2 LOCALIZAÇÃO....203
8.3 MONITORAMENTO HIDROSSEDIMENTOLÓGICO....206
8.4 REFERÊNCIAS....211

1. INTRODUÇÃO

1.1 Caracterização do problema e justificativa

Em rios de leito com granulometria extensa, caracterizados por grandes blocos associados a sedimentos móveis menores, a compreensão da dinâmica do transporte de carga de fundo é de suma importância. Isso porque, os sedimentos mais grossos, que se mobilizam das encostas, podem permanecer depositados nas margens e no leito dos rios, alterando a geometria da seção transversal do canal, a trajetória do escoamento preferencial e o coeficiente de resistência ao escoamento. Quando os sedimentos estão parados ou transportados com baixa intensidade, a presença de partículas de sedimentos na superfície do leito desses rios e seus impactos no escoamento são elementos que podem induzir a ocorrência de mudanças na resistência do leito do canal.

Compreender a dinâmica da interação entre o escoamento e os sedimentos presentes na seção transversal destes cursos de água favorece o conhecimento físico do transporte de sedimentos neste ambiente para melhor predizê-lo. Essas previsões são essenciais para avaliar o perigo relacionado a fluxos fortemente carregados de sedimentos e, mais especificamente, para direcionar os sedimentos através de redes fluviais, restaurar a funcionalidade e o habitat do rio e mitigar o impacto dos fluxos de detritos na população ribeirinha (LAMB; DIETRICH; VENDITTI, 2008a).

No Brasil, esses rios estão associados a regiões como a Serra do Mar, que acompanha o litoral do Sudeste e Sul do Brasil. Essa região é caracterizada por uma serra escarpada, com grande declividade, formando um paredão próximo ao mar. Além do clima úmido, há forte presença da Mata Atlântica, com intensa erosão e instabilidade de encostas (THOMPSON et al., 1998). Outras regiões de ocorrência desses rios no Brasil é a Serra Geral, abrangendo os estados de Santa Catarina, Rio Grande do Sul e Paraná, prolongando-se até o Mato Grosso do Sul e Paraguai em alguns contextos geológicos. No APÊNDICE A é mostrado o rio referência para o presente estudo, localizado no estado do Rio Grande do Sul Essa região marca o rebordo do Planalto Meridional e é uma região típica de canyons, campos e araucárias (RENNER et al., 2024). Por esses motivos, a dinâmica dos sedimentos nos rios dessas regiões é bastante diferenciada de outras regiões ao redor do mundo, principalmente por possuírem uma área fonte de sedimentos de granulometria menor e que, por vezes, estão associadas a áreas agrícolas.

Os leitos dos cursos de água em ambientes de alta declividade são caracterizados pela ocorrência de granulometria extensa. Isso é responsável por criar uma arquitetura de leito que apresenta distribuição de tamanho de grão multimodal e mal classificada (BATHURST, 1985; LENZI; MAO; COMITI, 2006; RICKENMANN, 2001; SCHNEIDER *et al.*, 2014; YAGER *et al.*, 2012b). Em alguns casos, blocos imóveis do leito induzem flutuações de carga de sedimentos de fundo, afetando a taxa de arrastamento e a deposição de partículas em sua vizinhança (MONSALVE; YAGER; SCHMEECKLE, 2017). Ao regular a deposição e a mobilização do material que chega, os blocos também alteram a estrutura da superfície do leito (GHILARDI; FRANCA; SCHLEISS, 2014; RECKING; VÁZQUEZ TARRÍO; PITON, 2022; YAGER; KIRCHNER; DIETRICH, 2007).

Embora esses rios geralmente sejam responsáveis por controlar o fornecimento de sedimentos para os rios de planície, relativamente poucos estudos foram realizados em canais de granulometria extensa, principalmente no que se refere a modelos físicos. Além disso, a influência desses rios, geralmente associados a áreas montanhosas, na geomorfologia do sistema fluvial e nas enchentes de caráter catastrófico é determinante. No entanto, historicamente, o conhecimento científico sobre rios em áreas planas de areia tem sido maior do que sobre rios de cascalho e montanha. Embora esses estudos forneçam equações de transporte de sedimentos, a maioria deles não leva em consideração as condições extremas que caracterizam os rios de granulometria extensa. Um exemplo disso é a presença de elementos de macro rugosidade, como grandes pedregulhos relativamente imóveis, que interrompem o fluxo e alteram a rugosidade do canal (GHILARDI; FRANCA; SCHLEISS, 2014).

Nesse sentido, a modelagem física desses processos garante um ambiente controlado, sendo possível, determinar com precisão as variáveis de entrada e quantificar as variáveis de saída. Explorando situações em que o sedimento atua como barreira/obstáculo ou em que ele age como rugosidade de superfície, busca-se entender como a granulometria extensa desses rios interfere nos parâmetros hidráulicos (profundidade, velocidades, resistência), na natureza do escoamento quanto à relação *h/D* (profundidade do escoamento/diâmetro de sedimento de fundo) e na taxa de transporte de sedimentos de arraste.

Ao utilizar dados de campo para criar condições de laboratório e, consequentemente, simular um rio natural, é possível controlar e quantificar variáveis

que, em campo, são difíceis. Assim, essa pesquisa tem o potencial de fornecer ferramentas para o avanço do conhecimento na área de hidráulica fluvial, contribuindo para uma melhor compreensão dos processos em rios de granulometria extensa e permitindo o desenvolvimento de estratégias mais eficazes para a gestão e conservação desses ambientes. Além disso, os resultados obtidos podem ter aplicações práticas em projetos de engenharia hidráulica e na tomada de decisões relacionadas à preservação dos recursos hídricos e à segurança da população ribeirinha.

1.2 Questão de pesquisa

Em rios com granulometria extensa, é possível diferenciar, por meio de simulação física baseada em dados coletados à campo, a influência da rugosidade sobre os valores da resistência ao fluxo?

1.3 Objetivos

1.3.1 Objetivo geral

O objetivo desta Tese é estudar a influência da rugosidade do leito no padrão de escoamento e no regime de transporte de sedimentos em rios de granulometria extensa por meio da simulação física.

1.3.2 Objetivos específicos

Os objetivos específicos desta Tese são:

- Conceber e projetar o aparato experimental e a metodologia para a simulação física do processo em estudo;
- Avaliar o efeito das deformações de fundo sobre o escoamento na busca de uma conformação morfológica em equilíbrio;
- Identificar como a granulometria de fundo controla o escoamento (resistência hidráulica) por meio da medição de perfis de velocidade.

1.4 Estrutura da Tese

Com o objetivo de atender aos propósitos delineados na introdução, este trabalho está organizado em seis capítulos, cada um com suas respectivas motivações, conforme detalhado a seguir:

- CAPÍTULO 1 – INTRODUÇÃO. Nesse capítulo é apresentado e caracterizado o tema principal da pesquisa. Além disso, é exposto a questão de pesquisa e delineado os objetivos.
- CAPÍTULO 2 - REVISÃO BIBLIOGRÁFICA: Neste capítulo, é apresentada uma revisão bibliográfica que fundamenta cientificamente o desenvolvimento deste estudo. Além disso, em cada artigo (Capítulo 3, 4 e 5) é realizada uma revisão específica sobre o assunto principal;
- CAPÍTULO 3 – ARTIGO I. Nesse capítulo é apresentado o artigo "*Explorando o equilíbrio morfológico e a resistência ao fluxo em rios de leito de cascalho: percepções da análise experimental em escala de canal*". O principal objetivo desse artigo foi desenvolver uma configuração morfológica que reproduza os padrões típicos observados em canais fluviais de leito de cascalho.
- CAPÍTULO 4 – ARTIGO II. Nesse capítulo é apresentado o artigo "*Rugosidade do leito em rios de leito de cascalho: respostas em escala de canal à dinâmica do escoamento e dos sedimentos*". O principal objetivo desse artigo foi investigar o comportamento da rugosidade do leito em resposta à supressão do suprimento de sedimentos em um canal de leito de cascalho, e estimar como a rugosidade do fundo evolui sob condições variáveis de escoamento e de transporte de sedimentos.
- CAPÍTULO 5 – ARTIGO III. Nesse capítulo é apresentado o artigo *"Efeitos hidrodinâmicos da rugosidade do leito sobre os perfis de velocidade em rios de leito de cascalho: uma abordagem experimental".* O principal objetivo desse artigo foi avaliar a rugosidade do leito com base em medições de perfis de velocidade sob diferentes condições de escoamento.
- CAPÍTULO 6 – CONCLUSÕES E PERSPECTIVAS. Nesse último capítulo são apresentadas as principais conclusões envolvendo o desenvolvimento desse estudo e como ele pode contribuir para o avanço de novos conhecimentos acerca do entendimento da dinâmica de rios de cascalho no Brasil.

Cada capítulo foi cuidadosamente planejado para promover o entendimento de aspectos relacionados a rios de leito de cascalho e o efeito dessa característica na resistência ao fluxo e no transporte de sedimentos.

2. REVISÃO BIBLIOGRÁFICA

2.1 Rios de granulometria extensa

Em rios de granulometria extensa o leito do canal é composto por sedimentos móveis grosseiros, encontrados geralmente nas piscinas (*pools*) a jusante dos degraus (*steps*), e por grandes blocos relativamente imóveis (PAPANICOLAOU; BDOUR; WICKLEIN, 2004; RICKENMANN, 2001; YAGER; KIRCHNER; DIETRICH, 2007). Nesses rios, a dinâmica do escoamento e a arquitetura dos sedimentos podem organizar os degraus abrangendo toda a largura do canal (morfologia *step-pool*) ou de uma maneira mais irregular (morfologia *cascade*) (MONTGOMERY; BUFFINGTON, 1997).

Geralmente, leitos de granulometria extensa estão associados a rios de montanha que exercem um controle significativo sobre o tamanho, quantidade e tempo de sedimentos entregues às regiões de menor gradiente da bacia hidrográfica (YAGER; KIRCHNER; DIETRICH, 2007). Em rios como esses, o transporte de sedimentos é predominantemente realizado pela carga de fundo devido ao tamanho relativamente grande do diâmetro médio das partículas. Nesse tipo de transporte, as partículas se deslocam através de deslizamentos, rolamentos e pequenos saltos a jusante (saltação) (HEYMAN *et al.*, 2013).

Leito de cascalho e riachos com leito de pedregulho (por exemplo, rios de montanha) são caracterizados por uma ampla distribuição de tamanho de grão que é composta por sedimentos mais finos e móveis e grandes grãos ou pedregulhos relativamente imóveis (PAPANICOLAOU; BDOUR; WICKLEIN, 2004; RICKENMANN, 2001; YAGER; KIRCHNER; DIETRICH, 2007). Devido à presença de blocos grossos, a resistência ao escoamento do fluxo no canal é alta (WILCOX; WOHL, 2006).

Como destacado por Wohl (2000), as equações hidráulicas desenvolvidas para canais arenosos de baixa declividade não se aplicam bem a canais de montanha. Nesses ambientes, a combinação de declividades acentuadas, grãos de grande porte e formas rugosas produz perfis de velocidade não logarítmicos. Também favorece a ocorrência de escoamento crítico e localmente supercrítico, além de um padrão de escoamento fortemente tridimensional. As equações de resistência comumente utilizadas, portanto, não estimam com precisão a velocidade do fluxo nem a tensão de cisalhamento nesses rios rasos e íngremes. Isso ocorre principalmente devido à presença de elementos de

macrorrugosidade, como pedregulhos, grandes detritos lenhosos e morfologia escalonada. As equações de transporte de fundo ampliam essa incerteza. Elas dependem de previsões acuradas da tensão de cisalhamento no leito e assumem que o transporte de sedimentos aumenta de forma não linear com o excesso de tensão de cisalhamento (YAGER *et al.*, 2012a).

Por essas razões, é necessário diferenciar, ao analisar o transporte de sedimentos em rios de granulometria extensa, quando o material do leito atua como resistência ao escoamento ou quando atuam como obstáculos ao escoamento. Muitos estudos investigaram a influência de elementos de macro rugosidade, como pedregulhos (isolados ou dispostos em etapas) e grandes detritos lenhosos, nas condições de fluxo sem suprimento de sedimentos (CANOVARO; PARIS; SOLARI, 2007; WILCOX; WOHL, 2006). No entanto, para rios brasileiros ainda não há estudos que realizam essa abordagem.

2.2 Morfodinâmica de rios com leito de cascalho

A ligação entre as mudanças morfológicas e o transporte de sedimentos em rios de leito de cascalho ainda é uma questão em aberto (CHURCH; FERGUSON, 2015; RECKING *et al.*, 2016). Rios de leito de cascalho são caracterizados por sedimentos mal classificados e, como resultado da interação entre grãos em movimento e estáticos, seu leito é auto-organizado. Muitas vezes ocorre uma distribuição vertical da granulometria, pois os grãos mais finos são preferencialmente transportados. Como consequência, os grãos grossos formam uma camada de proteção (*armor layer*) na superfície do leito, cobrindo o material mais fino (PARKER *et al.*, 1982; PITLICK *et al.*, 2008).

A camada de proteção aumenta a resistência do leito ao estresse de cisalhamento e, portanto, limita sua erosão (CHURCH; HASSAN; WOLCOTT, 1998). Ela é tipicamente observada na ausência de grandes entradas de sedimentos e quando o estresse de cisalhamento é menor que o valor crítico necessário para iniciar o movimento de todas as classes de tamanho de grãos (GOMEZ, 1994). No entanto, durante enchentes, a camada de proteção pode ser desmontada, liberando grandes quantidades de sedimentos. A dinâmica desses rios é, portanto, o resultado da interação mútua entre o fluxo da água e a morfologia do leito através do transporte de sedimentos, conforme mostrado na Figura 2-1.

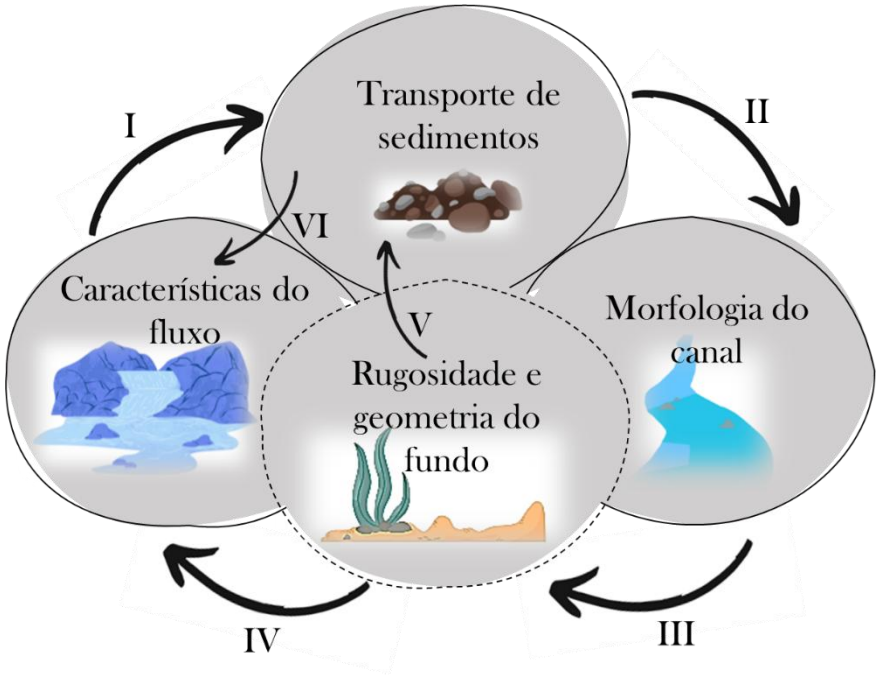


Figura 2-1 - Interação entre o fluxo do rio e a morfologia em rios de leito de cascalho

(I) o fluxo do rio transporta o sedimento, (II) o transporte do sedimento induz mudanças na morfologia do canal (erosão e deposição no leito); (III) as mudanças morfológicas afetam a geometria e a rugosidade do leito; (IV) as alterações do leito afetam as características do fluxo e, (V) o transporte do sedimento, e (VI) o transporte do sedimento também pode afetar as características do fluxo; adaptado de (PAQUIER *et al.*, 2008).

É importante destacar que a superfície do leito de um rio aluvial representa a principal interface entre o fluxo de água e o sedimento disponível para ser transportado. Como tal, é um componente crítico do sistema fluvial, exercendo uma influência na hidráulica do escoamento (FERRARO; COSCARELLA; GAUDIO, 2019; HARDY *et al.*, 2010), na resistência ao fluxo (RICKENMANN; RECKING, 2011a) e na taxa de transporte de sedimentos e na distribuição de tamanhos de grãos (WANG *et al.*, 2011). Além disso, devido à interação dinâmica entre o leito, o fluxo e o sedimento transportado, o leito do canal está livre para se ajustar às mudanças na vazão (POLVI, 2021; RACHELLY *et al.*, 2021) e no suprimento de sedimentos (DIETRICH *et al.*, 1989; LÓPEZ *et al.*, 2023). Assim, com o intuito de procurar uma maior estabilidade, a superfície de um leito de rio se molda livremente para acomodar os sedimentos disponíveis, resultando na formação de uma arquitetura característica do fundo (FERGUSON, 2007; NELSON; DUBÉ, 2016).

Vários estudos têm utilizado configurações ideais de leitos de cascalho para isolar os efeitos de diferentes configurações superficiais de depósito (FERRO, 2018; SCHMEECKLE; NELSON; SHREVE, 2007; SMITH et al., 2023), mas poucos

desenvolveram técnicas para recriar as condições de leito encontradas em rios de cascalho naturais. BUFFIN-BÉLANGER *et al.* (2003) e Spiller; Rüther; Baumann (2015) desenvolveram um procedimento de moldagem que reproduz com precisão a complexidade das superfícies de leitos de cascalho. Esses autores fizeram moldes a partir de uma seção de um leito de cascalho no campo e réplicas foram produzidas a partir desses moldes e colocadas no canal. Embora esse método crie uma superfície com a estrutura geométrica de um leito de cascalho natural, é importante observar que ela é impermeável, o fundo é estático e não reproduz a estratificação vertical do sedimento no leito.

Nesse sentido, para a compreensão da interação entre água e sedimentos, a modelagem física do fundo móvel exige uma fase preliminar de ensaios que permita a criação de uma calha de canal que apresente elementos morfológicos, distribuição dos sedimentos e caminhos de escoamento que reproduzam, o mais próximo possível, as suas condições naturais (calha de equilíbrio). A busca da calha de equilíbrio, se faz injetando, por um determinado tempo, vazão de diferentes magnitudes no canal, até se obter uma geometria do leito quase invariável, identificada através da quantificação do sedimento transportado.

2.3 Resistência hidráulica

2.3.1 Tipos de resistência ao fluxo

A resistência ao fluxo em rios é causada por qualquer característica da topografia do canal, forma ou textura do leito (tamanho de grãos e distribuição de tamanho de grãos) que retarda o fluxo do rio, sendo frequentemente considerada como uma dissipação de energia. A perda de energia ao longo de um determinado trecho de um rio é causada pelas interações entre o fluxo do rio e os limites do canal que dissipam a energia. Essa energia é dissipada à medida que a água se move ao redor e sobre irregularidades do leito e das margens, resultando em resistência ao fluxo (DAVID *et al.*, 2011).

Essa dissipação de energia se deve ao cisalhamento do escoamento sobre a superfície, causado pela pressão diferencial em torno dos objetos (DAVID *et al.*, 2011; FERGUSON, 2007) e para formar tensões induzidas (NIKORA *et al.*, 2001a). Isso se deve à intermitência espacial e temporal da turbulência do campo de velocidade com o leito heterogêneo do rio e a resistência ao escoamento.

As tensões induzidas se referem a dissipação de energia da aceleração e desaceleração do fluxo, geralmente ao longo ou a jusante de degraus (*Steps*) (CURRAN; WOHL, 2003; DAVID *et al.*, 2011). Elementos de grande rugosidade, como pedregulhos isolados, aglomerados de pedregulhos (degraus) e detritos lenhosos, encontrados em rios torrenciais, atuam como obstáculos ao fluxo ou, até mesmo, bancos de deposição. Uma força de arrasto é exercida sobre esses obstáculos quando o fluxo é forçado em torno deles. Praticamente qualquer coisa em um canal que cause a geração de turbulência (cisalhamento com o leito de sedimentos ou margens, formas no leito, vegetação, afloramentos de rochas, etc.) é uma forma de resistência dissipativa ao fluxo, assim, seu equacionamento é importante para o melhor conhecimento e previsão do comportamento em um rio natural.

2.3.2 Equacionamento

Nesse sentido, equações de resistência de fluxo são comumente usadas para a estimativa da velocidade de fluxo em rios. As equações usadas com mais frequência para calcular a velocidade do fluxo incluem as equações de Chézy, Manning e Darcy-Weisbach:

$$U = C\sqrt{RI} = \frac{1}{n}R^{\frac{2}{3}}I^{\frac{1}{2}} = \sqrt{\frac{8gRI}{f}} \quad (1)$$

Onde U é a velocidade média do fluxo (L/T), C é o coeficiente de Chezy ($L^{1/2}/T$), n é o coeficiente de Manning ($T/L^{1/3}$), f é o fator de perda de Darcy–Weisbach (adimensional), R é o raio hidráulico da seção (L), I é a inclinação (L/L) da linha de energia total e é considerada igual à inclinação do leito no caso de movimento permanente e uniforme e g é a aceleração devido à gravidade (L/T^2).

Em geral, a previsão da resistência ao fluxo para um contorno sólido rígido (fundo fixo) é feita assumindo um leito plano e apenas o cisalhamento junto à superfície do leito. As formas do leito são simuladas por uma altura de rugosidade selecionada, chamada de rugosidade de areia equivalente (k_s) (SIMONS e SENTURK, 1992). O k_s representa a rugosidade hidráulica do leito, tanto devido ao tamanho do grão quanto à forma como ele se dispõe ao movimentar-se.

Em canais com leitos aluviais (fundo móvel) são encontrados dois tipos de resistência: a resistência de forma (*form roughness*) e a resistência devido ao

cisalhamento na superfície (*surface roughness*). A resistência de forma está relacionada às deformações de fundo, que causam variações de pressão no escoamento, gerando variações locais na velocidade. Para uma compreensão completa da resistência ao fluxo em fundos móveis, é importante considerar também a resistência ao cisalhamento na superfície, a qual está relacionada ao cisalhamento atuante sobre a superfície do sedimento exposta ao fluxo.

A avaliação da resistência, portanto, é bastante complexa. Nesse sentido, várias abordagens foram desenvolvidas para a quantificação da resistência ao fluxo em leitos. A maioria das abordagens utiliza a seguinte forma:

$$\sqrt{\frac{8}{f}} = a + \frac{1}{\kappa}\ln\frac{h}{k_s} \tag{2}$$

onde f é o fator de perda de Darcy-Weisbach, κ é a constante de von Karman, h é a profundidade média, k_s é a rugosidade do leito e a é uma constante. Como o fator de perda de Darcy-Weisbach é um parâmetro adimensional, muitos pesquisadores derivaram equações para esse fator de perda (f), como por exemplo, Ferguson (2007) e Rickenmann e Recking (2011) que estudaram rios de leito de cascalho.

Strickler (1923) desenvolveu pela primeira vez a relação de lei de potência com a submersão relativa do fluxo. Então, em um dos trabalhos mais pioneiros ao considerar a lei da parede, Keulegan (1938) integrou o perfil de velocidade média (U) de Prandtl-Von-Karman-Nikuradse para desenvolver a equação de resistência ao fluxo da forma (Equação 3)

$$\sqrt{\frac{8}{f}} = \frac{U}{u_*} = 6{,}25 + \frac{1}{k}\ln\frac{h}{k_s} \tag{3}$$

onde k = 0,4 é o coeficiente de von-Karman, k_s é a rugosidade do leito, que Keulegan propôs ser equivalente ao tamanho médio do sedimento (D_{50}), e u_* é a velocidade de cisalhamento dada por (Equação 4)

$$u_* = \sqrt{gRI} \tag{4}$$

Desde então, os pesquisadores desenvolveram várias equações variando a lei adotada para expressar o perfil de velocidades, como por exemplo lei de potência, lei logarítmica e a equação de potência variável. No entanto, neste trabalho, escolhemos as oito equações a seguir com base em sua ampla aplicabilidade, estrutura simples e

trabalhos anteriores para a estimativa da resistência do fluxo em termos de $\sqrt{8/f}$ usando os parâmetros medidos durante os ensaios realizados (Tabela 2-1).

Tabela 2-1 - Equações utilizadas para cálculo da resistência ao fluxo

Referência	Equação	Nº da equação
Strickler (1923)	$\sqrt{\frac{8}{f}} = \frac{u}{u_*} = 8{,}3\left(\frac{h}{D_{90}}\right)^{\frac{1}{6}}$	(5)
Keulegan (1938)	$\sqrt{\frac{8}{f}} = \frac{u}{u_*} = 6{,}25 + 5{,}75\log\frac{h}{D_{50}}$	(6)
Hey (1979)	$\sqrt{\frac{8}{f}} = \frac{u}{u_*} = 6{,}25 + 5{,}75\log\left(\frac{h}{3{,}5D_{84}}\right)$	(7)
Smart e Jaggi (1983)	$\sqrt{\frac{8}{f}} = \frac{u}{u_*} = 5{,}75\left[1 - e^{\left(-0{,}05\frac{h}{D_{50}}\frac{1}{\sqrt{I}}\right)}\right]^{0{,}5}\log\left(8{,}2\frac{h}{D_{90}}\right)$	(8)
Bathurst (1985)	$\sqrt{\frac{8}{f}} = \frac{u}{u_*} = 4 + 5{,}62\log\frac{h}{D_{84}}$	(10)
Aberle e Smart (2003)	$\sqrt{\frac{8}{f}} = \frac{u}{u_*} = 3{,}86\ln\frac{h}{\sigma z} - 1{,}19$	(11)
Aberle e Smart (2003)	$\sqrt{\frac{8}{f}} = \frac{u}{u_*} = 0{,}91\frac{h}{\sigma z}$	(12)
Ferguson (2007)	$\sqrt{\frac{8}{f}} = \frac{u}{u_*} = \frac{(6{,}5 * 2{,}5)\left(\frac{h}{D_{84}}\right)}{\sqrt{6{,}5^2 + 2{,}5^2\left(\frac{h}{D_{84}}\right)^{\frac{5}{3}}}}$	(13)
Recking et al., (2008)	$\sqrt{\frac{8}{f}} = \frac{u}{u_*} = -1 + 9{,}5\log\frac{h}{D_{84}}$	(14)
Rickenmann e Recking (2011)	$\sqrt{\frac{8}{f}} = \frac{u}{u_*} = \frac{4{,}416\left(\frac{h}{D_{84}}\right)^{1{,}904}}{\left(1 + \left(\frac{h}{1{,}283D_{84}}\right)^{1{,}618}\right)^{1{,}083}}$	(15)

* f: fator de perda de carga de Darcy-Weisbach; u: velocidade; u_*: velocidade de cisalhamento; h: altura da lâmina d'água; D_x: diâmetro do grão correspondente a porcentagem acumulada de x%; σ_z refere-se ao desvio padrão das elevações do leito.

A equação de Keulegan, a equação de Smart e Jaggi (SMART E JAGGI, 1983) e a equação de Recking (RECKING *et al.*, 2008) foram desenvolvidas com base na investigação de canais experimentais em laboratório. Por outro lado, a equação de Manning Strickler (STRICKLER, 1923), a equação de Hey (HEY, 1979), a equação de Bathurst (BATHURST, 1985) e a equação de Rickenmann e Recking (RICKENMANN e RECKING, 2011) foram derivadas usando dados de campo. A equação de Ferguson (FERGUSON, 2007) foi derivada teoricamente pela combinação das equações de fluxo raso e profundo e é conhecida como uma equação de potência variável (EPV). Essa equação fornece uma única equação de resistência aplicável tanto a fluxos rasos quanto profundos em leitos de rio com partículas grosseiras. Ela quantifica o conceito de que as principais fontes de resistência se alteram à medida que o fluxo se torna mais raso e evita impor uma lei de resistência logarítmica a circunstâncias em que os perfis de velocidade não são logarítmicos.

A equação de Keulegan (1938) foi derivada para leitos de areia, enquanto Hey (1979), Smart e Jaggi (1983), Bathurst (1985), Ferguson (2007), Recking et al. (2008), Rickenmann e Recking (2011) foram derivadas principalmente para rios de leito de cascalho. As equações de Recking et al. (2008) e Smart e Jaggi (1983) foram deduzidos considerando os efeitos do transporte de sedimentos também em encostas íngremes.

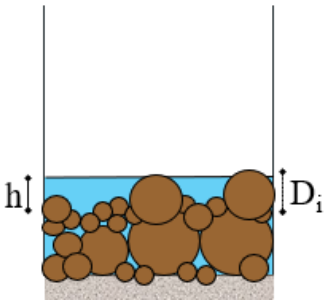
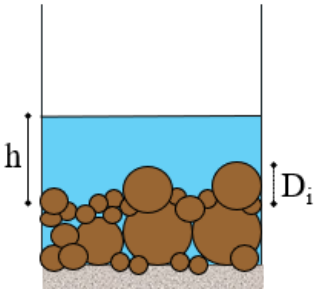
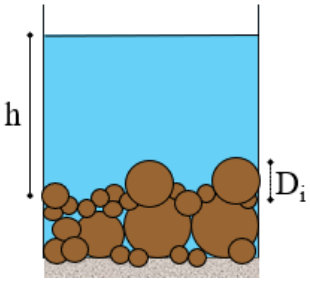
Aberle e Smart (2003) também utilizaram canais de laboratório utilizando material caracterizado por $D < 64$ mm. Esses autores introduziram o desvio padrão das elevações do leito (σ_z) como medida de rugosidade hidráulica. Este parâmetro pode ser facilmente derivado se perfis longitudinais escaneados com alta resolução estiverem disponíveis. O desvio padrão σ_z representa melhor os efeitos de rugosidade causados por formas de leito, como degraus e piscinas, em comparação com um diâmetro de grão característico D_i (CHEN *et al.*, 2020). Aberle e Smart (2003) propuseram ainda uma versão para expressar a resistência através de abordagem linear (Equação 12), que teve um desempenho semelhante em comparação com a abordagem logarítmica (Equação 11).

2.3.3 Submergência relativa

Um fator chave para o entendimento da resistência hidráulica e os padrões de deposição de sedimentos é a submersão relativa, que é a razão entre a profundidade média do fluxo na seção (h) e o tamanho característico de grão (D) (COOPER *et al.*, 2013; PAPANICOLAOU, TSAKIRIS e KRAMER, 2010). Conforme destacado, a submersão

relativa dos grãos no canal está presente em praticamente todas as equações de resistência ao fluxo. Bathurst *et al* (1985) categorizaram os mecanismos de resistência ao fluxo definindo diferentes escalas de rugosidade com base na taxa de submersão relativa (h/D_i) do fluxo, conforme apresentado na Tabela 2-2.

Tabela 2-2 - Submersão relativa do fluxo conforme categorizado por Bathurst (1985).

Escala de rugosidade	**Escala de submergência relativa ($\frac{h}{D_i}$)**	**Taxa de variação**	**Representação Esquemática**
Grande	Pequena	$\frac{h}{D_i} < 1{,}2$	
Intermediária	Intermediária	$1{,}2 < \frac{h}{D_i} < 4$	
Pequena	Grande	$\frac{h}{D_i} > 4$	

Em submersões relativas elevadas, onde $h/D > 4$ a tensão média no leito depende do número de Reynolds e a acumulação de sedimentos tende a ocorrer a jusante de grandes elementos de rugosidade (PAPANICOLAOU; KRAMER, 2006). Em regimes de submersão relativa baixa, a tensão média no leito pode depender do número de Froude e os sedimentos são normalmente depositados a montante de grandes grãos imóveis (THANOS *et al.*, 2011). No entanto, experimentos de laboratório no regime de baixa submersão foram realizados apenas para leitos não erodíveis (PAPANICOLAOU;

KRAMER, 2006; PAPANICOLAOU, TSAKIRIS e KRAMER, 2010) ou leitos sem fornecimento de sedimentos a montante (SHAMLOO; RAJARATNAM; KATOPODIS, 2001). Portanto, a maioria dos experimentos em baixa submersão relativa negligenciam a influência da erosão local e da formação concomitante de formas de leito, o que pode alterar significativamente as linhas de fluxo.

Em particular, sabe-se que as formas de leito e os grandes elementos de rugosidade causam independentemente desvios dos perfis de velocidade comumente assumidos (SHAMLOO; RAJARATNAM; KATOPODIS, 2001; THANOS *et al.*, 2011; TSAKIRIS *et al.*, 2014). Perfis de velocidade localizados próximo do leito - dentro da camada de rugosidade - foram assumidos como lineares (NIKORA *et al.*, 2001b), quase constantes (RECKING, 2009) ou quadráticos (LAMB; DIETRICH; VENDITTI, 2008b) e são usados para determinar as tensões de cisalhamento no contorno sólido, que são posteriormente utilizados em cálculos de transporte de sedimentos. Os testes dessas equações de perfil de velocidade foram limitados a geometrias de leito relativamente simples que podem não ser representativas de muitos riachos de montanha, que incluem formas de leito e grandes elementos imóveis. Muitas vezes é assumido que a tensão de cisalhamento média na seção é uma função direta da profundidade do fluxo e da inclinação do canal (I_c). Esses cálculos são baseados na suposição de fluxo uniforme, que pode ser violada pelas acelerações convectivas presentes ao redor de grãos imóveis. Nos rios de montanha, o fluxo é notadamente variado o que pode levar a incertezas associadas as suas estimativas.

2.4 Transporte de sedimentos

2.4.1 Condições iniciais

O transporte de sedimento de fundo diz respeito aos sedimentos mais grossos que são mobilizados ao longo do leito do canal por rolamento, deslizamento e/ou saltação. Conforme destacado anteriormente, em rios de leito de cascalho, a análise e quantificação do transporte de sedimentos de fundo é de fundamental importância para muitas aplicações. Além disso, os volumes de carga de fundo representam a principal fonte de preocupação, mais do que os volumes de água de inundação (LENZI; MAO; COMITI, 2004) na questão de desastres naturais. Assim, uma avaliação precisa do transporte de sedimentos é necessária para o mapeamento e gestão do risco.

Ainda, do ponto de vista ecológico, em muitas regiões montanhosas, os habitats de desova de espécies de peixes são fortemente afetados pelo transporte de sedimentos de fundo (VÁZQUEZ-TARRÍO; MENÉNDEZ-DUARTE, 2014). Nessas regiões, pode ocorrer a pavimentação do leito (*armouring*) devido à alta heterogeneidade nas estruturas do leito que faz com que as partículas menores sejam mais difíceis de serem mobilizadas do que se estivessem em um leito com material de tamanho uniforme, enquanto as partículas de tamanhos maiores podem ser mais facilmente mobilizadas (BATHURST, 2013).

Desenvolver uma compreensão do transporte do material do leito em rios tem sido um importante foco de pesquisa para geomorfólogos e engenheiros. Talvez um dos mais influentes trabalhos tenha sido o realizado por Shields (1936), que desenvolveu um modelo para arrastamento de partículas usando sedimento unimodal de tamanho *D*

$$\tau_c = \theta_c(\gamma_s - \gamma)D \tag{16}$$

Esta equação prevê a tensão de cisalhamento mínima (τ_c) necessária para arrastar uma partícula de tamanho *D* em função de seu peso unitário submerso (γ_s) e uma constante (θ_c) determinada empiricamente, que varia entre 0,03 e 0,06 para *D* maior que cerca de 3 mm.

Muitos outros modelos de transporte de sedimentos de fundo em rios foram desenvolvidos - uma revisão detalhada é apresentada em (GOMEZ, 1991). No entanto, o trabalho de Shields (1936) e Meyer-Peter e Muller (1948) se destacam e foram fundamentais para o desenvolvimento inicial da teoria do transporte de sedimentos para fluxos de leito de cascalho. Com base nesses trabalhos, levou-se à adoção do tamanho de grão mediano da superfície do leito (D_{50}) como o tamanho de grão característico mais apropriado, pois é a camada mais superficial com o qual o fluxo interage (Parker, 1990).

Inicialmente, Parker et al. (1982b) desenvolveram um modelo de transporte de sedimentos usando D_{50} e assumiram que a textura da superfície do leito se ajusta de modo que todos os tamanhos de grão sejam arrastados quase com a mesma tensão de cisalhamento. Essa ideia é chamada de hipótese de mobilidade igual (PARKER *et al.*, 1982). Nesse caso, D_{50} tem sido usado quase exclusivamente como o tamanho de grão característico em todos os tipos de estudos de transporte de sedimentos, por exemplo, Montgomery; Buffington, (1997); Scheingross et al., (2013); Wilcock; Asce; Crowe, (2003).

De acordo com Southard (2006), a igual mobilidade dos sedimentos diz que a razão da taxa de transporte de uma determinada fração granulométrica é a mesma para todas as frações de tamanho dos grãos. Porém, partículas maiores são mais difíceis de mover porque são mais pesadas (Figura 2-2a), isso significa que é mais difícil para um fluxo transportar as frações mais grosseiras do que as frações mais finas.

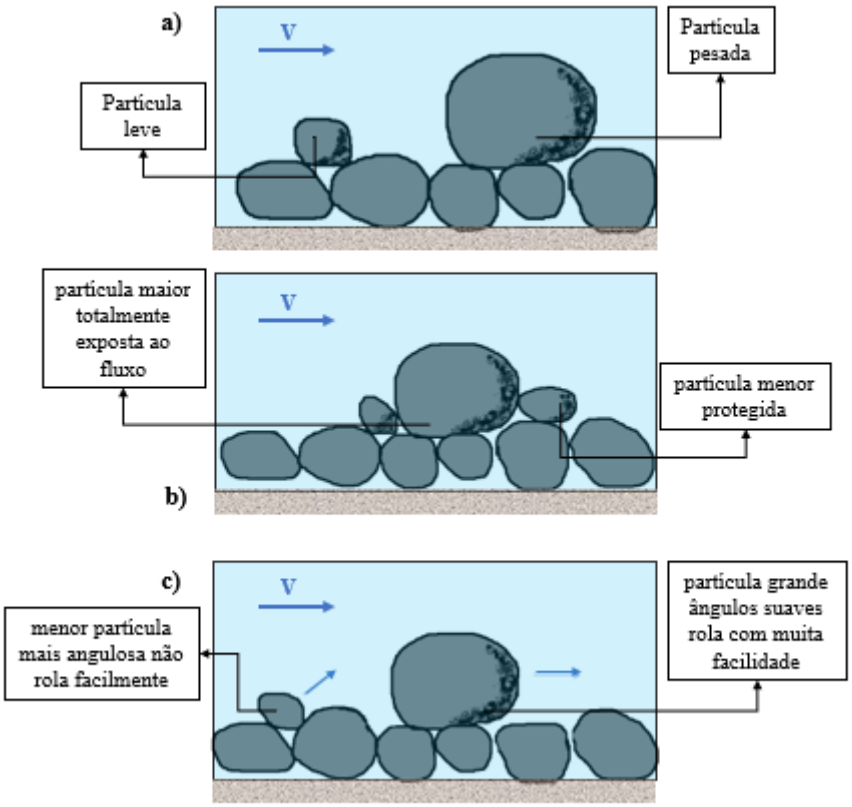


Figura 2-2 - Mobilidade dos sedimentos: a) o efeito do peso da partícula; b) o efeito de ocultação; c) o efeito de rolamento. Fonte: Adaptado de Southard (2006).

No entanto, dois importantes efeitos tendem a compensar o peso da partícula: (1) o efeito de ocultação: em que partículas maiores são mais expostas ao fluxo e, portanto, exercem sobre elas uma força de fluido maior, sendo que partículas menores tendem a ser protegidas das forças do fluxo pelas partículas maiores (Figura 2-2b); e (2) o efeito de rolamento: em que partículas maiores, se tiverem ângulos suaves, podem rolar facilmente sobre um leito de partículas menores, mas partículas menores não podem rolar facilmente sobre um leito de partículas maiores pois podem ficar presas entre as maiores, principalmente se foram angulosas (Figura 2-2c). A importância relativa do efeito do peso da partícula e a combinação do efeito de ocultação e o efeito de rolamento é um elemento

essencial no transporte de sedimentos de tamanho misto (SOUTHARD, 2006). Nesse sentido, é importante considerar diferentes frações de sedimentos no leito do canal.

2.4.2 Leito de granulometria não uniforme

Atualmente, os modelos de transporte de sedimentos de fundo mais comumente usados calculam as taxas de transporte individuais para cada fração de tamanho dos grãos em uma distribuição (e. g. BRENNA; SURIAN; MAO, 2020; MAO et al., 2017, 2020; RAINATO; MAO; PICCO, 2018). Esses modelos levam em consideração o efeito do tamanho de grão relativo no arrastamento de partículas:

$$\tau_{ri} = \tau_{r50} \left(\frac{D_i}{D_{50}} \right)^b \tag{17}$$

Nessa equação, o conceito de tensão de cisalhamento limite é substituído por uma tensão de cisalhamento de referência (τ_{ri}), seguindo Parker (1990). O expoente b descreve o grau em que o tamanho de grão relativo ($D_i = D_{50}$) afeta o arrastamento, sendo a mobilidade associada com $b = 0$ e transporte puramente seletivo de tamanho associado com $b = 1$. Wilcock e Crowe (2003) concluíram que o arrastamento de partículas não é bem descrito por uma lei de potência simples, e eles mostraram que b se aproxima de um expoente de 0,12 para $D_i << D_{50}$ e de um expoente de 0,67 para $D_i >> D_{50}$.

Para sedimentos heterogêneos, vários modelos para o transporte de sedimentos foram desenvolvidos empírica ou semiempiricamente (WILCOCK; ASCE; CROWE, 2003; EINSTEIN, 1950; EGIAZAROFF, 1965; ASHIDA E MICHIUE, 1973). Esses modelos geralmente consideram um "fator de ocultação", ou seja, a relação entre o diâmetro de um grão no limiar do movimento e o diâmetro (mediano) dos grãos circundantes.

De acordo com Komar e Li (1988), Egiazaroff (1965) assumiu que um grão é arrastado quando a velocidade do grão é igual à velocidade de sedimentação em água parada. Então, ele propôs um coeficiente de ocultação, ζ_i, para compensar a tensão de cisalhamento crítica em tal condição:

$$\tau_c = \tau_{r50} . \zeta_j \tag{18}$$

onde τ_c é a tensão de cisalhamento crítica para a mistura; τ_{r50} é a tensão de cisalhamento crítica para D_{50}; e ζ_j é o coeficiente de ocultação.

Então, Egiazaroff (1965) propôs que o coeficiente de ocultação pode ser calculado pela Equação 19:

$$\zeta_j = \left(\frac{\log 19}{\log 19 \frac{D_i}{D_{50}}} \right)^2 \tag{19}$$

No entanto, Ashida e Michiue (1973) modificaram o modelo de Egiazaroff (1965), pois eles observaram que a Equação (19) subestimou a mobilidade de partículas pequenas ($D_i < 0{,}4\ D$) embora tenha funcionado bem para partículas maiores. Então, os autores propuseram uma função condicional, conforme descrito abaixo

$$\zeta_j = \frac{\tau_{cr,i}}{g(\rho_s - \rho_f)D_i} = \left(\frac{0{,}1}{\left(\log \frac{D_i}{D_m}\right)^2} \right) \quad para\ \frac{D_i}{D_m} \geq 0{,}4 \tag{20}$$

$$\zeta_j = 0{,}0519 \frac{D_m}{D_i}\ para\ \frac{D_i}{D_m} < 0{,}4 \tag{21}$$

onde D_i é o diâmetro da fração de tamanho i e D_m é o diâmetro médio de todos os grãos.

Experimentos de laboratório e dados de campo mostram que a mobilidade total de muitas frações de tamanho de grão ocorre, mas que os maiores grãos no leito do canal são quase sempre imóveis ou apenas parcialmente móveis (CHURCH M., 2002a; MONSALVE; YAGER; SCHMEECKLE, 2017), mesmo durante fluxos de formação de canais (HASCHENBURGER; WILCOCK, 2003). Como consequência, a distribuição do tamanho de grão da carga de fundo em rios de leito de cascalho é frequentemente mais fina do que a distribuição na superfície (LISLE, 1995). É somente durante eventos de inundação excepcionalmente grandes que os grãos maiores são totalmente mobilizados e condições de mobilidade iguais para todos os tamanhos de grão do leito do canal são alcançadas (MAO; LENZI, 2007; PELLEGRINI *et al.*, 2021); no entanto, esses eventos são mais incomuns.

Alguns pesquisadores argumentaram que é desnecessário incluir grãos grandes na formulação de modelos de transporte de sedimentos, pois eles constituem apenas para uma pequena parte do total de sedimentos transportados (WILCOCK; KENWORTHY, 2002). Contudo, o que não é considerado, é o papel que esses grãos grandes desempenham na formação da camada superficial grosseira que controla a disponibilidade do material tipicamente mais fino abaixo. Vários estudos destacam que a mobilidade de grãos grandes controla a disponibilidade de material no leito (LENZI; D'AGOSTINO; BILLI, 1999;

MASTELLER; FINNEGAN, 2017), pois agem para prender grãos mais finos móveis que estão abaixo deles, diminuindo sua proporção na carga de fundo (WILCOCK; MCARDELL, 1997). Assim, quando grãos grandes são arrastados, eles não apenas se adicionam ao leito, mas também liberam uma grande quantidade de material mais fino abaixo.

2.4.3 Equações utilizadas em leito de granulometria extensa

As abordagens para estimar o transporte de sedimentos de fundo podem ser baseadas na tensão de cisalhamento do leito (FERNANDEZ LUQUE; VAN BEEK, 1976; RECKING *et al.*, 2008), na descarga de fluxo (RICKENMANN, 1991), na potência do fluxo (PARKER; CLIFFORD; THORNE, 2011) e em funções estocásticas para movimento de sedimentos (PARKER, 1990). Nesse sentido, a maioria das fórmulas de transporte de fundo tem a seguinte forma (RICKENMANN, 1997)

$$q_b = \alpha(X - X_{cr})^{\beta} I^{\gamma} \quad (22)$$

Onde q_bé o transporte de fundo por unidade de largura do canal, que pode ser expresso em unidades diferentes, dependendo da equação, α, β e γ são geralmente constantes empíricas, I é a inclinação do leito, X pode ser a descarga líquida por unidade de largura (q), potência de fluxo por unidade de largura (ω), ou mais geralmente a tensão de cisalhamento adimensional (τ_*), sendo X_{cr} o valor crítico correspondente, no qual o transporte de carga de fundo começa.

O coeficiente α frequentemente depende de alguns diâmetros de tamanho de grão e da massa específica da água (ρ=1000 kgm^{-3}) e do sedimento (ρ_s=2650 kgm^{-3}). O expoente β é frequentemente definido como 1 (RICKENMANN, 1991), mas pode variar entre 2 e 3 (FERNANDEZ LUQUE; VAN BEEK, 1976), e γ foi encontrado variando entre 1,5 e 2 (MEYER-PETER E MÜLLER 1948), mas também pode ser nulo (FERNANDEZ LUQUE; VAN BEEK, 1976). Existem outras formas mais complexas de fórmulas de transporte de sedimentos (SMART E JÄGGI 1983), mas muitas vezes podem ser reduzidas à forma mencionada anteriormente.

As leis de transporte de sedimentos de leito comumente citadas são apresentadas na Tabela 2-3. Embora nenhuma relação tenha obtido aceitação universal, algumas características gerais são aceitas.

Tabela 2-3 – Equações utilizadas para estimativa de transporte de sedimentos de fundo em rios de granulometria extensa

Referência	Equação	Nº da equação	Comentário
Meyer-Peter e Muller (1948)	$q_b = 8(\tau_* - \tau_{cr})^{\frac{3}{2}}$	(23)	Dados experimentais
Wong e Parker (2006)	$q_b = 3{,}97(\tau_* - \tau_{cr})^{\frac{3}{2}}$	(24)	Dados experimentais
Einstein (1950) [1]	$q_b = 12f1(\tau_* - \tau_{cr})^{\frac{3}{2}}$	(25)	Derivação teórica
Bagnold (1973)	$q_b = \frac{V}{\mu\sqrt{RgD}}(\tau_* - \tau_{cr})$	(26)	Derivação teórica
Ashida e Michiue (1973)	$q_b = 17(\tau_* - \tau_{cr})\left(\sqrt{\tau_*} - \sqrt{\tau_{cr}}\right)$	(27)	Derivação teórica e dados experimentais
Fernandez Luque e Van Beck (1976)	$q_b = 5{,}7(\tau_* - \tau_{cr})^{\frac{3}{2}}$	(28)	Dados experimentais
Engelund e Fredsoe (1976)	$q_b = 18{,}74(\tau_* - \tau_{cr})\left(\sqrt{\tau_*} - 0{,}7\sqrt{\tau_{cr}}\right)$	(29)	Derivação teórica
Bridge e Dominic (1984) [2,3]	$q_b = \frac{f3}{f2}(\tau_* - \tau_{cr})\left(\sqrt{\tau_*} - \sqrt{\tau_{cr}}\right)$	(30)	Derivação teórica e dados experimentais
Rickenmann (2001)	$q_b = 1{,}5(q - q_c)\ \ I^{1,5}$	(31)	Dados experimentais

1: $f1$é um parâmetro de ajuste; 2: $f2$ é um coeficiente de perda (fricção); 3: $f3$ é um parâmetro de ajuste. q_b:transporte sólido de fundo por unidade de largura do canal; τ_*: tensão de cisalhamento adimensional; τ_{cr}: tensão de cisalhamento crítica adimensional; μ: fator de fricção relacionado à viscosidade do fluido; R: raio hidráulico; g: aceleração da gravidade; D: diâmetro característico do sedimento; q: vazão líquida por unidade de largura; q_c: vazão crítica por unidade de largura, correspondente ao início do movimento dos sedimentos

Um número considerável de estudos científicos tem investigado o transporte de carga de fundo (sedimentos móveis no leito), e a maioria das teorias atuais tem suas raízes na literatura produzida durante a primeira parte do século XX. Uma das primeiras fórmulas de transporte de carga de fundo foi proposta por Du Boys (1879), que descreveu o transporte de carga de fundo como a progressão de camadas de grãos deslizantes. Sua teoria afirma que a taxa de transporte de carga de fundo depende da tensão de cisalhamento do fluido aplicada ao leito, que excede a tensão de cisalhamento crítica necessária para iniciar o movimento das partículas. Muitas equações de transporte de carga de fundo surgiram a partir de refinamentos desse conceito inicial, sendo a mais notória, talvez, a proposta por Meyer-Peter e Müller (1948). No entanto, um grande desafio dessa abordagem é a determinação da tensão de cisalhamento crítica, o que motivou alguns autores a usar critérios alternativos de início de movimento relacionados, por exemplo, à velocidade do fluxo.

As diferentes teorias destacadas anteriormente fornecem uma visão geral de alguns dos diversos processos físicos envolvidos no transporte de carga de fundo e ilustram sua complexidade (CHURCH M., 2002b). Uma revisão detalhada das equações citadas e dos conceitos a que se referem pode ser encontrada na vasta literatura dedicada a esse assunto (ANCEY, 2020; GOMEZ, 1991).

Apesar dos consideráveis esforços feitos para melhor prever o transporte de carga de fundo, as equações disponíveis muitas vezes superestimam as taxas de transporte de carga de fundo e seu desempenho parece aceitável apenas sob condições de fornecimento ilimitado de sedimentos (COMITI; MAO, 2012). Lenzi, D'Agostino e Billi (1999) estudaram o Rio Cordon, na Itália, e obtiveram previsões razoáveis de taxa de transporte de carga de fundo apenas durante enchentes extremas que mobilizaram todas as classes de tamanho de grãos (estado de mobilidade igual). Schneider *et al.* (2014) destacam que as condições complexas que caracterizam o transporte de sedimentos de fundo, a avaliação do volume mobilizado é frequentemente baseada em equações empíricas. Tais equações são normalmente derivadas de experimentos de canais de laboratório ou de áreas de estudo específicas e, portanto, exibem grandes incertezas (SCHNEIDER *et al.*, 2014).

Dessa forma, quanto mais integradas forem as abordagens empregadas na análise do transporte de sedimentos de fundo, maior será a eficiência e a confiabilidade dos

resultados. A conciliação entre monitoramentos de campo, simulações físicas em modelos reduzidos e modelagem numérica permite compreender os processos de forma mais abrangente e fundamentada. Dentro dessas abordagens, o uso combinado de diferentes técnicas, como, por exemplo, comparar modelos digitais de elevação antes e após os ensaios físicos, juntamente com a quantificação de sedimentos transportados a jusante, reduz significativamente os erros e aprimora a interpretação dos resultados experimentais. Assim, haverá maior precisão nas estimativas de transporte e rugosidade, conforme será visto nos capítulos seguintes.

3. ARTIGO I: EXPLORING MORPHOLOGICAL EQUILIBRIUM AND FLOW RESISTANCE IN GRAVEL-BED RIVERS: INSIGHTS FROM CHANNEL-SCALE EXPERIMENTAL ANALYSIS

Apresentação

Este capítulo baseia-se no seguinte artigo publicado na Revista Brasileira de Recursos Hídricos: Menezes, D. D., & Borges, A. L. D. O. (2025). Exploring morphological equilibrium and flow resistance in gravel-bed rivers: insights from channel-scale experimental analysis. RBRH, 30, e2.

O artigo foi publicado em inglês, e, por essa razão, apresenta-se aqui apenas uma síntese em português do tema principal, da metodologia empregada e dos principais resultados obtidos. O estudo teve como objetivo reproduzir, em ambiente controlado de laboratório, os distintos padrões morfológicos observados em canais de rios com leito cascalhoso, buscando compreender o equilíbrio morfológico e os mecanismos associados à resistência ao escoamento.

Para isso, foi utilizado um canal experimental de 10 m de comprimento, 0,56 m de largura e 0,40 m de profundidade, representando a escala reduzida (1:20) de um rio natural. O experimento foi conduzido em duas fases, totalizando 12 ensaios e aproximadamente 27 horas de observação contínua. Na primeira fase, com duração de 15 horas, monitoraram-se de forma detalhada as deformações do leito e o transporte de sedimentos sob diferentes vazões. Na segunda fase, após o ajuste das vazões, foram realizados novos ensaios com o objetivo de avaliar a evolução da rugosidade e sua influência sobre os parâmetros hidráulicos.

As medições envolveram o uso de instrumentos, como perfilador a laser e tubo de Pitot, além de dados de campo para calibração e validação. Os resultados indicaram que o aumento do diâmetro médio do material móvel do leito levou a um acréscimo na resistência ao escoamento, evidenciado pelos parâmetros de rugosidade *n*, fator de perda de carga de Darcy-Weisbach (*f*) e coeficiente de Chézy (*C*). Também se observou a deposição de partículas finas nos espaços intergranulares, bem como o aumento da rugosidade equivalente (k_s) associado à redução da vazão. Esses achados reforçam o papel

da rugosidade de fundo na dinâmica do escoamento e no transporte de sedimentos em canais de leito granular.

De modo geral, o estudo fornece subsídios importantes para a compreensão dos processos físicos que governam o transporte de água e sedimentos e contribui para o aprimoramento de futuros experimentos em modelos físicos reduzidos, voltados à investigação de rios de leito cascalhoso e à calibração de modelos numéricos complementares.

EXPLORING MORPHOLOGICAL EQUILIBRIUM AND FLOW RESISTANCE IN GRAVEL-BED RIVERS: INSIGHTS FROM CHANNEL-SCALE EXPERIMENTAL ANALYSIS

Abstract: Our aim is to recreate the distinct patterns observed in gravel-bed river channels for studies involving physical modeling by designing a morphological configuration and investigating bed resistance. We used a 10x0.56x0.4m experimental channel that scaled-down a natural river at a ratio of 1:20, utilizing sand as the bed material. Employing both field data and measuring instruments such as a laser profiler and pitot tube, we conducted a total of 12 tests spanning 27 hours. In the initial 15-hour phase, we closely monitored deformations and sediment transport under various flow rates. Subsequently, we adjusted the flow rates and proceeded with testing. The results indicated that a larger diameter of the movable bed led to increased flow resistance, evident in parameters like *n, f*, and *C*. Additionally, we observed the deposition of fines within intergrain voids and noted an increase in *ks* with reduced discharge volume, illustrating the influence on flow dynamics and sediment transport. Furthermore, this preliminary study provides valuable insights into the physical processes governing water and sediment transport, which are crucial considerations for future physical simulation studies.

Keywords: Physical modeling; Movable bed; Sediment transport; Bed roughness; Flow resistance.

3.1 INTRODUCTION

3.1.1 Definition of morphological equilibrium conformation

The bed surface of an alluvial river serves as the primary interface between flow rate and available sediment for transport. Therefore, it is a critical component of the river system, exerting influence on flow hydraulics (Hardy et al., 2010; Ferraro et al., 2019), flow resistance (Rickenmann & Recking, 2011), sediment transport rate, and grain size distribution (Wang et al., 2011). Additionally, due to the dynamic interaction among the bed, flow, and transported sediment, the channel bed is free to adjust to changes in discharge (Polvi, 2021; Rachelly et al., 2022) and sediment supply (Dietrich et al., 1989; López et al., 2023). In pursuit of greater stability, the riverbed surface freely adapts to accommodate available sediment, resulting in the formation of a distinct bed architecture (Ferguson, 2007; Nelson & Dubé, 2016).

An example of this can be seen in river restoration projects, which often involve constructing new channels or riverbeds that should take into account the balance between transport capacity and the transported sediment load in order to avoid problems of erosion or deposition. According to Cooper & Tait (2009), this approach may not faithfully replicate the hydraulic and ecological components of a gravel-bed river; instead, the bed should be constructed through sequential cycles of sediment transport and deposition.

Numerous studies have employed ideal gravel bed configurations to isolate the effects of different surface deposit settings (e.g., Schmeeckle et al., 2007; Ferro, 2018; Smith et al., 2023), but few have developed techniques to recreate the bed conditions found in natural gravel-bed rivers. Recent studies combine physical modeling with computational fluid dynamics (CFD) modeling, as exemplified by Kumar & Afzal (2023). These authors aimed to determine erosion at vertical wall encounters under conditions dominated by strong currents, both in combined wave and current scenarios and in current-only scenarios. Their experimental findings demonstrate that the initial phase of erosion development is faster under the combined flow of waves and currents, but the equilibrium erosion depth is greater in current-only conditions.

Bahmanpouri et al. (2021) also conducted a numerical and experimental investigation. In this case, the authors evaluated sediment transport and the morphological evolution of the erodible bed induced by dam-break flows. Experiments were conducted

in a specially designed channel for the dam-break flow process. Based on an initial flat bed, the effect of three different bed compaction rates was evaluated. Experimental data suggested that an increase in the bed compaction rate resulted in a decrease in erosion and sedimentation depth, as well as the sediment transport rate. Additionally, the increase in the bed compaction rate led to an increase in the wave front celerity, reducing the erosion rate and erosion depth.

Conversely, using only physical experiments, Alomari et al. (2018) investigated the effect of a diversion channel on the erosion of the main downstream channel, while Friedl et al. (2018) studied sediment replenishment with artificial gravel deposits as a method to compensate for sediment deficits in rivers and improve their ecological conditions.

These studies share the property of not utilizing a preliminary phase of shaping the movable bed to represent the natural watercourse. In this context, Buffin-Bélanger et al. (2003) and Spiller et al. (2015) devised a molding procedure that accurately replicates the complexity of gravel bed surfaces. Molds were created from a field section of a gravel bed, and replicas were produced from these molds and placed in the channel. While this method generates a surface with the geometric structure of a natural gravel bed, it's important to note that it is impermeable, the bed is static, and it doesn't reproduce subsurface vertical sorting.

In this context, for a better understanding of the water-sediment interaction, physical modeling of a movable bed necessitates a preliminary phase of experiments enabling the creation of a riverbed flume. This flume should exhibit morphological features, sediment distribution, and flow paths that closely resemble its natural conditions (Cooper & Tait, 2009).

3.1.2 Flow resistance in gravel-bed rivers

In mountain rivers, when sediments are at rest or transported with low intensity, the presence of sediment particles on the riverbed surface and their impacts on discharge are considered as the bed resistance of the channel. The resistance characteristics of mountainous rivers, composed of coarse bed material, are quite distinct from those of alluvial rivers with fine bed particles. One of the significant influencing factors is

roughness, which is responsible for providing flow resistance in mountainous rivers (Bathurst, 1985; Maxwell & Papanicolaou, 2001).

In Brazil, there are few studies focused on the understanding of gravel-bed rivers. However, in recent years, the characteristics of some of these rivers have been examined, particularly in the southern region of the country (e.g., Menezes & Kobiyama, 2023; Paixão et al., 2023; Paixão & Kobiyama, 2022; Bartels et al., 2021). Both studies emphasize the occurrence of different bed morphologies and the influence of macro-roughness in these Brazilian rivers.

These studies have a wide range of applications, such as in flood risk assessment. As highlighted by Vázquez-Tarrío et al. (2024), who conducted a thorough review of the scientific literature addressing the implications of sediment transport in flood risk assessment. According to their analysis, most studies on the influence of sediment transport on flood risk have focused on mountain streams due to their high sensitivity to changes in sediment supply. Additionally, the research has concentrated on explaining historical changes in channel conveyance capacity and flood frequency. These changes are typically interpreted in relation to long-term trends in sediment supply. Recent developments in hydrodynamic and morphodynamic numerical models provide opportunities to explicitly incorporate sediment transport into flood risk analysis. However, the review does not address how small-scale physical models can also be useful for this issue, when combined with numerical models and field observations.

In this context, the work by Sturm et al. (2018a, 2018b) highlights, through a reduced-scale physical model (1:30 scale), the influence of sediment transport and deposition on floods in the Austrian Alps and their impact on buildings exposed to this phenomenon. Compared to clear water, sediment transport and deposition significantly influence impact forces due to sediment accumulation near buildings in the alluvial fan (Sturm et al., 2018b).

During floods, increased flow velocity mobilizes sediments from upstream sources, transporting them downstream and leading to sediment deposition in lower-energy environments. On the other hand, floods can also erode and reconfigure existing sediment deposits, altering riverbed morphology and channel geometry. According to the work by Hamidifar et al. (2024), which studied the role of sediment transport in flood

mapping, sediments transported during floods influence channel erosion and deposition patterns, affecting the magnitude and extent of flood events and subsequent sediment transport dynamics. This reciprocal relationship underscores the complex interaction between floods and sediment dynamics, highlighting the need for a comprehensive understanding (Hamidifar et al., 2024).

From this perspective, the interaction between water and sediments in channel experiments can provide detailed insights into the hydro-sedimentological processes responsible for creating a channel geometry that closely resembles a natural river. This occurs because the water in the natural watershed environment, with its distinct velocity and behavior, interacts with the channel bed, inducing flow resistance. This resistance, as measured in physical models, is associated with the size, shape, and gradation of sediment particles, as well as the geometric form and flow magnitude of rivers. To calibrate this relationship, most studies use measured data from a specific river or river section (Recking et al., 2008).

There exists a multitude of formulas due to varying choices of roughness size and data differences. For steep channels with high relative flow submergence, certain researchers (e.g., Aberle & Smart, 2003; Ferguson, 2007) have found that flow resistance correlates with relative submergence and have noted that this correlation follows a logarithmic pattern. However, for channels with lower gradient and extensive bed granulometry, as is the case in this study, this behavior may not be the same. The corresponding hydraulic roughness, as a singular characteristic roughness scale, is frequently determined based on the equivalent grain size of the riverbed.

Although, it is important to highlight that in granular beds composed of a single layer on a flat surface, each bed elevation is directly related to the grain size; therefore, bed roughness can be adequately expressed through particle size. In contrast, in beds with multiple layers, surface particles nestle into cavities formed by the underlying particles. In natural beds, with a mixture of particle sizes, these formed cavities have varying dimensions, and a specific characteristic grain diameter will be less representative of the bed surface protrusions compared to the case of a single-layer bed (Smart et al., 2002).

This becomes more evident when considering that the majority of flow resistance equations were developed for fixed-bed channels. In this regard, predicting flow

resistance and velocity distribution in movable-bed channels is considerably complex. Two reasons can be cited: a) By increasing the bed shear stress beyond a critical value, bed sediments begin to move. Consequently, the shape of the alluvial bed can change. Depending on flow conditions and other influential factors due to sediment particles, this type of bed deformation increases flow resistance compared to rigid-bed channels. This makes it challenging or even impossible to predict flow resistance with a constant ratio; b) Sediments transported both as bedload and suspended load can alter flow characteristics, such as velocity distribution, particularly near the bed where sediment concentration is higher. Therefore, it is necessary to consider sediment transport, variation in bed roughness, and their interaction (Abrahams & Li, 1998).

Until now, significant efforts have been directed towards the first subject, primarily in estimating flow resistance using velocity equations based on power and logarithmic laws. Some researchers also emphasize that the bed shear coefficient, or the Chézy coefficient, should be divided into two parts: particle roughness and bed form resistance.

Furthermore, an important question arises regarding the effect of sediment movement on flow resistance, specifically whether sediment movement as bedload can increase flow resistance compared to clear water or not. This question has given rise to two general viewpoints among researchers. Gao & Abrahams (2004) observed that bedload movement can lead to reductions in near-bed velocity, mean velocity, and an increase in the roughness coefficient, depending on the thickness of the moving sediment layer.

The analysis by Di Stefano et al. (2020) revealed that, for mixtures of large-sized particles, the friction factor can be accurately estimated by disregarding the effect of average concentration of suspended sediments. However, for mixtures of small-sized particles, the friction factor decreases as the average sediment concentration increases. Gladkov et al. (2021) concluded that in simulating sediment transport and calculating channel deformations in rivers, it is convenient to employ Chézy coefficient calculation dependencies to assess the bed sediment mixture's roughness. However, studies involving other flow resistance factors such as the Manning coefficient (n) and the Darcy-Weisbach friction factor (f) have not been evaluated. An analysis encompassing a comprehensive

set of variables could potentially offer a deeper comprehension of processes governing discharge and sediment transport in rivers with extensive granulometry.

In this context, the primary objective of this exploratory study is to develop a morphological configuration that replicates the typical patterns observed in gravel-bed river channels. This effort seeks to provide crucial fundamental insights for analogous investigations in Brazilian river systems. Starting with the disposition of sedimentary material on an inclined plane, we seek to establish a channel that reproduces characteristics of gravel-bed rivers by injecting flow for a specific period until we reach a practically invariable bed geometry, discerned by measuring the sediment transported. Subsequently, taking advantage of this initial condition, our study moves on to explore the bed's resistance characteristics. It is our aspiration that the initial morphological configuration of the riverbed will provide valuable insights into the processes of interaction between the flow and the bed, thus promoting the progression of physical modeling studies for gravel-bed rivers in Brazil.

3.2 MATERIAL AND METHODS

3.2.1 Experimental setup

The experiments were conducted in an experimental channel located in the Fluvial Pavilion of the Density Current Research Center (NECOD), at the Hydraulic Research Institute (IPH) of the Federal University of Rio Grande do Sul (UFRGS). The rectangular cross-section channel has dimensions of 10 m in length, 0.56 m in width, and 0.4 m in height (Figure 3-1). The channel's lateral walls are made of glass, enabling the observation and recording of flow characteristics as well as hydrodynamic data. The liquid supply circuit comprises a triangular weir, a downstream reservoir, and a pump for water recirculation. The channel's inclination is adjustable via a support point where a hydraulic jack is employed.

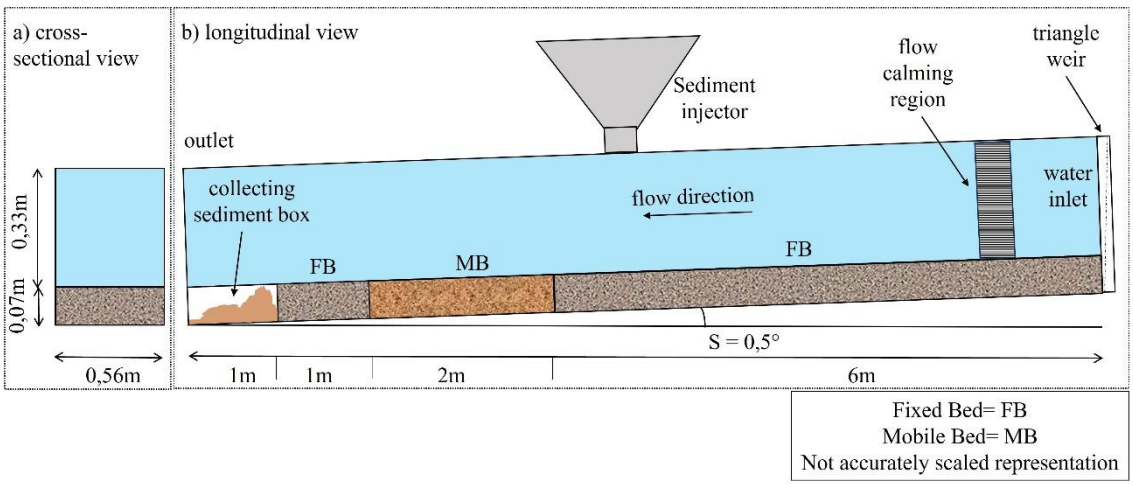


Figure 3-1 - Schematic representation of the experimental channel: a) cross and b) longitudinal view

Adjacent to the water inlet, there is a region of transition and stilling zone on the water surface. Over the subsequent 4.5 meters, a fixed bed (FB) was constructed using sand (D50 = 1.0 mm) to allow for flow development before entering the movable bed (MB) section. The MB region (effective testing area) spans a length of 2 meters for data collection. Subsequently, there is another FB region (1 meter), and finally, the sediment collection box for material transported from the MB (Figure 3-1).

3.2.2 Similarity analysis

Inspiration for selecting the sediment grain composition for the experiments was drawn from the Forqueta River (located in Maquiné/RS). The work by Menezes (2021) provides detailed insights into a stretch of this river, which served as a basis for the development of the physical model. Concerning the characteristics of this river, the mean D50 of the riverbed is 63.8 mm, classified as very coarse gravel. It has an average width of 10 meters and exhibits three distinct morphologies (step-pool, cascade, and plane-bed).

Classic Froude similarity rules for open-channel flow of liquids were applied.

$$Fr = \frac{v}{\sqrt{gh}} \quad (1)$$

The geometric scale factor (r) was established based on the dimensions of the experimental setup to be used (width: 0.56 m)

$$r = \frac{L_{model}}{L_{natural}} \quad (2)$$

$$r^{\frac{3}{2}} = \frac{Q_{model}}{Q_{natural}} \quad (3)$$

$$r^{\frac{1}{2}} = \frac{U_{model}}{U_{natural}} \quad (4)$$

By non-dimensionalizing all involved quantities, it is possible to demonstrate that the scale factor for particle diameters can be taken as equal to the r, provided the model is undistorted and the densities of natural and model sediment are the same. Table 3-1 presents the scaling relationships considering the geometric scale of 1:20. As highlighted, this scale was determined due to the limitation of the experimental channel, which is only 0.56 m wide. Additionally, this scale allows both vertical and horizontal scales to be the same.

Table 3-1 - Scale relationships between the model and the prototype

	S	***L***	D_{50}	Q_{med}	***U***
Model 1:20	0.00937m/m	0.56m	1mm	67L/min	0.22m/s
Prototype	0.00937m/m	11.2m	20mm	$2m^3/s$	1.0m/s

3.2.3 Inlet flow

The injected flow was supplied from a downstream reservoir with a capacity of 2,000 liters. The system operates through flow recirculation. To control and measure the flow rate (Q), a piezometer coupled with a triangular weir (60°) installed at the channel inlet is used to determine the water level on the weir (H). The obtained value of Q is cross-validated with the measured Q at the channel outlet, thus calibrating the weir discharge coefficient.

Subsequently, a rating curve for flow was established. The Excel Solver was employed to adjust the calculated values with the observed measurements, aiming to determine the parameters a and n of Equation 5.

$$Q = aH^n \quad (5)$$

where a and n are dimensionless adjustment parameters of the equation. With the calculated parameters a and n, Equation 6 is derived. Thus, based on the water level

reading on the weir (H in cm), the flow rate (Q in L/min) entering the channel through the weir can be determined.

$$Q = 0.60067H^{2,5} \quad (6)$$

3.2.4 Characterization of the Movable Bed (MB)

Sand (D_{50} = 1.0 mm) was employed as the material for the MB, as shown in Table 3-1. The grain size distribution curve of the utilized material can be observed in Figure 3-2.

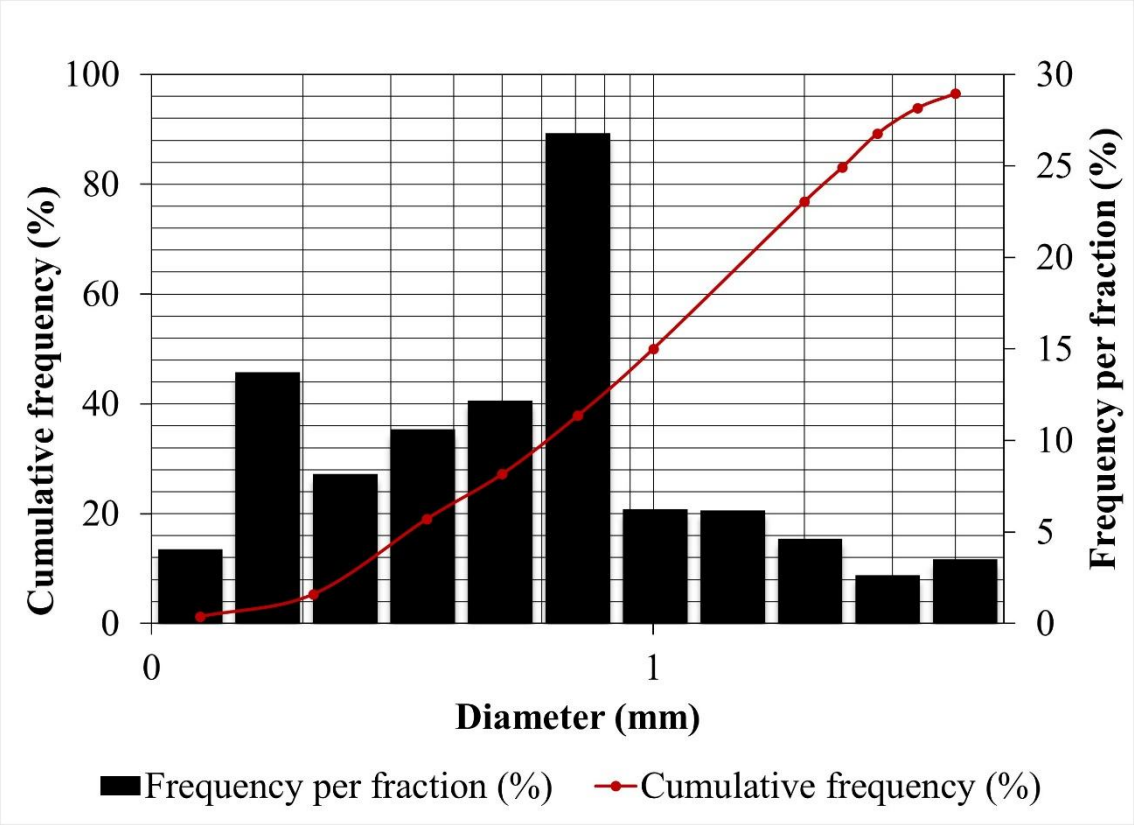


Figure 3-2 - Grain size distribution curve of the material for the channel's movable bed

3.2.5 Measurement of channel bed deformations

A laser profilometer was used to determine deformations in the MB. Thus, at the end of each test, the bed's topography was surveyed, enabling a comparison of bed modifications over time. The laser distance measuring equipment (model MD250 ADV) offers a precision of 0.1 mm and a reading speed of 100 measurements per second. Due to its high accuracy, it is suitable for evaluating distances, dimensions, relative positioning, and comparing elevations. It performs dynamic, point-to-point, and

continuous measurements without physical contact between the device and the target object. Further details are presented in Manica (2009).

This equipment is attached to a coordinate table, which allows highly controlled movement of the profilometer along the channel, ensuring precise scanning of the bed topography. The table's workspace is 0.5 m2, hence two position sheets are used: one for the first meter of the MB and another for the subsequent meter.

In order to analyze the texture of the profile generated by the data, a factor reflecting the surface roughness will be calculated, incorporating grain size and bed shape. This factor will be termed the transverse section bed elevation Oscillation Factor (FO), inspired by the factor described in Bogatin et al. (2013). The calculation is performed by dividing the length of the laser-generated surface (Ll) in a predetermined section by the width of the channel (L).

$$FO = \frac{L_l}{L} \tag{7}$$

3.2.6 Collector box for transported material

At the end of the experimental channel, a collector box is situated to collect the sediments transported in each test. The material is gathered, dried in a 105 °C oven, and subjected to granulometric analysis to determine characteristic diameters (D10, D16, D50, D84, and D90).

3.2.7 Measurement of velocities and water level

For velocity measurements, a Pitot tube coupled with an inclined piezometer (30°) was employed, as illustrated in Figure 3-3. Velocity was calculated using Equation 8.

$$U = \sqrt{2g\Delta h \sin \alpha} \tag{8}$$

where U is the flow velocity (m/s), g is the gravitational acceleration (9.81 m/s2), Δh is the difference between the dynamic and static heights of the piezometer, and α is the angle of the piezometer, in this case, 30°.



Figure 3-3 - (a) Pitot tube coupled with piezometer; (b) Measurement setup, (c) Pitot tube

Instantaneous velocities were measured at two cross-sections (sections 40 and 60 cm), and velocity profiles were captured at two other sections (sections 120 and 160 cm). Both types of measurements were taken along three verticals of each section (located at 15, 30, and 45 cm from the right channel wall) (Figure 3-4). Water depths across the cross-sections were also recorded during velocity measurements.

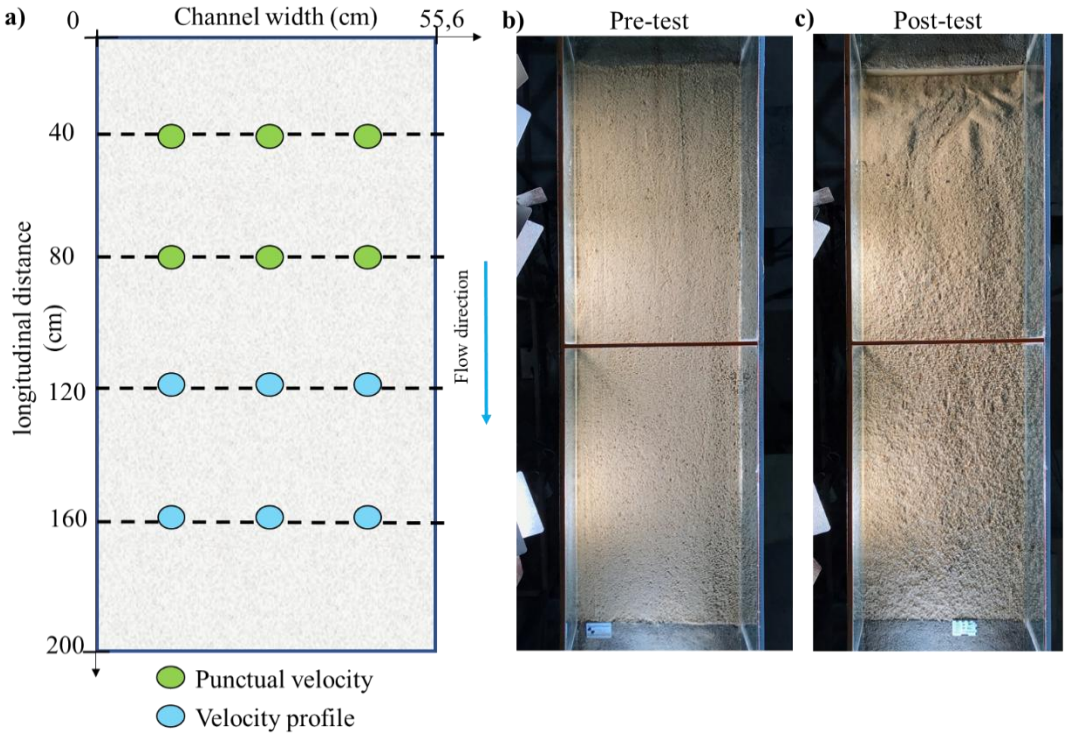


Figure 3-4 - Movable bed channel: (a) schematic showing evaluated cross-sections and respective velocity measurement points; (b) pre-test photos (inclined and ruled plane) and post-test photos (change in texture and creation of preferential pathways).

3.2.8 Treatment of velocity profiles

After measuring the velocity profiles, bed roughness coefficients and hydraulic resistance parameters were estimated. The velocity profile was adjusted considering a turbulent velocity distribution profile, as proposed by Prandtl (1926) prioritizing the velocities measured near the bottom.

$$\frac{u}{u*} = \frac{1}{\kappa} \ln y + c \tag{9}$$

where u is the velocity at a certain distance from the bottom (y), u∗ is the shear velocity, κ is the Von Karman constant, and c is a constant determined when y is equal to y0, corresponding to a specific distance from the bottom where the action of the viscous sublayer occurs. The constant y0 can be defined, in rough beds, as ks, which corresponds to a height where interaction between water and the channel bed takes place due to bed roughness.

$$\frac{u}{u*} = \frac{1}{\kappa} \ln \frac{y}{y_0} \tag{10}$$

Or, when rewritten following algebraic handling,

$$\frac{u}{u*} = 5{,}75 \log \frac{y}{k_s} + B \tag{11}$$

where B equals 8.5 for rough beds, as per Einstein (1950).

Einstein (1950) proposed a more comprehensive expression for the velocity profile in turbulent flow, incorporating a correction factor that varies depending on the flow regime being smooth, transitional, or rough (Figure 5).

$$\frac{U}{u*} = 5{,}75 \log\left(12{,}27 \frac{y}{k_s} x\right) \tag{12}$$

where x is a correction factor given by Figure 3-5 as a function of ks/δ, where δ is the thickness of the laminar sublayer.

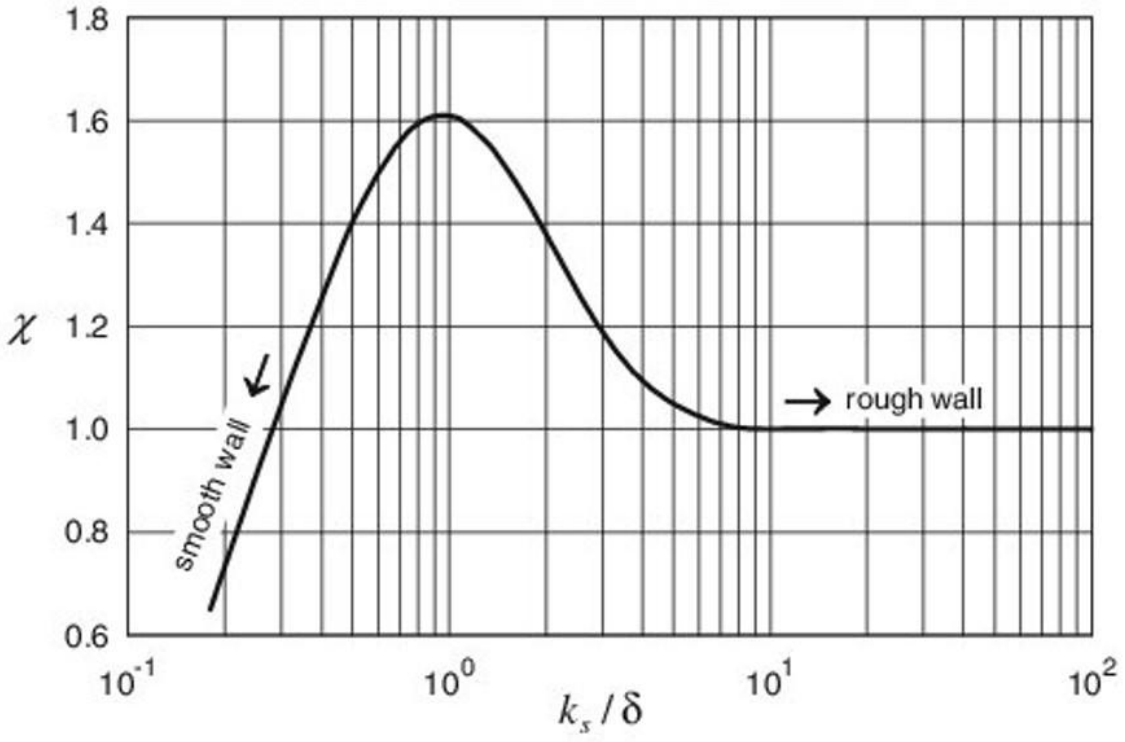


Figure 3-5 - Correction term (*x*) in the formula proposed by Einstein (1950)

The measured velocity profiles were fitted to the theoretical velocity profile, enabling the determination of the shear velocity at the location (u*), the roughness coefficient ks, through which the shear stress was estimated. Table 3-2 presents the equations utilized for the calculation of each parameter.

Table 3-2 - Equations used for the calculated variables

Variable	Equation	Equation number
$u*$	-	
k_s	-	
τ	$\tau = \rho u*^2$	(13)
δ	$\delta = 11.6\frac{\nu}{u*}$	(14)
k_s/δ	-	
h	-	
U	-	(15)
Fr	$Fr = \frac{V}{\sqrt{gh}}$	(16)
Re	$Re = \frac{Uh}{\nu}$	(17)
$Re*$	$Re* = \frac{u*d}{\nu}$	(18)
f	$\frac{U}{u*} = \sqrt{\frac{8}{f}}$	(19)
C	$\frac{V}{u*} = \frac{C}{\sqrt{g}}$	(20)
n	$\frac{V}{u*} = \frac{R^{\frac{1}{6}}}{n\sqrt{g}}$	(21)
I	$I = \frac{\tau}{\Upsilon h}$	(22)

3.2.9 Experimental design

The experiments were divided into two phases:

Phase 1: In this phase, the objective was to find a morphological bed configuration that exhibits equilibrium. This means that changes to the bed at a given flow rate do not result in variations in sediment transport. Thus, for a given liquid flow injected into the channel, a bed configuration was generated in which no variation occurred. This equilibrium condition was identified through the quantification of transported sediment.

This state was considered to be similar to the behavior of a natural river, indicating that the deformable medium had acquired a configuration compatible with the flow.

During this stage, 6 tests were conducted, each divided into time periods (0, 2, 6, 8, 10, 12, and 15 hours). At the end of each test, the bed topography of the channel was surveyed, and transported sediments were collected.

Phase 2: Evaluation of channel bed roughness. In this phase, the dynamics of water and sediment were evaluated in the presence of a specific channel bed roughness. This roughness was established after achieving phase 1 under a condition without sediment supply upstream of the section. The focus of this phase was on the flow's ability to shape (sculpt) its channel. Six tests were also conducted during this phase with decreasing flow rates, during which velocity profiles were measured as described in the velocity measurement section. At the end of each test (E1: 17h, E2: 19h, E3: 21h, E4: 23h, E5: 25h, and E6: 27 hours), the bed topography of the channel was surveyed, and transported sediments were collected. The Surfer software was used for visualization of the data obtained by the profiler.

The bed granulometry was determined after each test based on the percentage difference between the initial granulometric curve and the granulometric curve of the collected transported sediments. Thus, the relative submergence ratios were determined, and the hydraulic resistance parameters of the flow were calculated.

3.3 RESULTS AND DISCUSSION

In the first part, we will present the results obtained from the initial tests aimed at developing a channel bed that recreates the behavior and characteristics of a natural river. This bed configuration resulted from the balance between transported sediment and bed alterations.

Subsequently, we will present the analyses carried out on a previously worked bed. In this bed, the velocity profiles were examined at different Q values, all of them lower than the Q that generated the initial configuration of this channel. The focus will be on flow resistance parameters and related variables.

3.3.1 Evaluation of bed morphological configuration

3.3.1.1 Evaluation of flow and transported sediment

The total time for stabilization of the channel bed was 15 hours. Initially, the experiment began with a near-maximum Q of approximately 250 L/min. During this period, it was observed that the quantity of transported sediment stabilized at a constant value (~2 g/min) (Figure 3-6). Subsequently, the Q was increased to 318 L/min, which corresponds to a return period (TR) of 2 years in the prototype (Table 3-3). This Q was maintained for 5 hours until the exhaustion of sediment that was susceptible to transport in the channel. As time passed, transport reduced, indicating sediment deposition and immobilization in the channel.

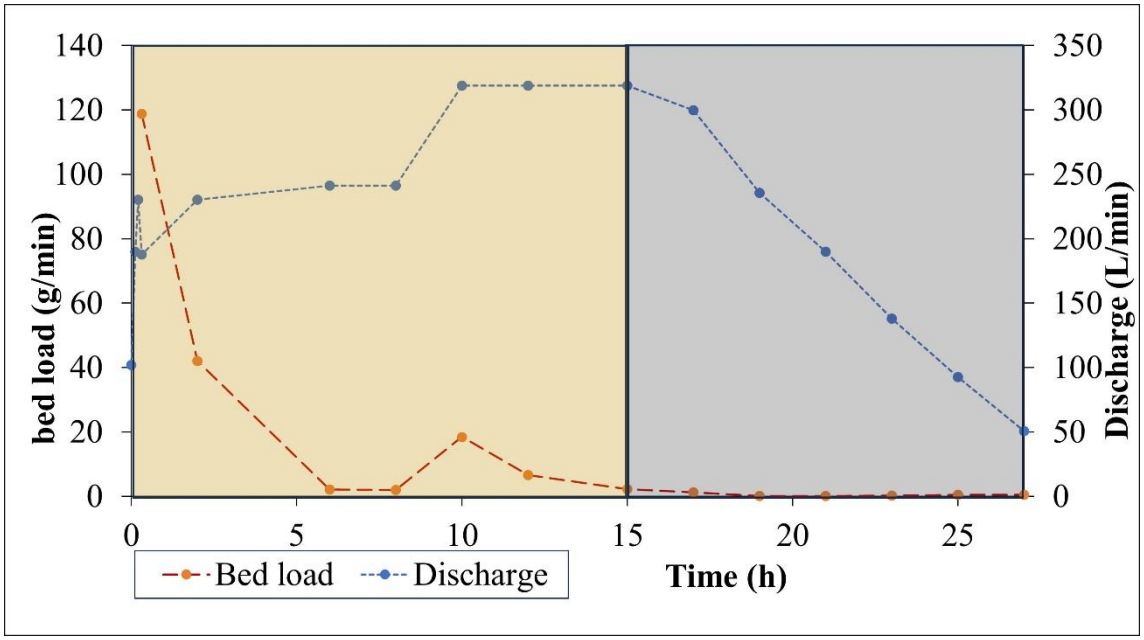


Figure 3-6 - Flow and transported sediment until stabilization of the mobile bed channel

Table 3-3 - Flow and transported sediment rates before bed stabilization

Time (h)	Flow rate (L/min)	Amount of transported sediment (g)	Cumulative amount of transported sediment (g)	Bed load (g/min)
0	102.06			
0.12	189.95			
0.2	230.25			
0.32	187.58	2256.1	2256.1	322.3
2	230.25	4245.2	6501.3	42.03
6	241.06	498.9	7000.2	2.08

Time (h)	Flow rate (L/min)	Amount of transported sediment (g)	Cumulative amount of transported sediment (g)	Bed load (g/min)
8	241.06	236.8	7237	1.97
10	318.71	2214.2	9451.2	18.45
12	318.71	792.1	10243.3	6.6
15	318.71	411.7	10655	2.29

Figure 3-6 illustrates the inserted Q in the system and the amount of transported and collected sediments at the end of the channel. It can be observed that when the Q is increased to 318 L/min, there is an increment in the total amount of transported sediments, and thereafter, the values tend to decrease. According to Masteller & Finnegan (2017), who assessed different sediment bed accommodation timescales, at short timescales, sediment transport rates decrease as the bed stabilizes.

Regarding the characteristics of the transported material, the D10, D16, and D50 of this material showed an increase during the initial Q (Figure 3-7), which coincided with the majority of the transported material (Figure 3-6). After 2 hours of testing, the values decreased and remained relatively constant, indicating that only a small fraction of the bed was mobilized by the flow (Kirchner et al., 1990) until the next Q increment.

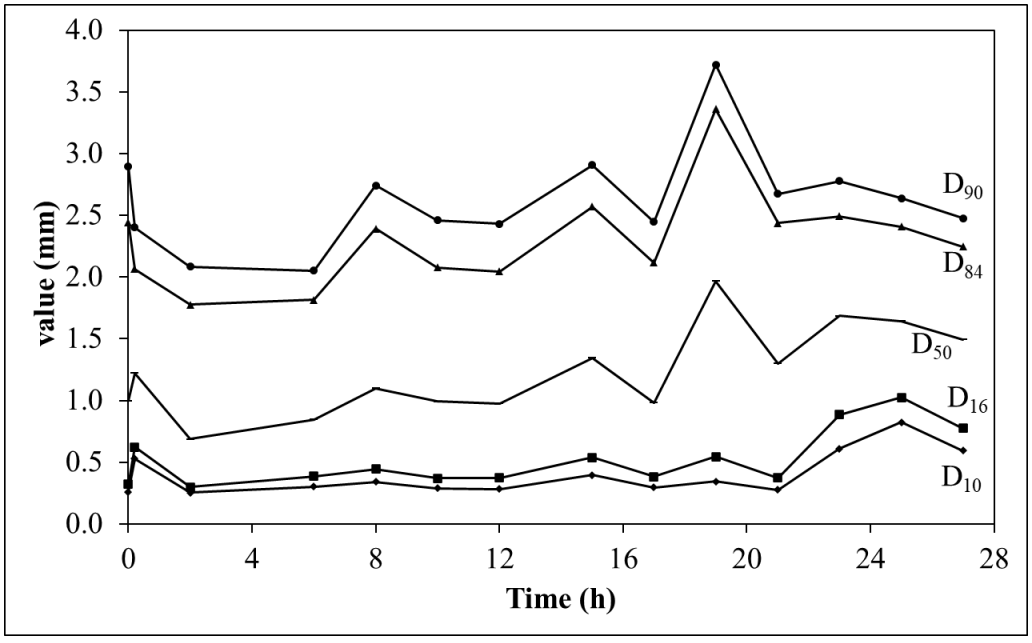


Figure 3-7 - Behavior of transported characteristic diameters throughout the morphological configuration phase

On the other hand, with the increase in Q, the D84 and D90 of the transported material were larger than the other analyzed diameters, as observed in Figure 3-7. Subsequently, both diameters decreased until the 12-hour mark of testing. In the following 3 hours, totaling 15 hours of testing, the sediment diameter values exhibited an increase in their magnitudes, as the finer sediment available had already been transported. Paphitis & Collins (2005) and Haynes & Pender (2007) suggest that, under prior accommodation, the bed is never fully stabilized, and the grains most exposed to flow (protruding grains) are always available for transport.

3.3.1.2 Evaluation of bed modifications

In Surfer software, bed surfaces were generated and evaluated for volume changes before and after each test. The volumes were multiplied by the density of quartz (2.65) and converted into mass (grams), with this difference referred to as calculated reworked sediment. At the 8-hour and 10-hour marks, the balance of reworked sediment material was negative (Table 3). As there was no increase in Q at these times, it is assumed that there might have been a bed material reconfiguration, seeking sediment transport stabilization, since these were among the lowest values observed. However, at the 10-hour mark, there was a Q increment, suggesting sediment mobilization and deposition within 2m of the mobile bed section. This led to the establishment of preferred Q paths and accommodation of finer sediments within voids of the mobile bed, ultimately influencing increased sediment deposition in the channel.

The values of transported sediments collected at the end of each test differed significantly from the reworked sediment values calculated by Surfer, as observed in Table 3-4. This difference could be attributed to the fact that the material became trapped or confined within the mobile bed itself (reworked by flow within the 2m of mobile bed). This difference was more pronounced at the beginning of the test when the surface texture was finer, potentially representing the removal of fines and bed accommodation under the influence of the water column. Additionally, fines might not have been captured by the collection box and could have clouded the water in the tank. In Figure 7, the smallest values for the characteristic diameters of the transported sediment's granulometric curve were recorded after 2 hours of testing.

Table 3-4 - Erosion vs. deposition balance through analysis of surfaces in Surfer

Time (h)	Eroded volume (cm^3)	Deposited volume (cm^3)	Net volume (cm^3)	Calculated reworking sediment (g)	Collected transported sediment (g)	Difference
2	14780.72	0	14780.72	39.17	6.5	32.67
6	891.01	452.98	438.04	1.16	0.5	0.66
8	128.38	992.04	-863.66*	-2.29	0.24	-
10	142.15	2696.97	-2554.82*	-6.77*	2.21	-
12	1073.82	420.65	653.18	1.73	0.79	0.94
15	1211.27	449.27	762.01	2.02	0.41	1.61

Hence, it is presumed that the bed material could be accommodating, compacting, and forming a channel more similar to a natural river, even though limited by the duration of the experiment. Previous experiments with channels have indicated that measurable compaction required several days of execution (Charru et al., 2004). For a deeper understanding of subsurface behavior, Cooper & Tait (2009) suggest quantifying the hydraulic conductivity and porosity of the studied bed.

Figure 3-8 illustrates the bed dynamics throughout the tests. It can be observed that a depression or pool formed at the beginning of the mobile bed (white portion of the bed) due to the interaction between the fixed bed (FB) and the start of the mobile bed (MB). However, if we observe a natural river, this behavior is typical of such rivers (also known as step-pools, as described by Montgomery & Buffington, 1997). The figure also demonstrates the occurrence of preferential flow paths, even though water occupies the entire width of the channel. Close to the 100cm mark, an iron rod is integrated into the channel structure, causing a noticeable discontinuity in the data at this specific location.

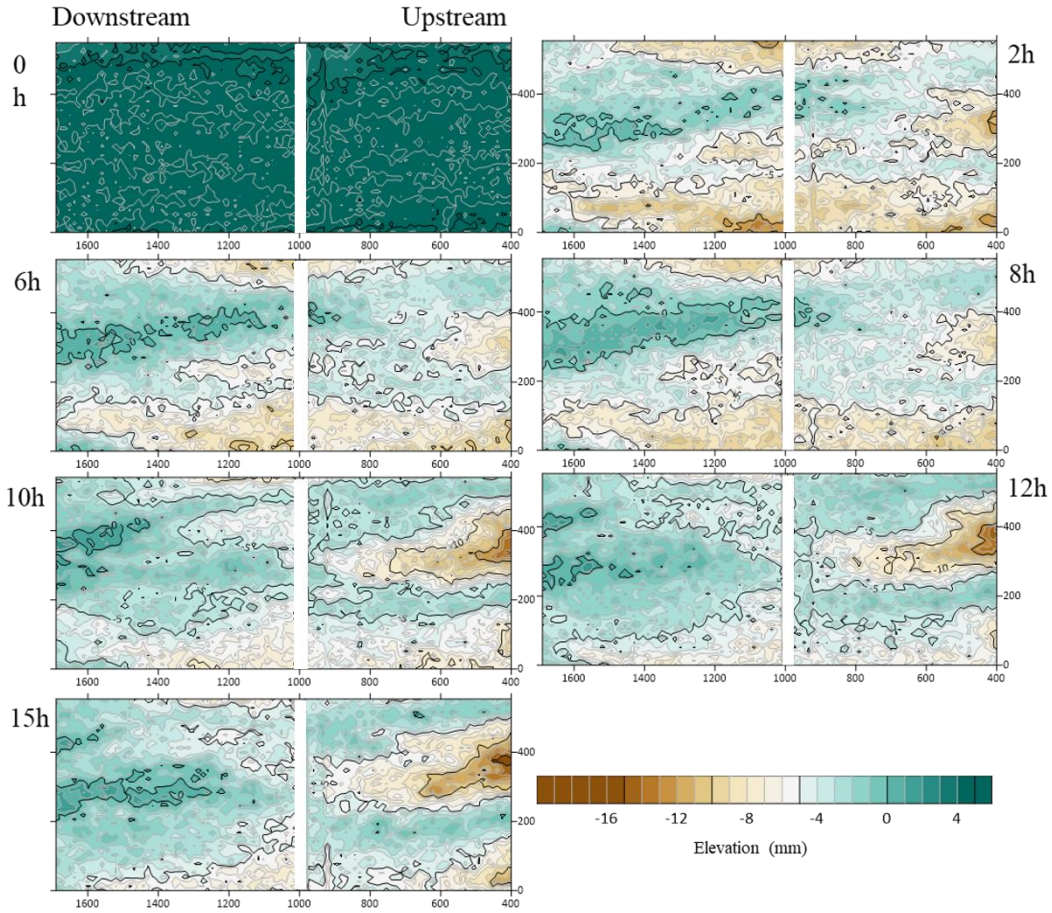


Figure 3-8 - Changes in the channel bed (between 40 and 170 cm of the MB) during the initial bed configuration tests (greener color indicates positive elevation, while browner colour indicates negative elevation)

Note: at a distance of 1000mm there is a structural limitation of the channel for taking profiler readings

Subsequently, three longitudinal profiles were selected, located at 15, 30, and 45 cm from the right channel bank. Figure 3-9 depicts the behavior of these two longitudinal sections throughout the tests. The difference between the profiles highlights significant material removal as soon as flow begins. After this initial accommodation, there is a shift in the average elevation of the sediment bed, where subsequent bed deformations will occur. It is also noticeable that the localized erosion pool generated by the transition between roughness elements remains relatively stable throughout the tests, ceasing to be a sediment source for the channel.

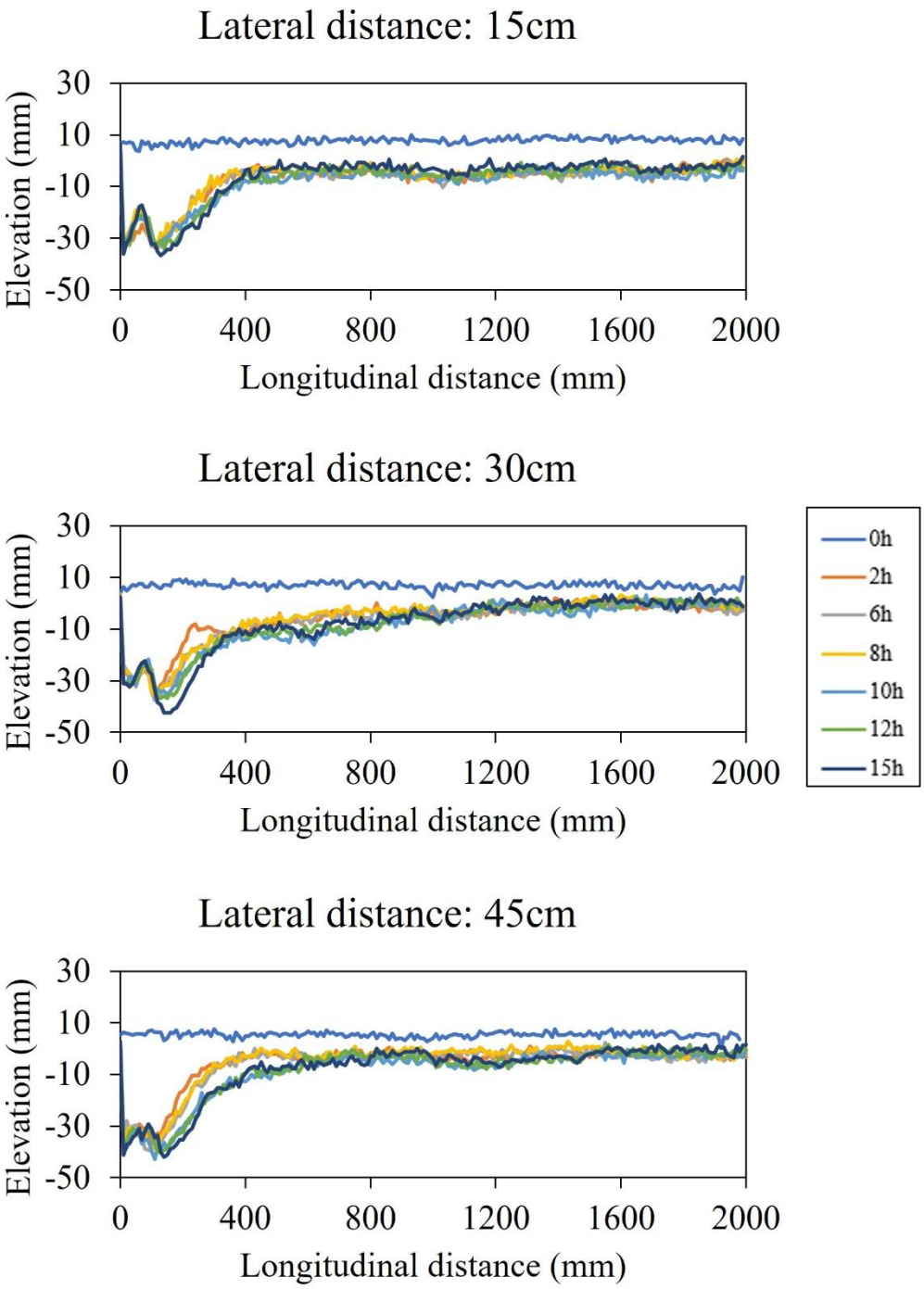


Figure 3-9 - Longitudinal profile at positions 15, 30, and 45cm (from right to left)

The evaluation of bottom diameter values showed little variation after 12 hours of testing (Figure 3-10). The D10 and D16 decreased from 0.259 to 0.255 mm and from 0.322 to 0.316 mm, respectively, suggesting the transport of this particle size class or perhaps the filling of voids in the mobile bed. The D50 remained nearly constant, ranging from 1.0 to 1.18 mm. On the other hand, the D84 and D90 increased from 2.445 to 2.522

mm and from 2.894 to 3.0 mm, respectively. This indicates an increase in bed roughness over time.

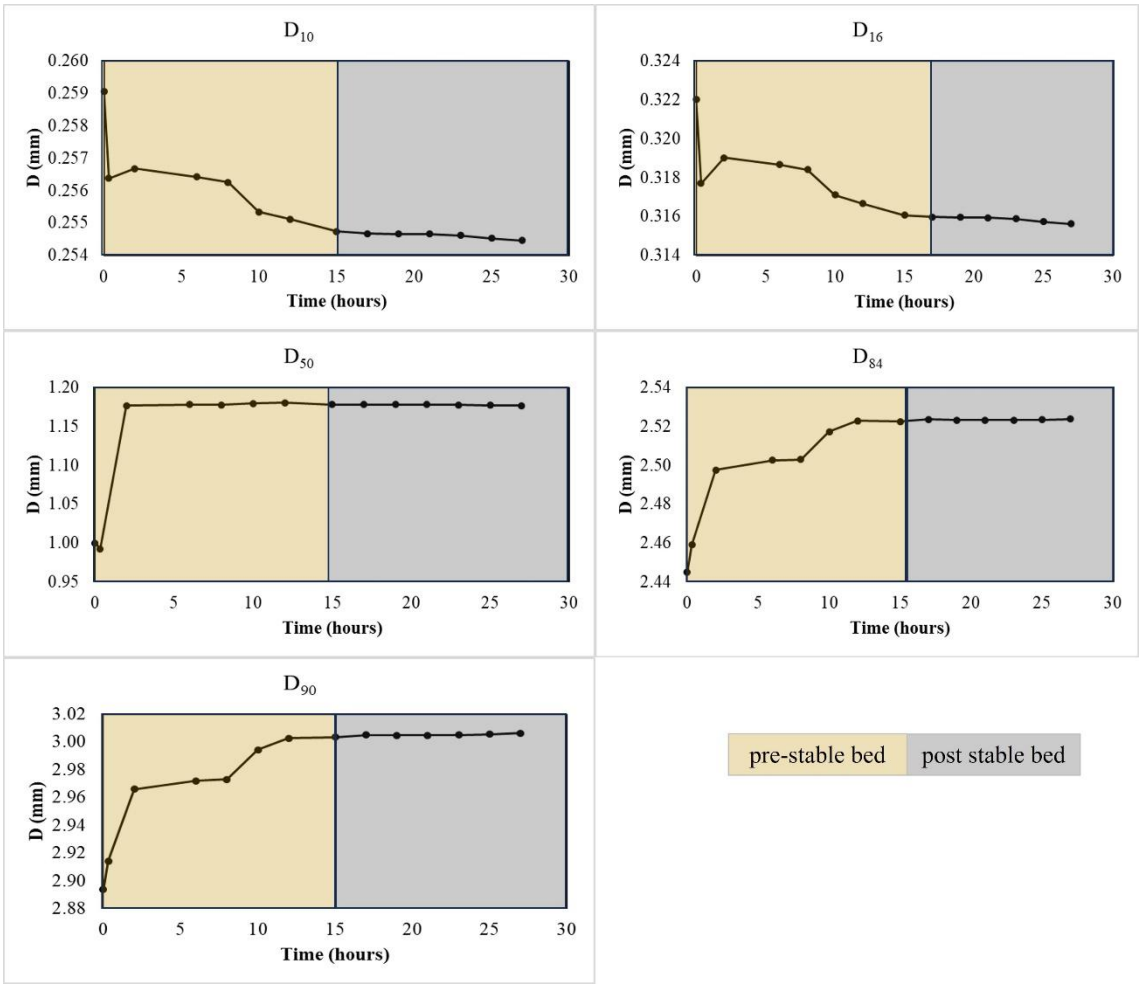


Figure 3-10 - Variation of bed diameters throughout the experiment

It is interesting to note that this pattern was also observed for the transported sediments. In other words, the same sediment size class that increases or decreases in the channel bed is the one being transported by the channel itself. This behavior occurs due to variations in the availability of sediment size classes during the tests. These results suggest a direct link between the number of protruding grains available, and the number of grains transported (Masteller & Finnegan, 2017). These grains project further from the mean bed elevation, making them available and facilitating transport (Kirchner et al., 1990). Additionally, they are exposed to higher fluid drag, resulting in increased mobility (Fenton & Abbott, 1977).

Natural rivers mostly consist of a wide range of sediment sizes, creating stable bed conditions, but this condition is not maintained all the time. This is because these rivers experience low, medium, and high flow conditions. Often, conditions are subcritical, meaning that the flow is insufficient to significantly disturb the bed, or the stresses imposed by the flow create a transient situation where the bed is adjusting to a new state as sediment supply from upstream allows (Church et al., 1998). Thus, by including a pre-channel formation phase that is morphologically analogous to a natural channel, more robust insights are provided for understanding phenomena associated with water and sediment flow in gravel-bed rivers.

3.3.2 Evaluation of velocity profiles and flow resistance

3.3.2.1 Flow and sediment transport behavior

The sediment transport rate throughout the tests remained very low, as depicted in Table 3-5. This is evident as the flow rate decreased from 317.85 L/min in Test E1 to 53.88L/min in Test E6.

Table 3-5 - Characterization of flow rates and sediments for the conducted tests

Tests	Time (h)	Flow rate (L/min)	Amount of transported sediment (g)	Cumulative amount of transported sediment (g)	Bed load (g/min)
E1	17	317.85	145.4	145.4	1.21
E2	19	249.94	17.5	162.9	0.15
E3	21	201.5	7.2	170.1	0.06
E4	23	146.38	34.7	204.8	0.29
E5	25	98.16	61.67	266.47	0.51
E6	27	53.88	52.79	319.25	0.44

Figure 3-6 illustrated the behavior over time, considering the period of stable bed formation where the Q was increased up to 317.85 L/min, and the period after bed stabilization where a successive series of flow rate reductions occurred. Sediment transport remained low despite the mobilization generated in the first 15 hours. Spatial characterization by sections will be presented in the subsequent sections.

3.3.2.2 Analysis of velocity profiles between sections

The velocity profiles obtained for the sections at 120 and 160 cm for Tests E1, E2, E3, E4, and E5 are depicted in Figure 3-11. For Test E6, velocity measurement was not

possible due to extremely low values, rendering the measurement methodology unfeasible. It is observed that the velocity intensity decreased with decreasing flow rates, except for Test E1, which could indicate a greater influence of bed roughness during the measurement process.

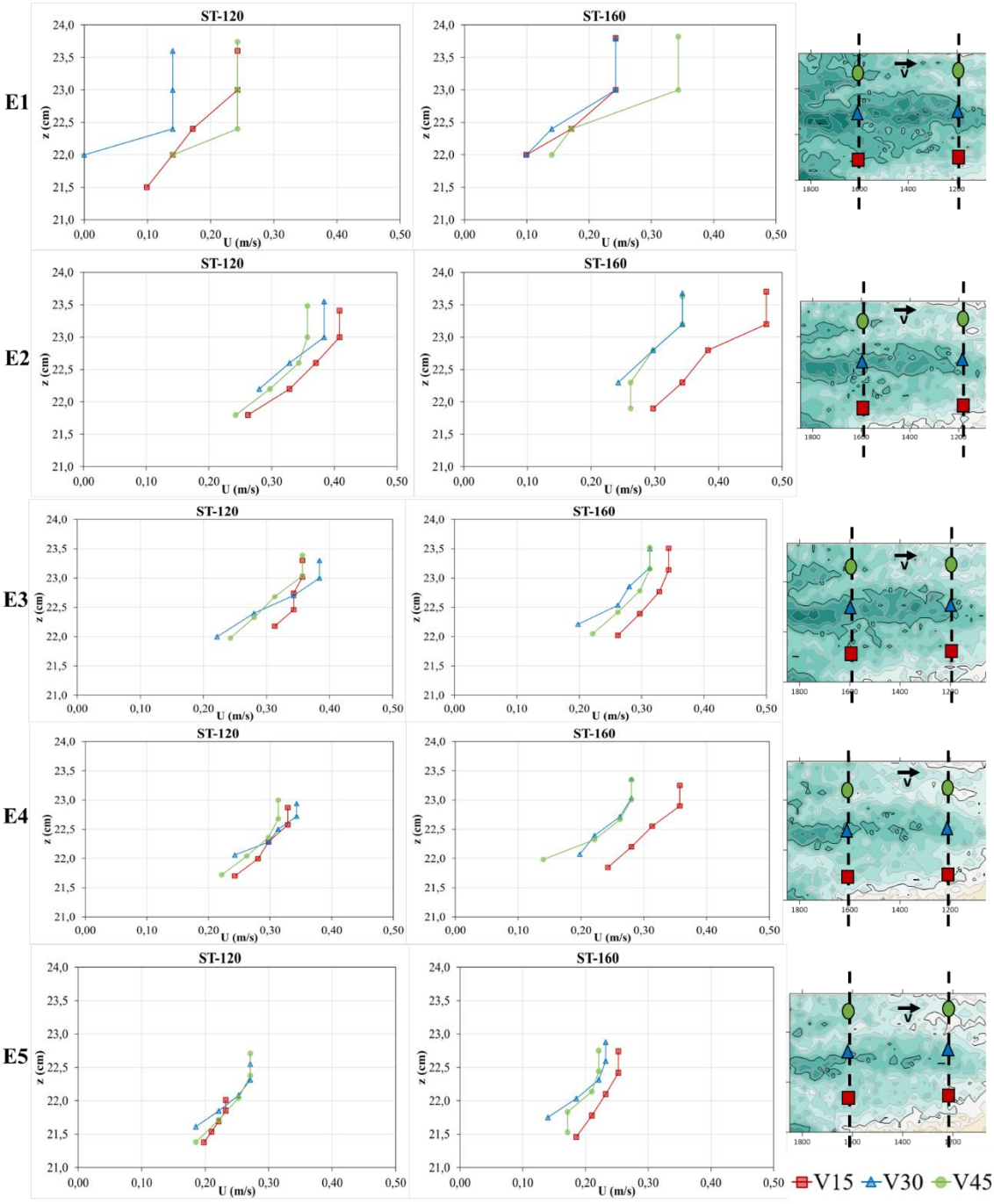


Figure 3-11 - Velocity profiles obtained for verticals (V14, V30, and V45) at sections (ST-120 and ST-160) for the conducted tests (E1, E2, E3, E4, and E5)

Figure 3-12 displays velocity profiles per vertical across the tests. It can be observed that during Test E1, the bed elevation values were higher, suggesting bed mobilization. However, during Test E2, these bed elevation values appear to be higher.

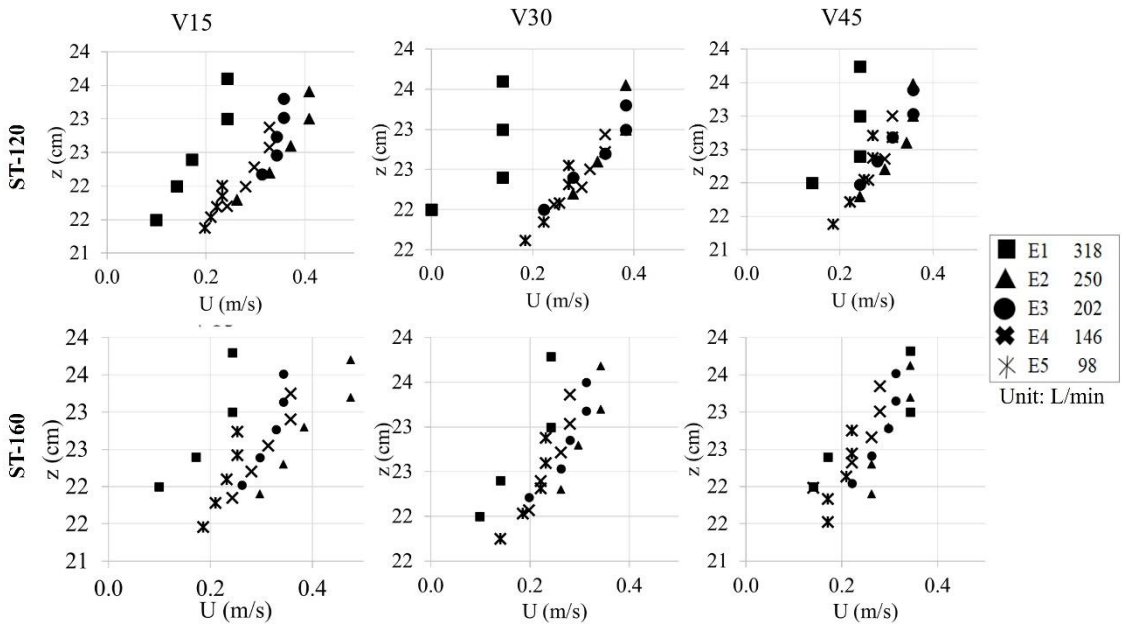


Figure 3-12 - Velocity profiles for each vertical at ST-120 and ST-160 cm

3.3.3 Evaluation of bed roughness

To assess the influence of bed roughness, the velocity distribution profile was adjusted, and the ks (bed roughness coefficient) was calculated for each measured vertical. The average behavior for each section can be observed in Figure 3-13. Upon analyzing the figure, it is evident that as the flow rate decreases across the tests, the values of ks increase, indicating an elevation in bed roughness. This behavior is reflected in the velocity data, where values decrease as flow rate diminishes and ks values increase. Additionally, when considering the two sections separately, in ST-120, U values are higher compared to ST-160, while ks values are greater in ST-160.

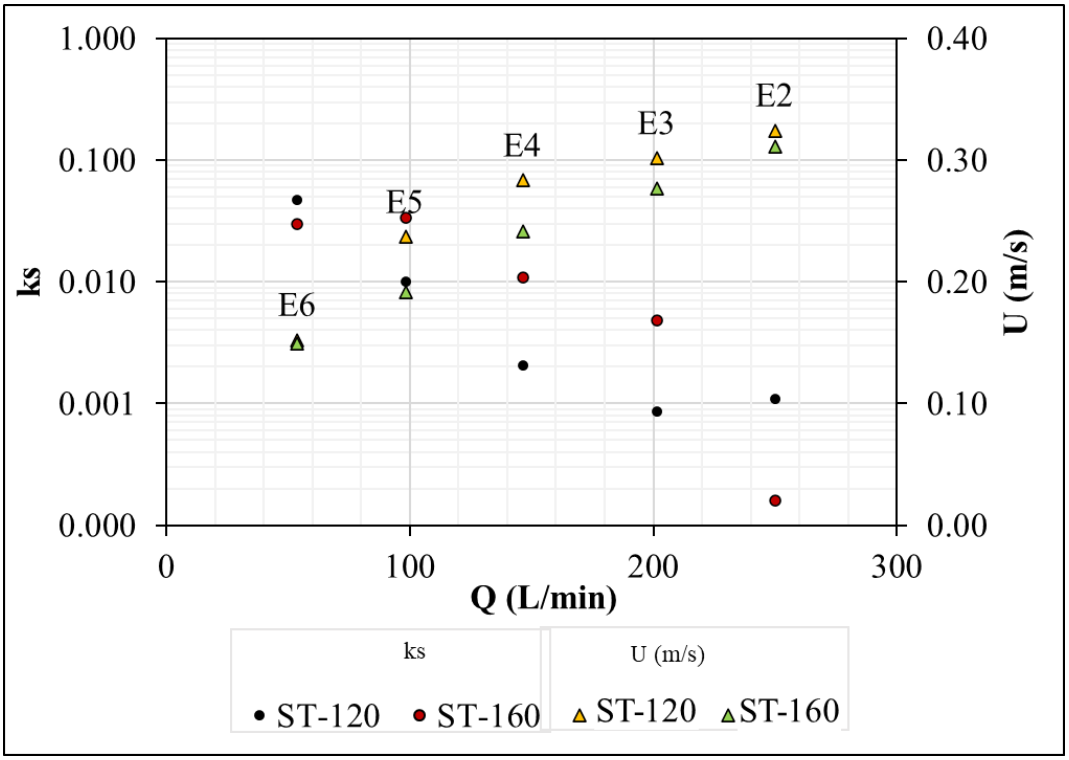


Figure 3-13 - Behavior of ks and U across the tests for the two velocity profile measurement sections

During the tests, it was observed that this behavior may be associated with the deposition that occurred in the downstream portion of the mobile bed, closer to ST-160. In this section, finer sediments filled empty spaces, and larger sediments contributed to creating a higher level of roughness compared to the other sections. By examining the bathymetry of both sections, it can be concluded that deposition is taking place, resulting in increased roughness in this section (Figure 3-14).

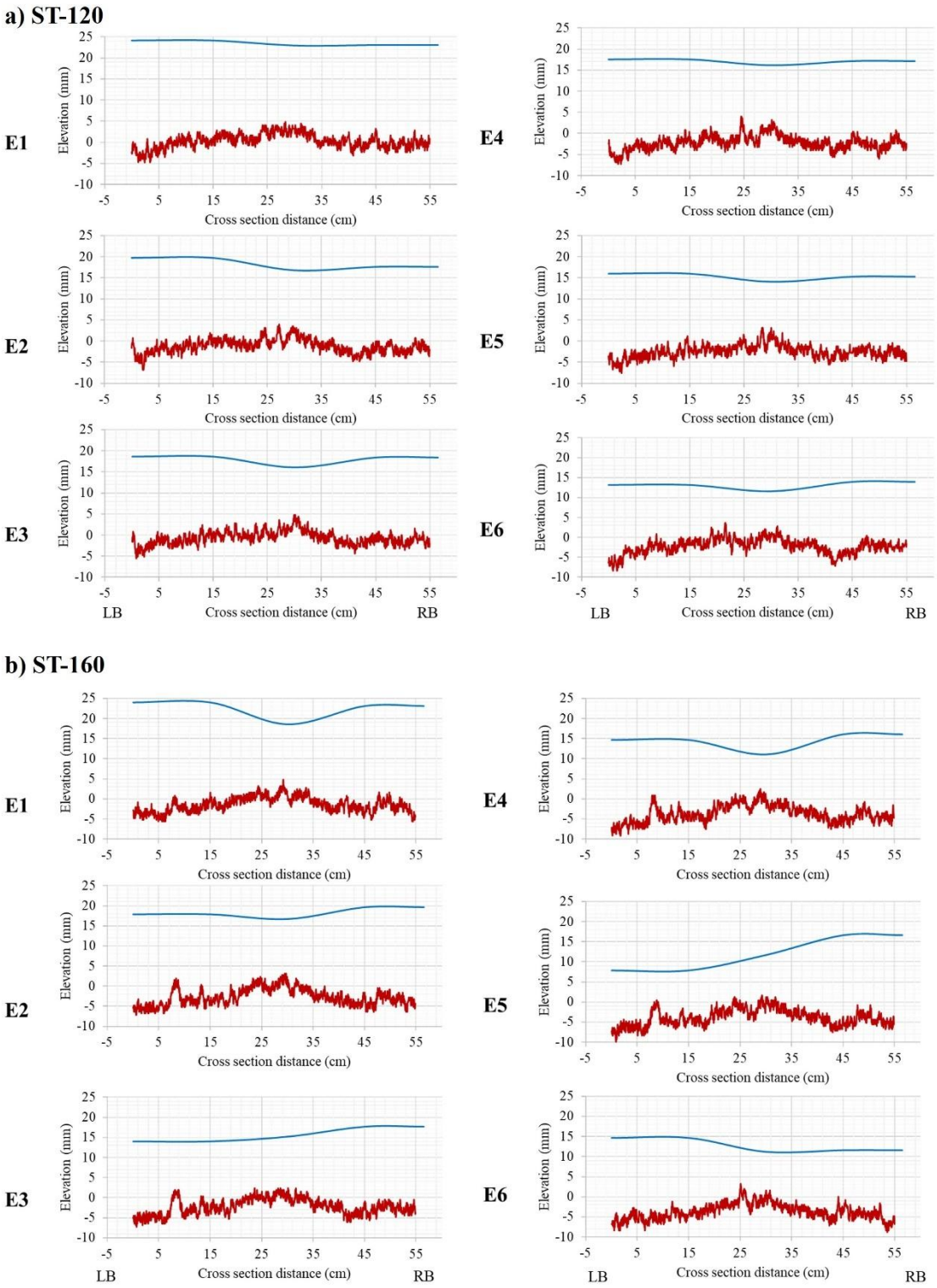


Figure 3-14 - Bathymetry of transverse sections (a) at 120 cm (ST-120) and (b) at 160 cm (ST-160) at the end of each test, along with the water depth measured during the test

Note: E1: Q = 317.85L/min; E2: 249.94L/min; E3: 201.5L/min; E4: 146.38L/min; E5: 98.16L/min; E6: 53.88L/min. Water depth shown in blue, and channel bed in red. LB: left bank; RB: right bank.

Figure 3-15 illustrates this behavior of the mobile bed during the tests. The measurements were taken at the end of each test. It is worth highlighting that from E1 to E6, a sequence of decreasing flow rates, velocities, and depths occurred, leading to the plan-view stabilization of the channel bed. This figure depicts only the section between 40 and 190 cm, where ST-120 and ST-160 are located.

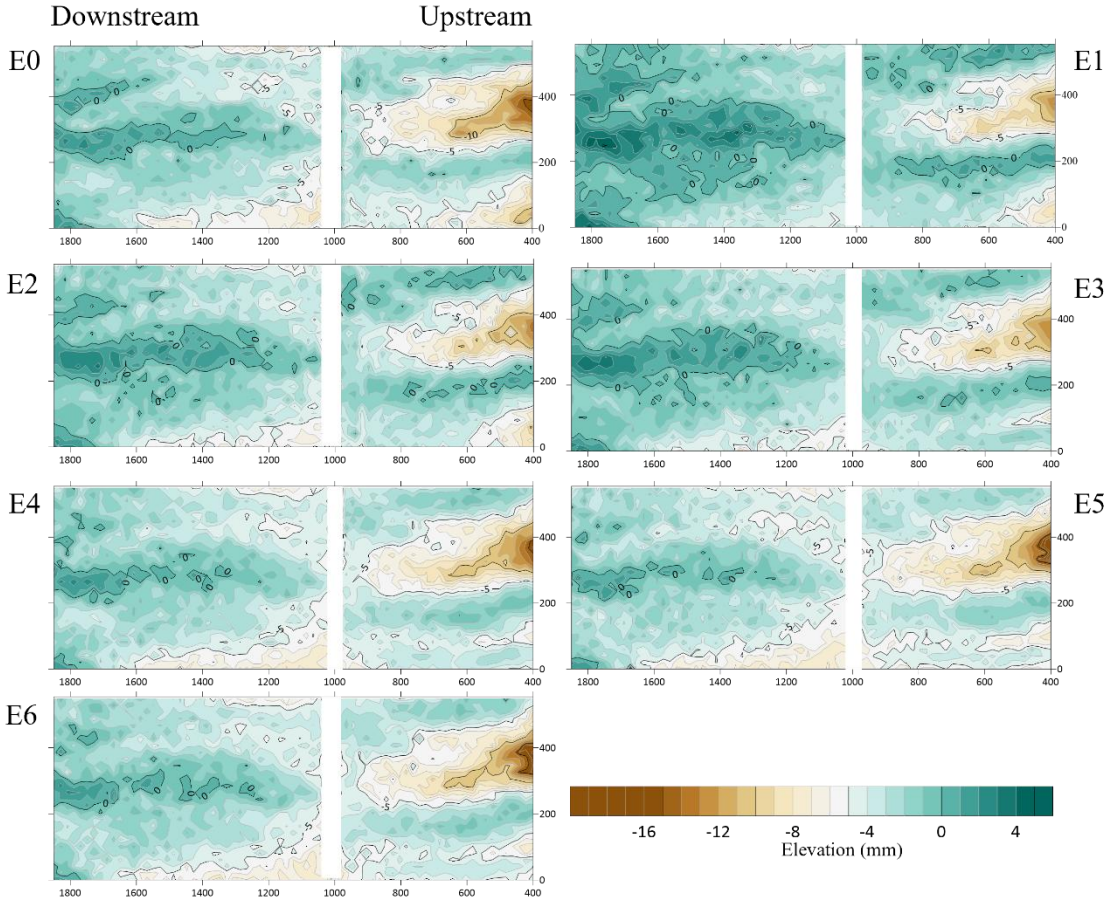


Figure 3-15 - Channel bed throughout the tests (greener color indicates positive elevation, and browner color indicates negative elevation)

Note: at a distance of 1000mm there is a structural limitation of the channel for taking profiler readings.

In this regard, the oscillation factor (OF) of the bed elevation was also evaluated after each test, as shown in Figure 3-16. Directly looking at sections ST-120 and ST-160, it is notable that the oscillation value is lower for ST-160, with the exception of E4. However, as seen in Figure 15, for the last test, ks was higher in ST-120, and the oscillation factor continued to be lower for ST-160. This behavior could be related to the filling of voids by sediments of lower granulometry.

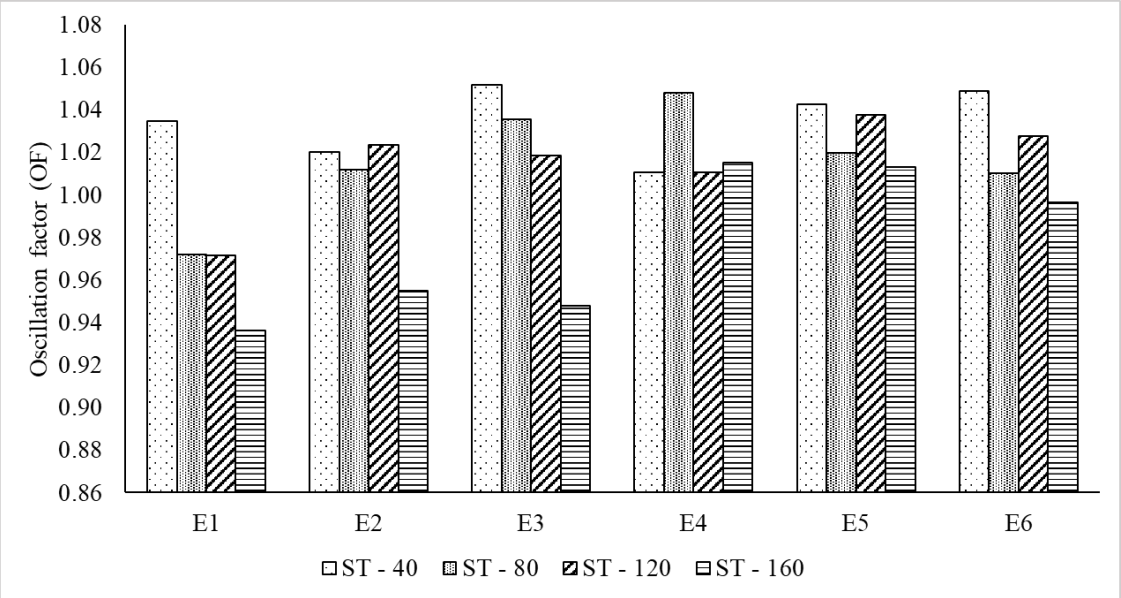


Figure 3-16 - Oscillation factor (OF) of the bed elevation in transverse measurement sections of the channel

Currently, there is no consensus on the ideal approach to relate bed characteristics in high-gradient or shallow flow rivers to flow resistance, primarily due to the lack of agreement on how to quantify roughness and the limited availability of combined measurements of flow velocity and bed roughness in the field. Additionally, the description of roughness often relies on a single parameter, and none of the proposed roughness measures to date can fully explain the observed variability in flow velocity between different locations.

3.3.3.1 Relationship between flow resistance for the tests

For a clearer visualization of the data, the averages for each test were extracted through the averages for each section (Figure 3-17). In this way, the main flow resistance parameters (n, f, and C) were calculed. Except for E1, the values of n and f for the other tests increased as the Q in the channel decreased, indicating a reduction in flow energy. The average data obtained for each test can be seen in Table 3-6.

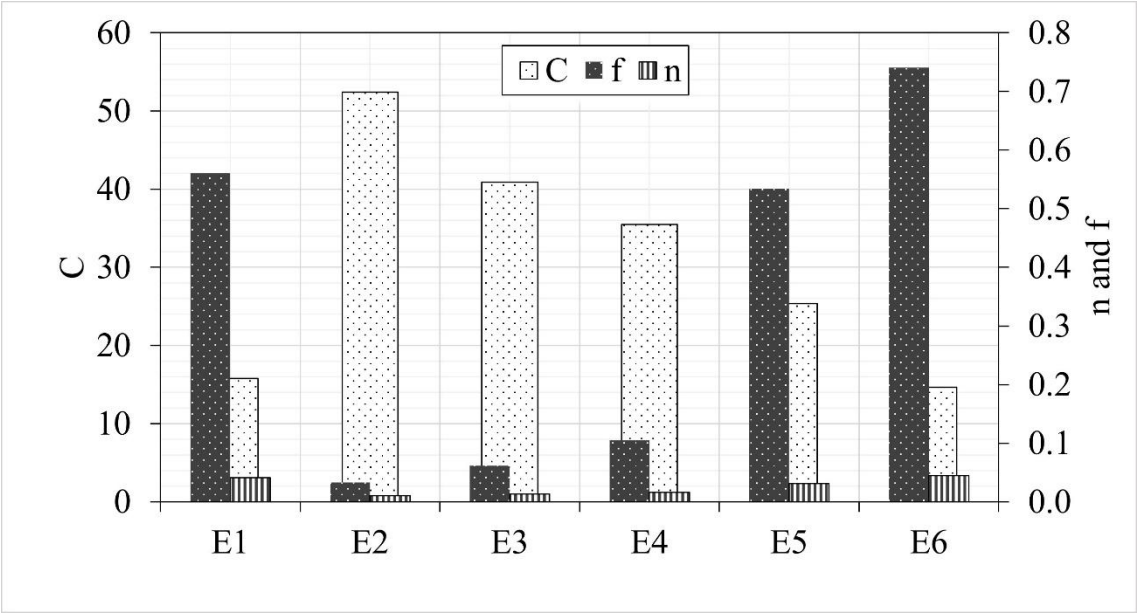


Figure 3-17 - Behavior of resistance variables throughout the tests: C (Chezy coefficient), F (Darcy–Weisbach coefficient), and n (Manning coefficient).

Table 3-6 - Measured and calculated variables for the tests conducted in the channel

		Tests					
	Variable	**E1**	**E2**	**E3**	**E4**	**E5**	**E6**
		Average values					
Observed	**h (cm)**	2.309	2.046	1.816	1.678	1.508	1.382
	Q (weir) (L/min)	317.85	249.94	201.5	146.38	98.16	53.88
	U obs (m/s)	0.23	0.299	0.273	0.261	0.215	0.124
	Qst (g)	145.4	17.495	7.2	34.7	61.672	52.785
	Qst (g/min)	1.212	0.146	0.06	0.289	0.514	0.44
	D_{10} bed	0.255	0.255	0.255	0.255	0.255	0.254
	D_{16} bed	0.316	0.316	0.316	0.316	0.316	0.316
	D_{50} bed	1.178	1.178	1.178	1.178	1.177	1.177
	D_{84} bed	2.523	2.523	2.523	2.523	2.523	2.524
	D_{90} bed	3.005	3.005	3.005	3.005	3.006	3.006
	D_{10} st	0.296	0.346	0.277	0.611	0.825	0.595
	D_{16} st	0.382	0.546	0.374	0.885	1.025	0.774
	D_{50} st	0.983	1.969	1.3	1.688	1.645	1.495
	D_{84} st	2.117	3.36	2.438	2.493	2.407	2.246
	D_{90} st	2.449	3.722	2.675	2.778	2.639	2.477
Derived from velocity profile	**u* (m/s)**	0.043	0.02	0.024	0.026	0.04	0.042
	ks	0.052	0.001	0.003	0.006	0.022	0.039
	τ (N/m^2)	2.329	0.414	0.601	0.811	2.511	1.978

Variable	Tests					
	E1	E2	E3	E4	E5	E6
	Average values					
δ (m)	3.70E-04	6.10E-04	5.20E-04	5.10E-04	4.40E-04	3.40E-04
ks/δ	249.75	1.26	7.86	23.88	153.06	159.15
U (m/s)	0.168	0.318	0.289	0.263	0.214	0.151
Fr	0.358	0.755	0.717	0.681	0.592	0.428
Re	3804.16	5741.25	4803.84	4007.26	2876.06	1921.05
Re*	2897.08	14.62	91.21	276.98	1775.52	1846.15
f	0.561	0.033	0.062	0.105	0.535	0.741
C	15.78	52.41	40.9	35.47	25.37	14.67
n (1/s.m$^{1/3}$)	0.041	0.01	0.014	0.016	0.031	0.045
S (m/m)	0.011	0.002	0.004	0.005	0.018	0.016

By observing some dimensionless parameters shown in Table 3-6, Figure 3-18 was constructed, where we can see that the behavior of Re and Fr shows a relationship with U/u* (R^2 = 0.77 and 0.89, respectively).

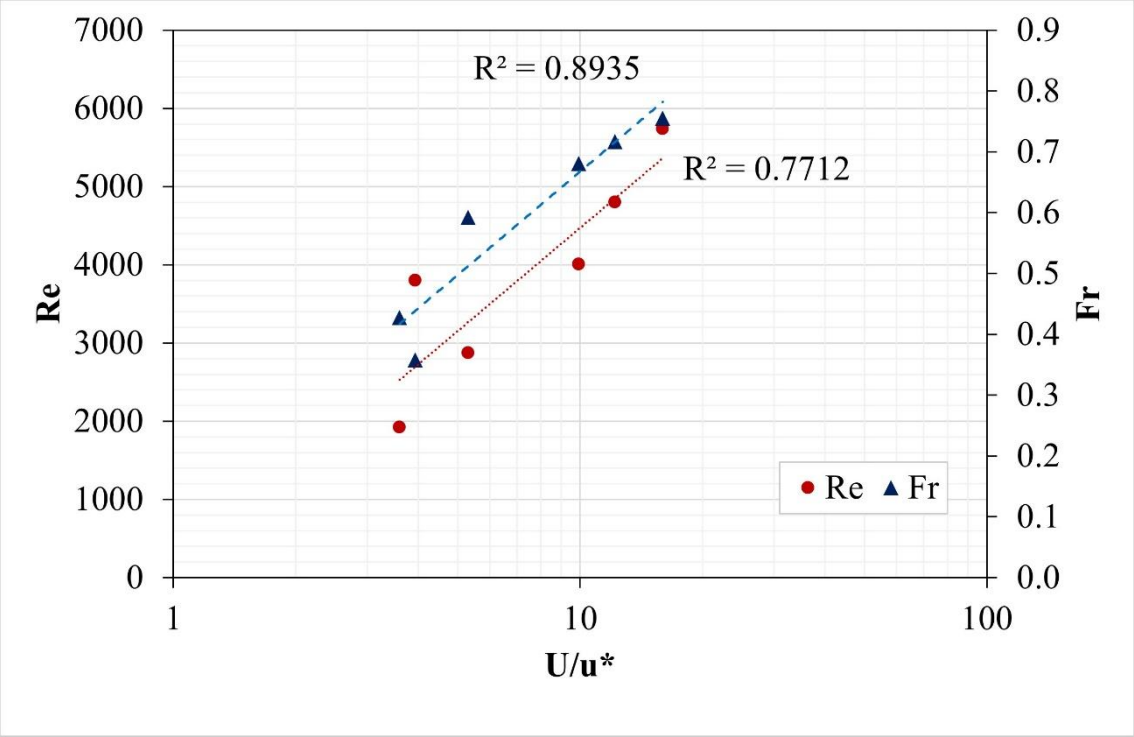


Figure 3-18 - Relationship between Re and Fr versus U/u*

3.3.3.2 Relationships between dimensionless variables q* and U*

Rickenmann and Recking (2011) utilized a dataset of 2890 field measurements to test the ability of various conventional flow resistance equations to predict the average

flow velocity in gravel-bed rivers. The authors emphasize the use of two dimensionless parameters.

$$q^{**} = \frac{q}{\sqrt{g.I.{D_{84}}^3}} \quad (23)$$

$$U^{**} = \frac{U}{\sqrt{g.I.D_{84}}} \quad (24)$$

When plotting the obtained results on the diagram developed using these dimensionless parameters by Rickenmann & Recking (2011), the points from our study fall within the cluster of points of the results found by these authors. In Figure 3-19, it is highlighted that these points converge towards small (h/D <1.2) and intermediate (1.2 < h/D< 14) scale roughness. According to Ferguson (2007), Comiti et al. (2009), and Zimmermann (2010), a significant advantage of the U** versus q** representation is that equations based on discharge to predict flow velocity are more robust (with fewer errors in input variables) than equations based on D, especially when applied to steep and high-roughness channels.

Furthermore, we incorporated data from Menezes (2021), which illustrates the prototype inspiring this physical model. We noted consistent behavior in dimensionless values. Notably, certain data points along the Forqueta river deviate from the trend. This variance may have its origin in differing channel morphologies, such as cascades and plane-beds, as elaborated in Menezes (2021).

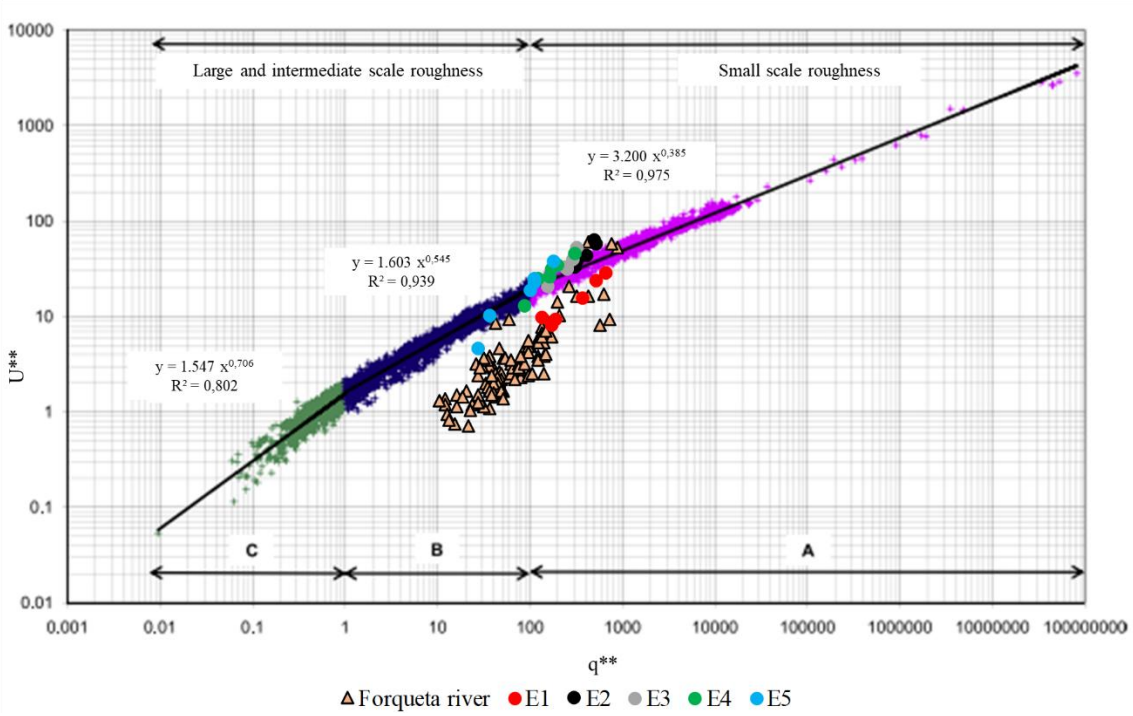


Figure 3-19 - Comparison between the dimensionless variables proposed by Rickenmann and Recking (2011)

The understanding among these dimensionless parameters allows comparison with other studies in this field and enables the improvement of conventional equations for application in beds with extensive particle size distribution. However, there are still questions that deserve further observations and detailing for a complete understanding of the involved processes. For instance, some studies highlight that, in order to estimate the bed roughness height, D_{84} is not always a reliable predictive parameter. Aberle & Smart (2003) achieved more favorable results by using the standard deviation of bed elevation (σ_z) as a roughness indicator in gravel-bed streams. Chen et al. (2020) and Ferguson et al. (2019), employing the same roughness indicator, also obtained promising results. However, both of them used data collected from natural rivers under a specific condition. In this regard, there is still a gap in research conducted in situations with more irregular beds, especially when using scale reductions.

3.4 CONCLUSIONS

The preliminary phase allows the laboratory channel bed to develop appropriate geometric and surface characteristics, ensuring that the experiment reproduces hydrodynamic patterns similar to those of natural shallow-flow fluvial systems.

Maintaining a flow rate characteristic of the modeled environment has allowed the generation of a channel bed that incorporates morphological elements, sediment distribution and flow paths that more closely resemble natural conditions. This provides a more accurate and realistic basis for physical simulation studies on rivers with variable grain size.

Looking at the velocity profiles obtained from the formed bed experiments, several important features can be highlighted: the thickening of the diameter of the moving bed which leads to increased resistance to flow (indicated by the parameters n, f and C), the deposition of fines in the empty spaces between the grains and the increase in ks as the discharge volume decreases. It was also observed that the dimension values obtained in the physical model correspond to those observed in nature.

Thus, through this preliminary study it was possible to reveal insights into the physical processes involved in water and sediment transport that need to be considered in physical simulation studies. This is important because understanding these processes is crucial for various fields, including hydrology, fluvial geomorphology and river engineering.

3.5 REFERENCES

Aberle, J., & Smart, G. M. (2003). The influence of roughness structure on flow resistance on steep slopes. *Journal of Hydraulic Research*, *41*(3), 259-269.

Abrahams, A. D., & Li, G. (1998). Effect of saltating sediment on flow resistance and bed roughness in overland flow. *Earth Surface Processes and Landforms*, *23*(10), 953-960.

Alomari, N. K., Yusuf, B., Mohammad, T. A., & Ghazali, A. H. (2018). Experimental investigation of scour at a channel junctions of different diversion angles and bed width ratios. *Catena*, *166*, 10-20.

Bahmanpouri, F., Daliri, M., Khoshkonesh, A., Montazeri Namin, M., & Buccino, M. (2021). Bed compaction effect on dam break flow over erodible bed; experimental and numerical modeling. *Journal of Hydrology*, *594*, 125645.

Bartels, G. K., Castro, N. M. R., Collares, G. L., & Fan, F. M. (2021). Performance of bedload transport equations in a mixed bedrock-alluvial channel environment. *Catena*, *199*, 105108.

Bathurst, J. C. (1985). Flow resistance estimation in mountain rivers. *Journal of Hydraulic Engineering*, *111*(4), 625-643.

Bogatin, E., DeGroot, D., Huray, P. G., & Shlepnev, Y. (2013).

Which one is better? Comparing options to describe frequency dependent losses. Faculty Publications. 1665.

Buffin-Bélanger, T., Reid, I., Rice, S., Chandler, J. H., & Lancaster, J. (2003). A casting procedure for reproducing coarse-grained sedimentary surfaces. *Earth Surface Processes and Landforms*, *28*(7), 787-796.

Charru, F., Mouilleron, H., & Eiff, O. (2004). Erosion and deposition of particles on a bed sheared by a viscous flow. *Journal of Fluid Mechanics*, *519*, 55-80.

Chen, X., Hassan, M. A., An, C., & Fu, X. (2020). Rough correlations: meta-analysis of roughness measures in gravel bed rivers. *Water Resources Research*, *56*(8), e2020WR027079.

Church, M., Hassan, M. A., & Wolcott, J. F. (1998). Stabilizing self-organized structures in gravel-bed stream channels: field and experimental observations. *Water Resources Research*, *34*(11), 3169-3179.

Comiti, F., Cadol, D., & Wohl, E. (2009). Flow regimes, bed morphology, and flow resistance in self-formed step-pool channels. *Water Resources Research*, *45*(4), 2008WR007259.

Cooper, J. R., & Tait, S. J. (2009). Water-worked gravel beds in laboratory flumes–a natural analogue? *Earth Surface Processes and Landforms*, *34*(3), 384-397.

Di Stefano, C., Nicosia, A., Palmeri, V., Pampalone, V., & Ferro, V. (2020). Flow resistance law under suspended sediment laden conditions. *Flow Measurement and Instrumentation*, *74*, 101771.

Dietrich, W. E., Kirchner, J. W., Ikeda, H., & Iseya, F. (1989). Sediment supply and the development of the coarse surface layer in gravel-bedded rivers. *Nature*, *340*(6230), 215-217.

Einstein, H. A. (1950). *The bed-load function for sediment transportation in open channel flows* (No. 1026). US Department of Agriculture.

Fenton, J. D., & Abbott, J. E. (1977). Initial movement of grains on a stream bed: the effect of relative protrusion. *Proceedings of the Royal Society of London. Series A, Mathematical and Physical Sciences*, *352*(1671), 523-537.

Ferguson, R. (2007). Flow resistance equations for gravel-and boulder-bed streams. *Water Resources Research*, *43*(5), 2006WR005422.

Ferguson, R. I., Hardy, R. J., & Hodge, R. A. (2019). Flow resistance and hydraulic geometry in bedrock rivers with multiple roughness length scales. *Earth Surface Processes and Landforms*, *44*(12), 2437-2449.

Ferraro, D., Coscarella, F., & Gaudio, R. (2019). Scales of turbulence in open-channel flows with low relative submergence. *Physics of Fluids*, *31*(12), 125114.

Ferro, V. (2018). Assessing flow resistance in gravel bed channels by dimensional analysis and self-similarity. *Catena*, *169*, 119-127.

Friedl, F., Weitbrecht, V., & Boes, R. M. (2018). Erosion pattern of artificial gravel deposits. *International Journal of Sediment Research*, *33*(1), 57-67.

Gao, P., & Abrahams, A. D. (2004). Bedload transport resistance in rough open-channel flows. *Earth Surface Processes and Landforms*, *29*(4), 423-435.

Gladkov, G., Habel, M., Babiński, Z., & Belyakov, P. (2021). Sediment transport and water flow resistance in alluvial river channels: modified model of transport of non-uniform grain-size sediments. *Water*, *13*(15), 2038.

Hamidifar, H., Nones, M., & Rowinski, P. M. (2024). Flood modeling and fluvial dynamics: a scoping review on the role of sediment transport. *Earth-Science Reviews*, *253*, 104775.

Hardy, R. J., Best, J. L., Lane, S. N., & Carbonneau, P. E. (2010). Coherent flow structures in a depth-limited flow over a gravel surface: the influence of surface roughness. *Journal of Geophysical Research. Earth Surface*, *115*, F03006.

Haynes, H., & Pender, G. (2007). Stress history effects on graded bed stability. *Journal of Hydraulic Engineering*, *133*(4), 343-349.

Kirchner, J. W., Dietrich, W. E., Iseya, F., & Ikeda, H. (1990). The variability of critical shear stress, friction angle, and grain protrusion in water-worked sediments. *Sedimentology*, *37*(4), 647-672.

Kumar, L., & Afzal, M. S. (2023). Experimental and numerical modelling of scour at vertical wall abutment under combined wave-current flow in low KC regime. *Ocean Engineering*, *285*, 115394.

López, R., Ville, F., Garcia, C., Batalla, R. J., & Vericat, D. (2023). Bed-material entrainment in a mountain river affected by hydropeaking. *The Science of the Total Environment*, *856*, 159065.

Manica, R. (2009). *Geração de correntes de turbidez de alta densidade: condicionantes hidráulicos e deposicionais* (Tese de doutorado). Programa de Pós-graduação em Recursos Hídricos e Saneamento Ambiental, Universidade Federal do Rio Grande do Sul, Porto Alegre.

Masteller, C. C., & Finnegan, N. J. (2017). Interplay between grain protrusion and sediment entrainment in an experimental flume. *Journal of Geophysical Research. Earth Surface*, *122*(1), 274-289.

Maxwell, A. R., & Papanicolaou, A. N. (2001). Step-pool morphology in high-gradient streams. *International Journal of Sediment Research*, *16*(3), 380-390.

Menezes, D. (2021). *Caracterização hidrossedimentológica de trecho do rio Forqueta, Maquiné, RS* (Dissertação de mestrado). Programa de Pós-graduação em Recursos Hídricos e Saneamento Ambiental, Universidade Federal do Rio Grande do Sul, Porto Alegre.

Menezes, D., & Kobiyama, M. (2023). Hydrosedimentological characterization of a reach in the Forqueta River catchment, south Brazil. *Journal of South American Earth Sciences*, *128*, 104430.

Montgomery, D. R., & Buffington, J. M. (1997). Channel-reach morphology in mountain drainage basins. *Geological Society of America Bulletin*, *109*(5), 596-611.

Nelson, A., & Dubé, K. (2016). Channel response to an extreme flood and sediment pulse in a mixed bedrock and gravel-bed river. *Earth Surface Processes and Landforms*, *41*(2), 178-195.

Paixão, M. A., & Kobiyama, M. (2022). Flow resistance in a subtropical canyon river. *Journal of Hydrology*, *613*, 128428.

Paixão, M. A., Kobiyama, M., Poleto, C., Mao, L., Ávila, I. G., Takebayashi, H., & Fujita, M. (2023). Relationship between morphology and sediment transport in a canyon river channel, Southern Brazil. *Journal of Soils and Sediments*, *23*(12), 1-15.

Paphitis, D., & Collins, M. B. (2005). Sand grain threshold, in relation to bed 'stress history': an experimental study. *Sedimentology*, *52*(4), 827-838.

Polvi, L. E. (2021). Morphodynamics of boulder-bed semi- alluvial streams in northern Fennoscandia: a flume experiment to determine sediment self-organization. *Water Resources Research*, *57*(3), e2020WR028859.

Prandtl, L. (1926). *Application of the" magnus effect" to the wind propulsion of ships*. NACA-TM. 367.

Rachelly, C., Vetsch, D. F., Boes, R. M., & Weitbrecht, V. (2022). Sediment supply control on morphodynamic processes in gravel- bed river widenings. *Earth Surface Processes and Landforms*, *47*(15), 3415-3434.

Recking, A., Frey, P., Paquier, A., Belleudy, P., & Champagne, J. Y. (2008). Feedback between bed load transport and flow resistance in gravel and cobble bed rivers. *Water Resources Research*, *44*(5), 2007WR006219.

Rickenmann, D., & Recking, A. (2011). Evaluation of flow resistance in gravel-bed rivers through a large field data set. *Water Resources Research*, *47*(7), 2010WR009793.

Schmeeckle, M. W., Nelson, J. M., & Shreve, R. L. (2007). Forces on stationary particles in near-bed turbulent flows. *Journal of Geophysical Research. Earth Surface*, *112*, F02003.

Smart, G. M., Duncan, M. J., & Walsh, J. M. (2002). Relatively rough flow resistance equations. *Journal of Hydraulic Engineering*, *128*(6), 568-578.

Smith, H. E., Monsalve, A. D., Turowski, J. M., Rickenmann, D., & Yager, E. M. (2023). Controls of local grain size distribution, bed structure, and flow conditions on sediment mobility. *Earth Surface Processes and Landforms*, *48*(10), 1990-2004.

Spiller, S. M., Rüther, N., & Baumann, B. (2015). Form-induced stress in non-uniform steady and unsteady open channel flow over a static rough bed. *International Journal of Sediment Research*, *30*(4), 297-305.

Sturm, M., Gems, B., Keller, F., Mazzorana, B., Fuchs, S., Papathoma-Köhle, M., & Aufleger, M. (2018a). Understanding impact dynamics on buildings caused by fluviatile sediment transport. *Geomorphology*, *321*, 45-59.

Sturm, M., Gems, B., Keller, F., Mazzorana, B., Fuchs, S., PapathomaKöhle, M., & Aufleger, M. (2018b). Experimental analyses of impact forces on buildings exposed to fluvial hazards. *Journal of Hydrology*, *565*, 1-13.

Vázquez-Tarrío, D., Ruiz-Villanueva, V., Garrote, J., Benito, G., Calle, M., Lucía, A., & Díez-Herrero, A. (2024). Effects of sediment transport on flood hazards: lessons learned and remaining challenges. *Geomorphology*, *446*, 108976.

Wang, X., Yang, Q., Lu, W., & Wang, X. (2011). Effects of bed load movement on mean flow characteristics in mobile gravel beds. *Water Resources Management*, *25*(11), 2781-2795.

Zimmermann, A. (2010). Flow resistance in steep streams: an experimental study. *Water Resources Research*, *46*(9), W09536.

4. ARTIGO II: BED ROUGHNESS IN GRAVEL-BED RIVERS: CHANNEL-SCALE RESPONSES TO FLOW AND SEDIMENT DYNAMICS

Apresentação

Este capítulo baseia-se no seguinte artigo aceito para publicação em 12 de outubro/2025 na Revista Advances in Water Resources: Menezes, D. D., & Borges, A. L. D. O. (2025). Bed roughness in gravel-bed rivers: channel-scale responses to flow and sediment dynamics.

O artigo foi redigido em inglês e, portanto, apresenta-se aqui uma síntese em português de seu conteúdo, destacando o tema central, a metodologia empregada e os principais resultados alcançados. O estudo aborda o comportamento da rugosidade de fundo em canais de leito cascalhoso, investigando como ela responde às variações de escoamento e à dinâmica sedimentar em condições de supressão de aporte de sedimentos. A compreensão desses processos é essencial tanto para a pesquisa científica quanto para aplicações de engenharia, incluindo estimativas de transporte de sedimentos, análises de morfodinâmica de rios, avaliação de cheias e previsão de habitats ecológicos.

Os experimentos foram conduzidos em um canal experimental retangular de 10 m de comprimento e 0,56 m de largura, com leito móvel composto por material granular. O estudo foi dividido em duas fases complementares. Na Fase 1, buscou-se a formação de uma configuração morfologicamente estável, permitindo o estabelecimento de um equilíbrio entre o escoamento e o transporte de sedimentos sob determinada vazão. Essa etapa de estabilização mostrou-se fundamental, pois o ajuste do material de fundo e o preenchimento dos vazios intergranulares por partículas finas influenciaram significativamente a resposta hidráulica do escoamento.

Na Fase 2, a rugosidade hidráulica do leito estabilizado foi avaliada sob diferentes condições de escoamento. Os resultados indicaram que a resistência ao escoamento tende a diminuir com o aumento da submergência relativa, enquanto condições de baixa vazão e baixa submergência resultaram em maior rugosidade, devido à microtopografia do leito

e à formação de camadas de “armoring”. Além disso, as equações empíricas tradicionalmente empregadas mostraram-se inadequadas para representar os casos de alta rugosidade relativa, evidenciando a necessidade de formulações mais específicas para canais de leito grosso.

Este estudo é o primeiro trabalho experimental voltado à análise de processos de rugosidade de fundo em rios de regiões montanhosas brasileiras, oferecendo novas perspectivas para a compreensão e modelagem desses ambientes. Os resultados confirmaram conceitos clássicos de transporte de sedimentos, como seleção granulométrica, formação de “*armoring*” e existência de vazão crítica para mobilização de partículas, contribuindo para o avanço do conhecimento em hidráulica de canais e para o aprimoramento da parametrização de modelos numéricos aplicados a sistemas naturais.

BED ROUGHNESS IN GRAVEL-BED RIVERS: CHANNEL-SCALE RESPONSES TO FLOW AND SEDIMENT DYNAMICS

Abstract: Understanding flow resistance is fundamental for both scientific research and the development of engineering applications in fluvial systems. Accurate estimation is crucial for assessing flood magnitude, predicting ecological habitats, estimating sediment transport, and analyzing river morphodynamics. However, natural gravel beds exhibit complex three-dimensional organization, shaped by continuous processes of transport, deposition, and sediment reworking during flow events. This study investigates bed roughness behavior under sediment supply suppression in gravel-bed channels, assessing its variation with flow conditions and sediment dynamics. Experiments were conducted in a 10 m-long, 0.56 m-wide rectangular flume with a mobile bed, divided into two phases. In Phase 1, a morphologically stable bed configuration was established, achieving equilibrium and consistent sediment transport under a given discharge. Preliminary bed stabilization proved essential, as material adjustment and fine sediment infilling significantly influenced hydraulic response. In Phase 2, the hydraulic roughness of the stabilized bed was evaluated. Results showed that flow resistance decreases with increasing relative submergence, whereas low-flow and low-submergence conditions led to higher roughness due to bed microtopography and armoring layer development. Empirical equations underestimated resistance under high relative roughness, indicating the need for more specific formulations. Importantly, this is among the first experimental studies addressing bed roughness processes for a Brazilian mountainous river, providing novel insights for similar environments. The study also confirmed classical sediment transport concepts, such as grain-size sorting, armoring formation, and a critical discharge threshold for sediment mobilization. These findings contribute to improved parameterization of numerical models and advance the understanding of fluvial hydraulics.

Keywords: Physical modeling, Sediment transport, Bed roughness, Flow resistance.

4.1 INTRODUCTION

4.1.1 Roughness in gravel-bed rivers

The understanding of flow resistance is of great interest both for scientific research and for the development of technical projects in river engineering. Estimating this resistance is essential for determining flood magnitudes, predicting ecological habitats, estimating sediment transport rates, and understanding river morphodynamics. However, the hydraulics of gravel-bed channels remains relatively poorly understood (Ferguson, 2007).

Much of the fundamental knowledge in fluid dynamics that underpins conventional approaches to predicting flow resistance has been developed based on regular geometries (Nicosia, Carollo, & Ferro, 2023). This poses a significant challenge, as gravel-bed channels exhibit multiscale topographic features, where both individual grains and grain assemblages ('forms') on the bed surface contribute variably to the total flow resistance across different channel types.

In this context, conventional empirical approaches—based solely on grain diameter - should ideally be replaced by methods that consider multiple scales (Adams, 2020). The decomposition of roughness elements across different scales, or the consideration of both grain and form roughness through detailed bed surface surveys, can contribute to a better understanding of channel morphodynamics, as energy dissipation is increasingly recognized as a key driver of fluvial system behavior (Church & Ferguson, 2015).

According to Ancey (2020), the partitioning of bed shear stress between grain-scale and form-scale elements is an essential step for predicting bedload transport. However, this partitioning is non-trivial, as both flow and sediment dynamics interact with these elements simultaneously, jointly defining bed roughness. Only when roughness acts as an obstacle to flow does the grain-scale contribution become more direct. In this sense, the present study seeks to understand this combined influence, as riverbed roughness depends on the interaction of both factors.

Several authors have highlighted many challenges associated with estimating bed roughness. Ferguson et al. (2024) emphasize that the calibration and testing of new flow resistance prediction methods require flow data from reaches with well-characterized roughness statistics. This need should be addressed in part through field measurements or

physical modeling of such areas, but also through laboratory flume experiments and numerical simulations using synthetic roughness (Ferguson et al., 2024). Recently, Dey and Ali (2024) conducted a comprehensive review of studies addressing turbulence in canonical flows and provided an overview of roughness height—e.g., Nikuradse's equivalent sand roughness ks or the root-mean-square value k_{rms} (Shockling et al., 2006)—and its relationship with wall topography. Their work emphasizes that, despite notable advances, a major challenge remains in reliably estimating ks. Furthermore, the phenomenological theory of turbulence has recently been applied to explore the origin of friction in fluvial hydraulics (Ali and Dey, 2018).

However, in the context of physical modeling studies, care must be taken to ensure that the bed adequately represents prototype flow conditions. Studies such as those by Menezes and Borges (2025) and Padhi et al. (2018) emphasize that laboratory experiments simulating gravel-bed channels should be conducted using beds that have already been exposed to flow, allowing the grains to be rearranged.

This is because the surface topography of a natural gravel bed exhibits a spatially three-dimensional organization - such as orientation, alignment, spacing, and clustering of gravel deposits - which is shaped by transport processes as a result of continuous deposition and reworking by multiple flow events. Thus, in a natural river, the gravel bed is actively shaped by the flow itself.

In the context of sediment transport, friction plays a pivotal role in revealing the scaling laws governing sediment dynamics (Ali and Dey, 2017). The authors demonstrated that, for the incipient motion of sediment particles, the densimetric Froude number follows a specific scaling law with relative roughness (defined as the ratio between particle diameter and approach flow depth).

4.1.2 Sediment supply in gravel-bed rivers

In steep mountain rivers, channel morphology evolves in response to hydraulic conditions and sediment supply over a range of spatial scales (Llena et al. 2020). According to Weichert et al. (2009), these adjustments span from grain-scale surface armoring to variations in channel gradient, the latter being influenced by the stability of surrounding hillslopes and the presence of bedrock exposures at the reach scale. The interplay between flow resistance, sediment transport, and bed stability in such systems has been the subject

of considerable research within geomorphology and river engineering (e. g. Powell, 2014; Comiti and Mao, 2012; Lamb et al. 2017).

The scales of response to changes in sediment supply are commonly investigated at the grain scale, bedform scale, and reach or section scale. To examine the grain-scale response to variations in sediment supply, Dietrich et al. (1989) conducted experiments in a flat-bed flume and observed that a 90% reduction in sediment feed rate led to a 32% increase in the median grain size of the surface layer. These authors proposed q*, defined as the ratio between the predicted sediment transport with and without the development of an armored bed surface.

$$q^* = \left(\frac{\tau_b - \tau_{cs}}{\tau_b - \tau_{ct}}\right)^{1.5} \quad (1)$$

Where, q* is the transport ratio, τb is the boundary shear stress estimated using the shear stress equation (ρgdS, where ρ is the water density, g is the gravitational acceleration, d is flow depth, and S is the energy slope), τcs is the critical shear stress for the surface material, and τct is the critical shear stress for the material being transported on the bed.

When q* = 1, the sediment supply is so high that no surface armoring develops; when q*=0, no sediment is being transported. Lisle (1995) observed a similar, though more pronounced, textural adjustment in flume experiments simulating braided rivers. A 90% reduction in sediment feed rate resulted in a 62% increase in median surface grain size.

In addition to the coarsening of the bed surface, a reduction in sediment supply—or, as shown by Church, Hassan, and Wolcott (1998), the complete elimination of sediment input - can also contribute to the development of bed surface structures. Laboratory experiments by Mazumder, Ghosal, and Dalal (2005) showed that suspension concentration increases with bed roughness up to a certain point, then decreases as roughness continues to rise. This indicates that a higher fraction of coarse sediment and particle trapping prevent grains from being entrained into suspension, defining a “critical bed roughness.

Hassan and Church (2000) investigated reduced sediment feed rates over a previously armored and structured bed. They found that increasing sediment supply led to a reduction in surface armoring, but the underlying bed structures remained relatively unchanged.

This suggests that bed structures may play a more significant role in channel stability across a wider range of sediment supply variations than surface armoring alone. Sengupta (1979) showed that the coarser grains resist erosion due to their weight, while the finer grains are either insufficient in quantity or too homogeneous to be eroded. This grain-size sorting occurs at the bed surface and is directly linked to bedform migration (Sengupta, 1979).

Iseya and Ikeda (1987) and Lisle et al. (1991) observed that the bed surface organized into three distinct textural zones in response to local variations in sediment supply. These zones included a smooth zone, composed mainly of sand over which gravel moved at high velocities; a congested zone, characterized by mostly immobile, interlocked gravel; and a transition zone (Iseya & Ikeda, 1987).

Similarly, field investigations by Dietrich et al. (2005) revealed that sediment transport rates were substantially higher over finer-textured surfaces than over coarser areas. A comparable response was documented by Smith (2004) in flume experiments, where the greatest transport rates were observed when fine-grained zones were longitudinally connected rather than spatially isolated.

Overall, the channel may respond in three principal ways: (1) through the formation of a surface armoring layer; (2) through the development of bed structures; or (3) through the formation of textural patches. High sediment supply inhibits the development of armoring and promotes surface fining, in which finer particles settle in the interstices between coarser grains (Lisle, 1982; Lisle & Hilton, 1992; Madej & Ozaki, 1996). This process reduces the roughness associated with gravel bars (Lisle, 1982; Buffington & Montgomery, 1999b; Kasai et al., 2004), thereby increasing the transport capacity (Buffington & Montgomery, 1999a; Lisle & Church, 2002). These findings point to a strong link between channel response and flow resistance.

Lisle et al. (2000) examined how a channel responds to changes in sediment supply at the reach scale and concluded that the response typically results from the interaction between channel morphology, local grain size, and flow dynamics, which together control bed mobility. Channels with high sediment supply exhibit larger extents of fully mobile beds, while those with low sediment supply are characterized by broader areas of partial

mobility. However, under both supply conditions, substantial portions of the channel displayed little or no mobility.

They also found that finer-grained areas were more sensitive to sediment supply variations, whereas coarser areas remained relatively stable. Two reach-scale parameters measured at bankfull discharge—the modified Shields number (θ) and Q*—showed a reasonable correlation with sediment supply. The modified Shields number (θ), which represents the ratio between tractive and gravitational forces acting on bed particles, is defined as:

$$\theta = \frac{\rho g d S_g}{g(\rho_s - \rho) D_{50s}} \quad (2)$$

Here, ρgdSg represents a modified boundary shear stress (τs), in which the channel slope (S) is replaced by Sg, the energy slope attributed specifically to grain resistance; ρs is the sediment density, and D_{50S} is the median grain size of the surface material.

Lisle et al. (2000) defined q* - a modified form based on Dietrich et al. (1989) - as the ratio between the predicted mean transport rate for the median grain size of the subsurface material, accounting for surface armoring, and the predicted transport rate assuming no armoring. Of the two reach-scale parameters analyzed, they concluded that q* was the more suitable metric, as it can be directly related to sediment supply variations and therefore may offer greater predictive capacity regarding channel response (Lisle et al., 2000).

A range of field and experimental studies have investigated the impacts of changes in sediment size on channel response, particularly sediment transport. Since Gilbert (1914), who observed that the addition of finer sediments increased the mobility of coarser grains, up to Dingle and Venditti (2023), who demonstrated through experiments that the flux of grain-size gap material is enhanced by sand deposition, making gravel beds mobile at the threshold of motion. Similarly, Jackson and Beschta (1984) added sand to their laboratory experiments and observed increases in gravel transport rates, as well as instability in previously stable riffles. Other studies (e.g., Church and Hassan, 2023) highlight the existence of the so-called grain size gap in sediment transport involving sand–gravel mixtures. Another factor raised by Dey and Ali (2018) is the influence of particle size,

particle exposure, and packing conditions under near-bed turbulent flow in controlling the bed shear stress required to initiate particle motion.

Wilcock et al. (2001) also found that higher sand content led to greater gravel transport rates, even when the proportion of gravel in the bed was reduced. Their findings suggest that the enhanced transport capacity associated with increased sand content may, in turn, limit the magnitude of channel response to large sediment inputs, as the channel becomes more efficient at evacuating excess material (Wilcock et al., 2001).

This study presents one of the first channel-scale experimental investigations of bed roughness dynamics in a Brazilian mountainous river, following Menezes and Borges (2025). In contrast to most previous research carried out in alpine or temperate environments, our experiments address rivers characterized by rainfall-driven hydrology and distinct channel slopes. This perspective provides novel insights into roughness processes under conditions that remain underrepresented in the literature. By advancing the understanding of roughness controls in such settings, the study contributes to improved parameterization of numerical models, thereby enhancing their reliability for flood risk assessment, habitat prediction, and sediment transport modeling in regions with similar hydro-geomorphological contexts. In this context, the present study aims to investigate the behavior of bed roughness in response to the suppression of sediment supply in a gravel-bed channel, and to estimate how bed roughness evolves under changing flow and sediment transport conditions.

4.2 MATERIAL AND METHODS

4.2.1 Experimental setup

The study was conducted in a laboratory flume located in the Fluvial Pavilion of the Density Current Research Center (NECOD) at the Hydraulic Research Institute (IPH) of the Federal University of Rio Grande do Sul (UFRGS). The facility comprises a rectangular channel measuring 10 m in length, 0.56 m in width, and 0.4 m in height (Figure 1). Further details are provided in Menezes and Borges (2025), which presents the previous stage of this research. In the present study, the main modification to the flume configuration concerns the length of the mobile bed (FM), defining an effective testing area of 3 m used for data collection, as illustrated in Figure 4-1.

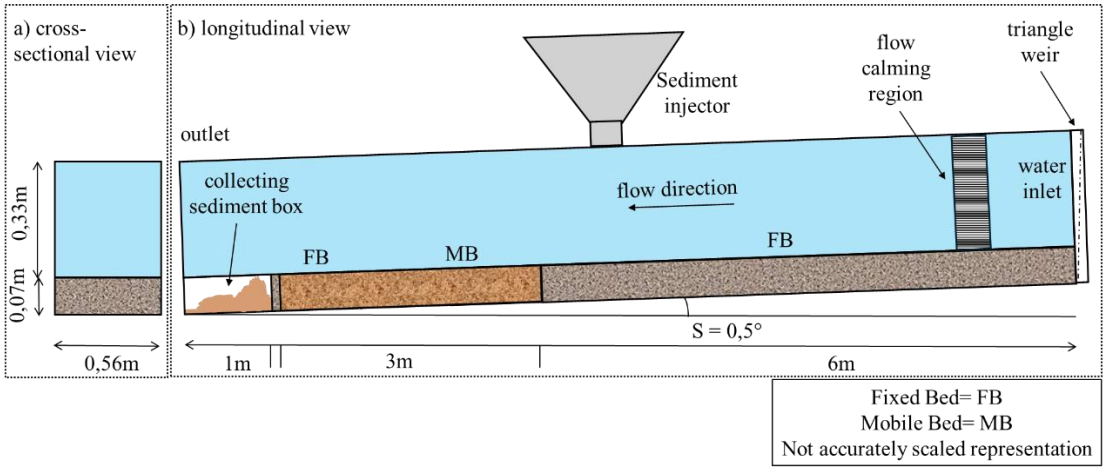


Figure 4-1 - Schematic representation of the experimental channel: a) cross and b) longitudinal view

4.2.2 Similarity Analysis

The sediment mixture used in the experiments was selected based on the grain-size characteristics of the Forqueta River, located in Maquiné/RS. A detailed description of a specific reach of this river is presented in Menezes (2021), which supported the design of the physical model. In this reach, the mean D_{50} of the bed material is 63.8 mm, corresponding to very coarse gravel. Additional characteristics can be found in Menezes (2021).

The same scaling approach adopted by Menezes and Borges (2025) was applied in the present study, including, for instance, the use of classic Froude similarity rules for open-channel liquid flows.

$$Fr = \frac{v}{\sqrt{gh}} \tag{3}$$

The geometric scale factor (r) was determined considering the dimensions of the experimental facility, specifically the channel width of 0.56 m.

$$r = \frac{L_{model}}{L_{natural}} \tag{4}$$

$$r^{\frac{3}{2}} = \frac{Q_{model}}{Q_{natural}} \tag{5}$$

$$r^{\frac{1}{2}} = \frac{U_{model}}{U_{natural}} \tag{6}$$

Following Menezes and Borges (2025), non-dimensionalization of all relevant variables shows that the scale factor for particle diameters can be taken as equal to the geometric

scale factor *r,* provided the model remains undistorted and the natural and model sediments have the same density. Table 4-1 presents the corresponding scaling relationships using a geometric scale of 1:20. This particular scale was selected due to the limited width of the experimental channel (0.56 m) and allows for uniformity between vertical and horizontal scaling.

Table 4-1 - Scale relationships between the model and the prototype

Parameter	Slope	Section Width	Diameter	Average Discharge	Flow Velocity
Symbol	(S)	(W)	(D_{50})	(Q_{med})	(U)
Model 1:20	0.00937m/m	0.56m	3,92mm	67L/min	0.22m/s
Prototype	0.00937m/m	11.2m	63mm	2m³/s	1.0m/s

4.2.3 Inlet Flow

As reported by Menezes and Borges (2025), the flow was introduced from a downstream reservoir with a 2,000-liter capacity, operating under a recirculating system. Flow rate (Q) was controlled and measured using a piezometer coupled with a 60° triangular weir installed at the channel inlet, which allowed determination of the water level on the weir (H). The calculated flow rate was then cross-checked with measurements at the channel outlet to calibrate the weir discharge coefficient. Following this, a flow rating curve was developed, with the coefficients a and b in Equation 3 determined by fitting the observed data using Excel Solver.

$$Q = aH^b \tag{7}$$

In this equation, a and n are dimensionless calibration parameters. Once these parameters are obtained, Equation 4 is established. Consequently, the flow rate (Q, in L/min) entering the channel can be determined from the water level on the weir (H, in cm) using the formulation described by Menezes and Borges (2025).

$$Q = 0.60067H^{\frac{5}{2}} \tag{8}$$

4.2.4 Characterization of the Movable Bed (MB)

For the composition of the MB, sand and gravel (D50 = 3.92 mm) were used, based on the granulometry of the prototype. Figure 4-2 shows the grain size distribution of the material used. The material was placed inside the channel, and an initial thalweg was manually excavated in the channel to guide the flow.

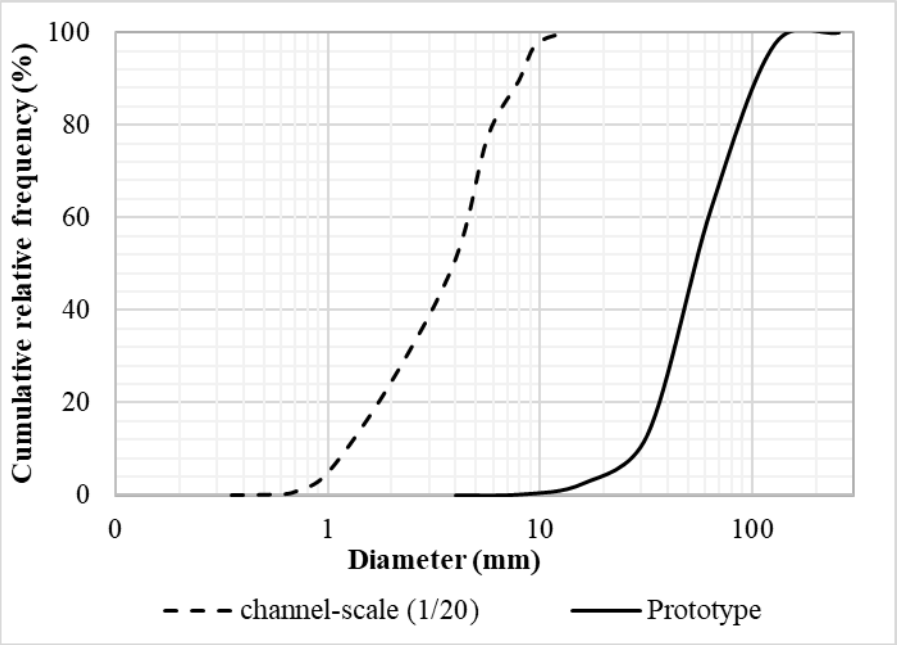


Figure 4-2 - Grain size distribution curve of the material for the channel's movable bed

4.2.5 Measurement of channel bed deformations

A laser profilometer was employed to measure deformations in the mobile bed, with further details provided in Menezes and Borges (2025). To assess the texture of the resulting cross-section, a surface roughness indicator was calculated, taking into account both grain size and bed morphology. This metric, named the Transverse Section Bed Elevation Oscillation Factor (FO), is based on the approach proposed by Bogatin et al. (2013). FO is obtained by dividing the length of the laser-scanned surface (Ll) within a given section by the channel width (L).

$$FO = \frac{L_l}{L} \tag{9}$$

The arithmetic absolute roughness (Ra) was calculated using equation 10

$$\mathrm{Ra} = \frac{1}{N}\sum_{i=1}^{N}|z_i - z| \tag{10}$$

Where N is the total number of points in the profile; z_i is the height of point i and z is the average height of the profile. Another analysis factor also considered was the standard deviation (σ)

$$\sigma = \sqrt{\frac{1}{N}\sum_{i=1}^{N}(z_i - z)^2} \quad (11)$$

In addition to these parameters, in each evaluated cross section (ST-40, 80, 120, 160, 220, and 260), bed elevation data obtained via profiler were organized in order to analyze bed roughness at the respective section. To assess this roughness, each elevation value was subtracted from the mean elevation of the section (the resulting values were converted to absolute values to ensure they were always positive), representing each bed fluctuation.

Following this step, these values were grouped into classes, to perform a frequency analyses classes used in the grain size distribution of sediments. Each measured bed elevation value (zi) was subtracted from the mean elevation of the corresponding cross-section (za), and only the absolute values of these differences were considered, i.e., |zi−za|. This dataset was then analyzed in terms of frequency of occurrence to represent fluctuations in channel bed elevations.

This allowed for counting how many values fell into each class (absolute frequency). Subsequently, the absolute frequency of each class was divided by the total number of data points to obtain the relative frequency of occurrence. Finally, each relative frequency was cumulatively summed to derive the cumulative relative frequency of occurrence.

Based on the cumulative relative frequency plotted for each class, thresholds corresponding to 90%, 84%, 50%, 16%, and 10% of occurrence were determined. These thresholds were then adopted as bed roughness coefficients (R), referred to respectively as R90, R84, R50, R16, and R10.

4.2.6 Collector box for transported material

A collector box was positioned at the downstream end of the experimental channel to capture the sediments transported during each test. The collected material was then dried in an oven at 105°C and analyzed granulometrically to determine its characteristic particle sizes (D10, D16, D50, D84, and D90).

4.2.7 Experimental Design

The experiments were divided into two phases based on preliminary tests carried out by Menezes and Borges (2025):

Phase 1: Morphological bed channel conformation. This phase aimed to achieve a morphological bed configuration in equilibrium, meaning that, at a given flow rate, bed adjustments did not lead to changes in sediment transport. For each fixed liquid discharge injected into the channel, a bed arrangement was established in which no further variations occurred. The equilibrium condition was verified by quantifying the transported sediment and was considered analogous to the behavior of a natural river, indicating that the mobile bed had adapted to a configuration consistent with the imposed flow.

During this stage, four tests were carried out, each lasting 5, 10, 15, and 20 hours, respectively (Table 4-2). Sediment was injected at a constant rate of 0.7 g/s, with particle sizes smaller than those of the bed material so that they would be partially transported by the flow. The grain size distribution of the injected sediment is presented in Figure 4-3. At the end of each test, the bed topography was surveyed and the transported sediments were collected for analysis.

Table 4-2 – Experiments design

Phase	Test	Discharge (L/min)	Total Test Duration (h)	Cumulative Time (h)	Injected Sediment Discharge (g/s)	Cumulative Injected Sediment (kg)
I - Morphological bed channel conformation	E1	366	5	5	0.7	12.6
	E2		5	10		25.2
	E3		5	15		37.8
	E4		5	20		50.4
II - Evaluation of channel bed roughness	E5	10.16	5	25	0	0
	E6	19.22	5	30		
	E7	40.7	5	35		
	E8	83.55	5	40		
	E9	105.37	5	45		
	E10	204.52	5	50		

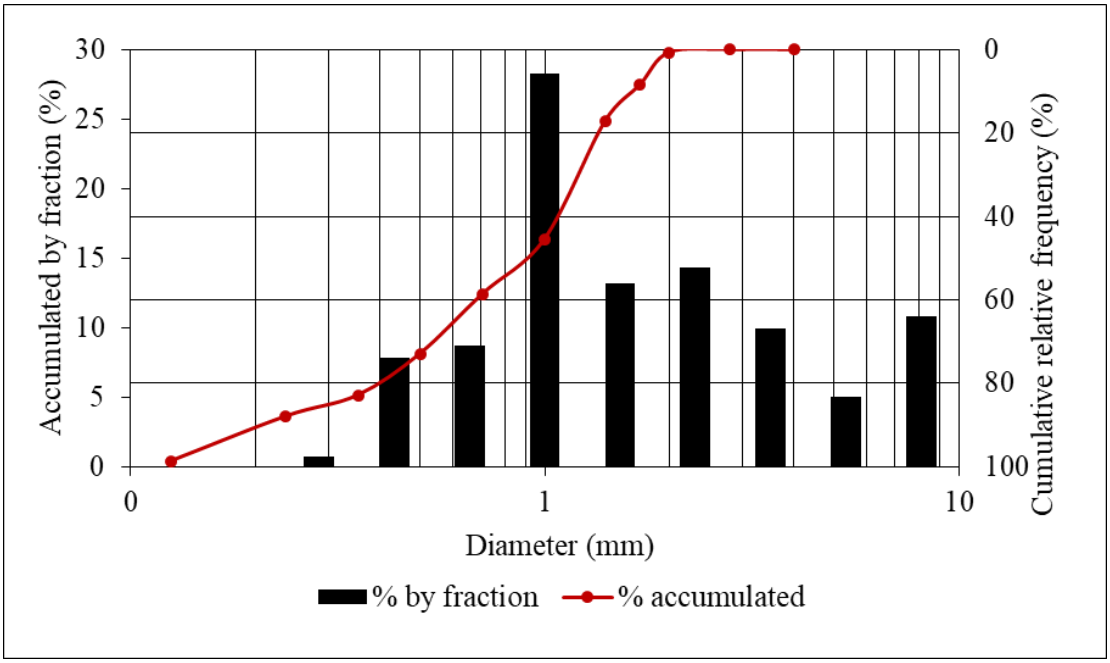


Figure 4-3 - Sediment inlet grain size distribution

Phase 2: Evaluation of channel bed roughness. In this phase, the interaction between water flow and sediment transport was examined under a channel bed roughness previously established in Phase 1, when sediment supply was introduced upstream of the section. Six experiments were conducted with progressively decreasing flow rates (Table 2) to enable the assessment of the roughness generated on the bed surface. After each run, the bed topography was surveyed, and the transported sediments were collected. Data acquired with the profiler were processed and visualized using Surfer software.

Figure 4-4 presents the flow rates applied in each experiment for Phases I and II. Phase I refers to tests conducted with constant flow rates, whereas Phase II comprises experiments in which the flow rate was progressively increased, starting from the lowest value introduced into the flume. The figure also depicts the sediment injection dynamics and the discontinuation of sediment supply from test 5 onward.

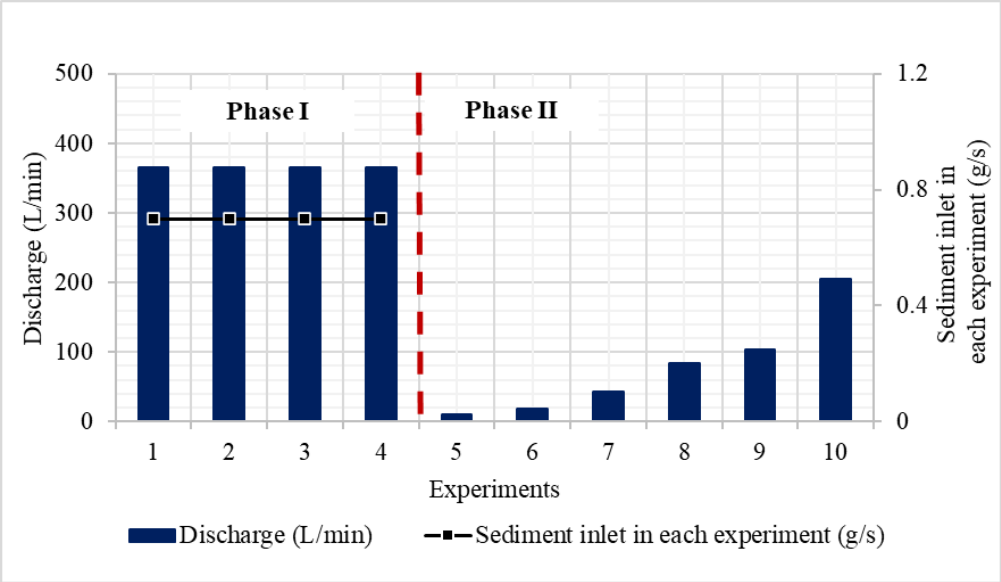


Figure 4-4 - Flow rate and sediment introduced into the channel during the experiments (Phases I and II)

4.3 RESULTS AND DISCUSSION

First, the results of the experiments conducted during Phase I are presented. This phase corresponds to the initial bed adjustment, during which both the flow discharge and sediment feed rate were kept constant in the flume. Based on this bed configuration, the behavior of the characteristic variables was analyzed throughout the tests.

Subsequently, the results from Phase II are presented, during which sediment feed was suppressed. In this phase, the flow discharge was varied, and sediment supply was discontinued.

Finally, the flow resistance parameters obtained in Phase II are analyzed, emphasizing their implications for the physical processes governing water and sediment transport, particularly the influence of bed roughness on channel dynamics.

4.3.1 Phase I: Bed conformation

To assess the effect of the initial bed conformation, the flow hydraulic variables and bed characteristics were obtained. This required, as a first step, the acquisition of bed elevation profiles for the evaluated sections and the water surface level for each experiment. For this reason, this section is divided into two subsections: 1 - Bed topography and water level for each experiment; 2 - Behavior of the variables throughout the experimental runs.

4.3.1.1 Bed topography and water level for each experiment

The bed topography was processed to establish the fundamental geometric relationships of the channel cross-section, thereby enabling the calculation of cross-sectional area (Am), wetted perimeter (Pm), and hydraulic radius (Rh). Appendix A presents the observed cross-sections for the experiments conducted during Phase I. As shown in all these cross-sections, there is an initial deposition of the injected sediment (initial thalweg gradually decreases in depth), which progressively propagates along the channel until reaching the final section (ST-260). In other words, a portion of the injected sediment is deposited, while the remainder is transported downstream.

It is important to note that the total duration of the experiment was defined based on the condition closest to equilibrium between the injected sediment and the sediment transported and collected at the channel outlet. Accordingly, at the end of Phase I (after 20 hours of testing), a mobile armored layer was observed. According to Parker and Klingeman (1982), this layer forms as a compensatory mechanism to balance the mobility of sand and gravel particles transported by the flow. Since coarse particles are naturally more resistant to mobilization than fine particles, they tend to become more prominent on the bed surface. In natural gravel-bed rivers, grain sizes larger than the median bed particle size are typically mobilized only during peak flood flows (Gilbert; Wilcox, 2024).

In addition to the data in Appendix A, digital elevation models were generated to represent the final bed surface after each experiment, enabling spatial analysis of bed behavior (Figure 4-5). The figure reveals sediment mobilization throughout the channel, with pronounced deposition particularly in the upstream third. A similar pattern was observed for the initial thalweg, which exhibited mild sediment accumulation over the course of the experiments.

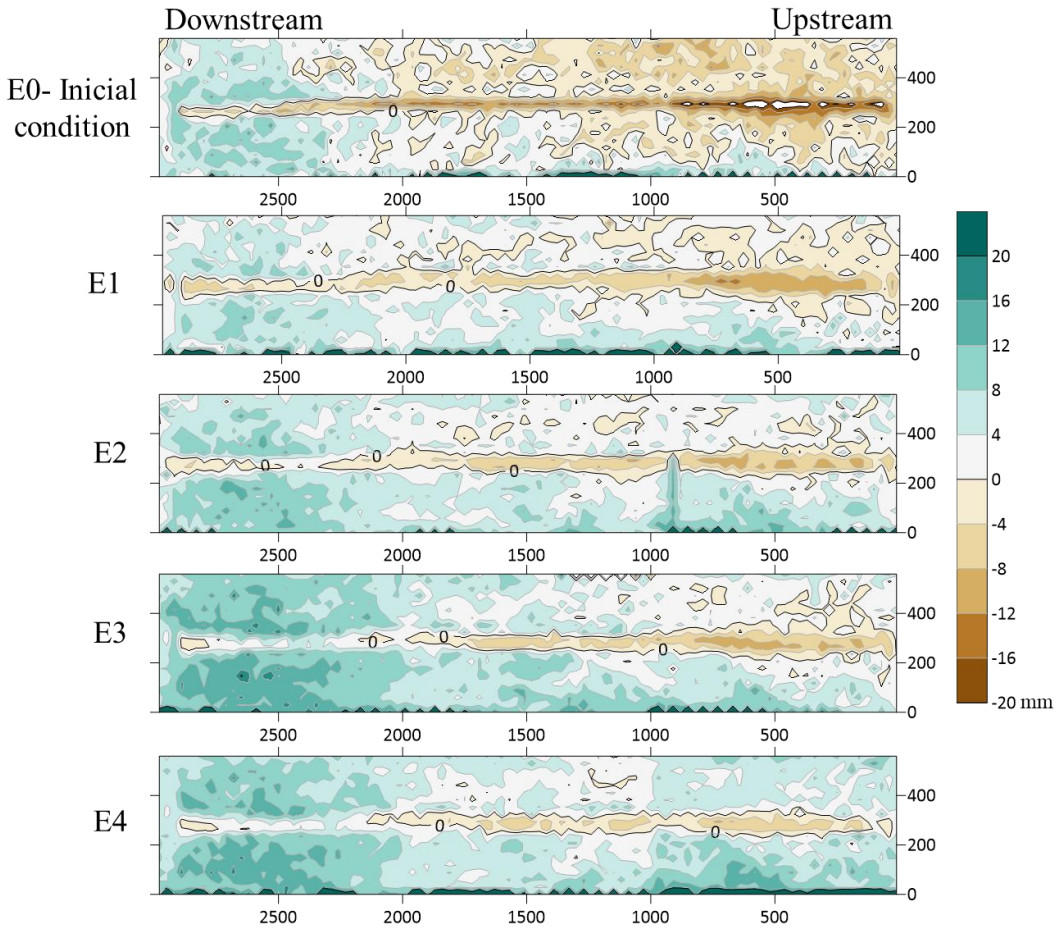


Figure 4-5 - Channel bed survey after Phase I experiments, both conducted with Q = 366 L/min and Qs = 0.7 g/s. All values shown in the figure are in millimeters

Based on the changes observed between the experiments, it is possible to evaluate the morphological alterations of the channel bed, which correspond to increases or decreases in roughness in response to new bed configurations. The quantitative values related to these changes are presented in Section 3.1.2.

4.3.1.2 Behavior of variables throughout the experiments

The geometric parameters of the cross-sections were determined to calculate the hydraulic variables related to flow velocity and flow resistance factors (Appendix B). Appendix B presents these variables for the six analysis sections across all four experiments. Based on the discharge value—which remained constant throughout the tests—velocity and other hydraulic variables were calculated.

Figure 4-6 shows the behavior of the parameters Pm, Rh, Am, and velocity (U) throughout the experiments. Test 1 exhibited more variable Pm values due to the initial arrangement of the sediment. In the subsequent tests, the variables tended toward equilibrium, as pore

spaces between the grains were gradually filled and the rates of sediment deposition and transport approached a steady state. This led to the conformation and rearrangement of the initial bed particles.

An analysis of these results underscores the importance of incorporating an initial bed conformation stage to facilitate particle rearrangement, alignment, and the infilling of pore spaces by finer particles. Similar observations were reported by Menezes and Borges (2025), who investigated the influence of initial bed shaping in flume experiments. Maintaining a flow rate characteristic of the modeled environment allowed the development of a channel bed with morphological features, sediment distribution, and flow paths more representative of natural river conditions. This provides a more robust and realistic basis for physical modeling studies of gravel-bed rivers with variable grain size distributions.

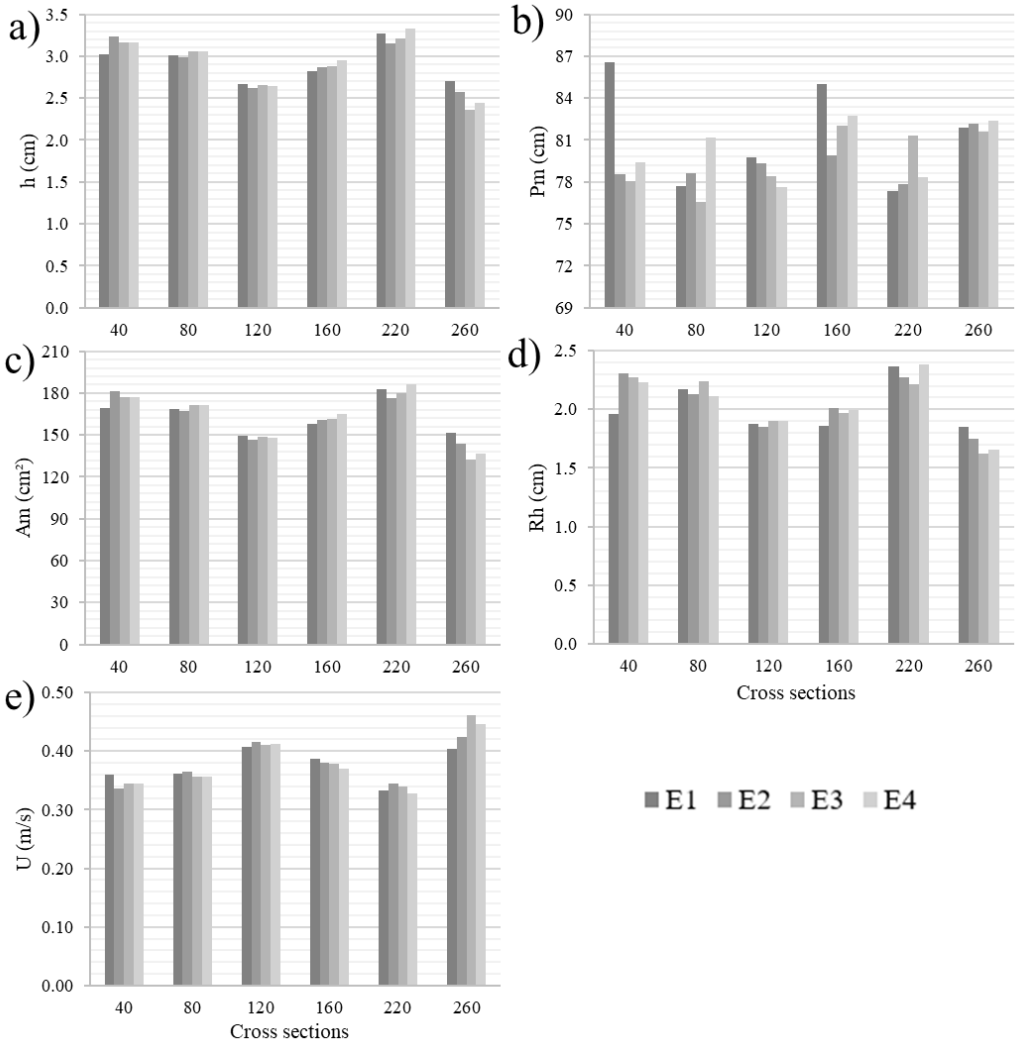


Figure 4-6 - Behavior of a) water depth (h), b) wetted perimeter (Pm); c) wetted area (Am), d) hydraulic radius (Rh), and e) velocity (U) along the cross-sections – Phase I

4.3.1.3 Bed roughness analysis

When analyzing bed roughness, we first extracted the oscillation factor and the standard deviation of bed elevation measurements recorded by the profiler (Figure 4-7). It can be observed that the initial state (E0) exhibited higher values, which were attenuated as the simulation progressed, as shown in the figure. However, section ST-260 showed an increase already in E1, which may be due to the absence of sediment deposition at this section, since the injected sediment was deposited along the upstream sections of the channel. Furthermore, the remaining sections exhibited relatively constant values throughout the subsequent experiments, with only minor variations.

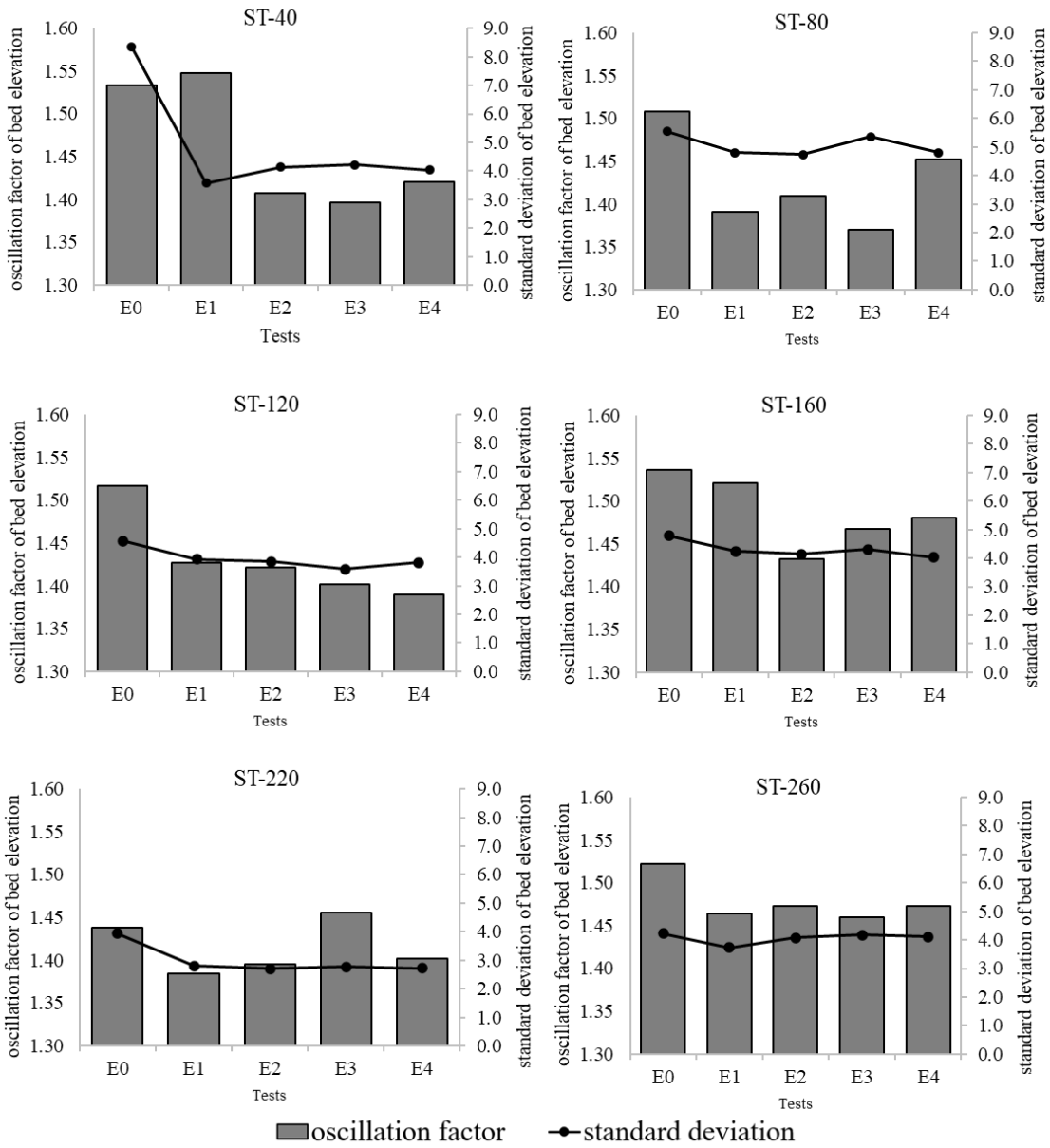


Figure 4-7 - Oscillation factor and standard deviation of bed elevation fluctuations - Phase I

For the calculation of the Manning roughness coefficient (n) and the Darcy–Weisbach friction factor (f), Equations 12 and 13 were used, respectively

$$n = \frac{1}{U} R_h^{\frac{2}{3}} S^{\frac{1}{2}} \tag{12}$$

$$f = 8 \frac{g\, S\, R_h}{U^2} \tag{13}$$

Here, U is the mean velocity in the cross-section (m/s), obtained from the continuity equation; Rh is the hydraulic radius of the section (m); S is the channel slope (0.0094 m/m); and g is the acceleration due to gravity (m/s²). Sections ST-120 and ST-260

exhibited the lowest values of n and f, as shown in Figure 4-8. On the other hand, sections ST-40 and ST-220 recorded the highest values. In ST-40, a localized erosion was observed, likely due to the interface between mobile and fixed bed sections, which may have influenced the roughness values. In contrast, ST-220 had a high concentration of coarser grains. These grains were more exposed (protruding) on the surface, which may have resulted in higher values of both f and n.

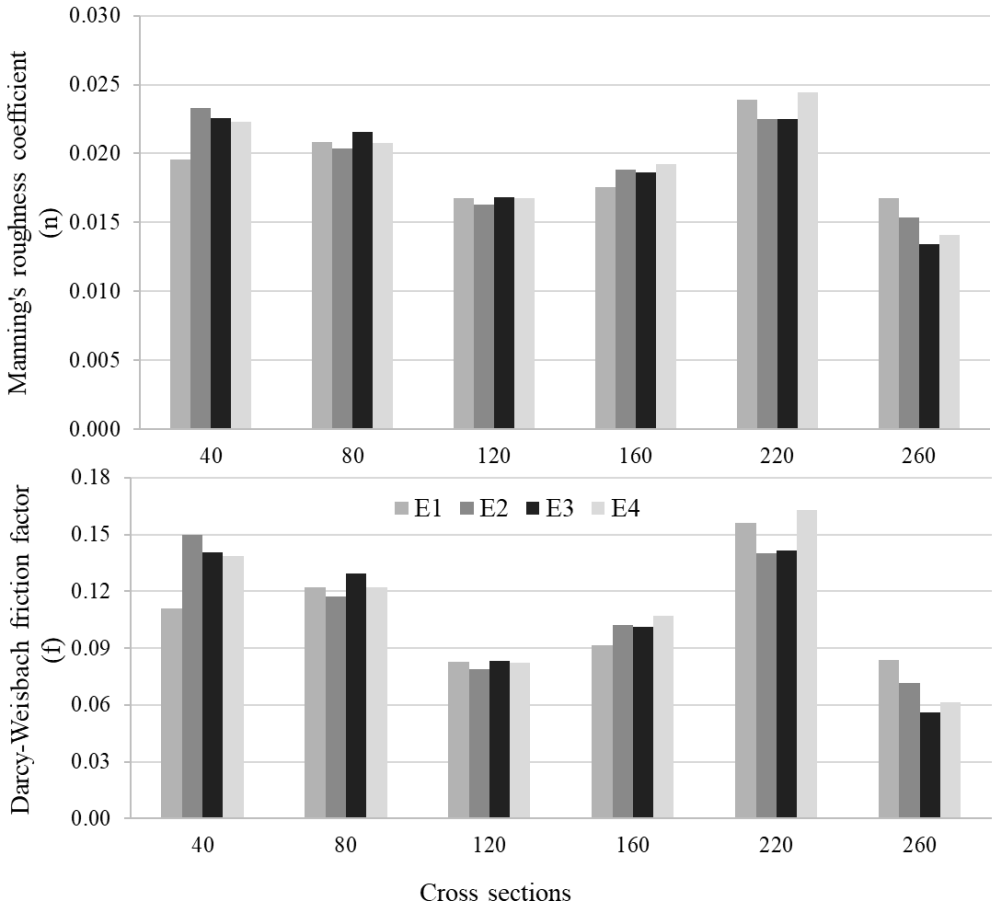


Figure 4-8 - Behavior of Manning's roughness coefficient (n) and Darcy-Weisbach friction factor (f) – Phase I

4.3.2 Phase II: suppression of sediment injection

Once again, bed elevation profiles were obtained for the evaluated sections, along with water level measurements taken during each experiment at every section and vertical. For this reason, this section is divided into two subsections: 1 – Bed topography and water level for each experiment, 2 – Behavior of the variables throughout the experiments, and 3 – Bed roughness analysis.

4.3.2.1 Bed topography and water level

As previously mentioned, the channel bed topography was processed in order to establish the basic geometric relationships of the cross-sections. Thus, it was possible to directly obtain data for Am, Pm, and Rh.

Appendix C presents the cross-sections observed during the experiments conducted in Phase II. As shown in these sections, there was an initial deposition of the injected sediment, which propagated along the channel throughout the experiments, eventually reaching the final section (ST-260).

In conjunction with Appendix D, the bed surface behavior was analyzed using the profiler data (Figure 4-9). The figure reveals that sediment mobilization occurred throughout the entire channel, with a greater emphasis on sediment deposition, particularly in the first third of the channel. A similar pattern was observed for the initial thalweg, which exhibited slight sediment deposition over the course of the experiments.

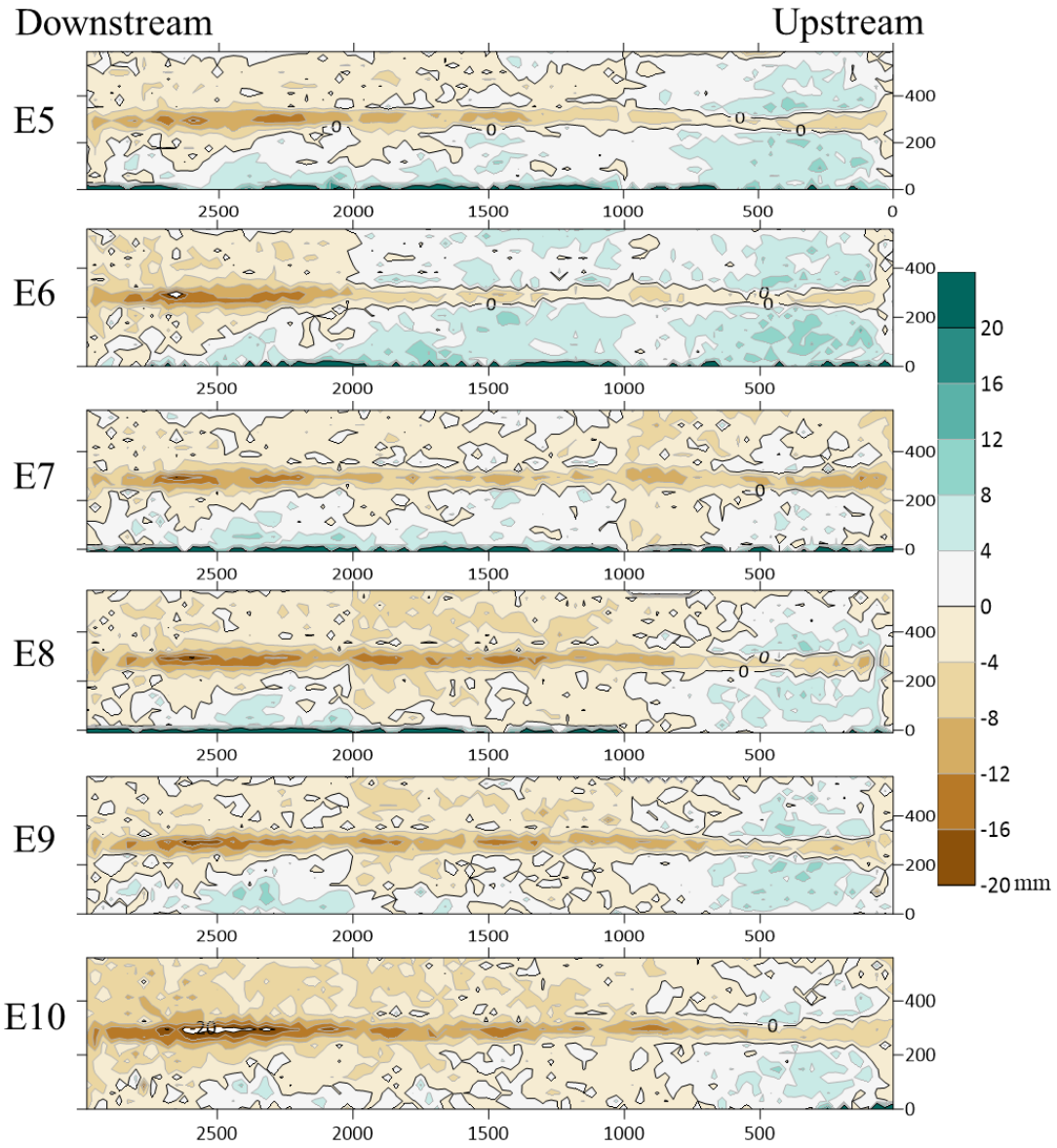


Figure 4-9 - Channel bed elevation survey after tests from Phase II experiments. All values shown in the figure are in millimeters

4.3.2.2 Behavior of the variables throughout the experiments

Based on the discharge values for each experiment, flow velocity and other hydraulic variables were computed. In this phase of the experimental set, discharge values were gradually increased in order to observe the relative submergence of the bed under the flow.

In the initial experiments (E5 and E6), discharge was very low. At the beginning, the water flow was concentrated in the main thalweg, and a layer of fine sediments—originating from Part I of the experiment—was deposited on the channel bed. Over time, discharge gradually increased, along with values of hydraulic radius (Rh), which ranged

from 0.27 cm in ST-220 (E5) to 1.75 cm in ST-80 (E10), and wetted perimeter (Pm), which ranged from 12.43 cm in ST-260 (E5) to 83.42 cm in ST-40 (E9) (Figure 4-10).

Flow velocity values increased steadily with rising discharge, as did the flow area and depth. However, this trend does not apply to the velocity values measured at ST-220 and ST-260 in E5. In these cases, due to the shallow water depth associated with the low discharge of 10 L/min, the flow was confined to an initial thalweg, which may have resulted in higher velocity values.

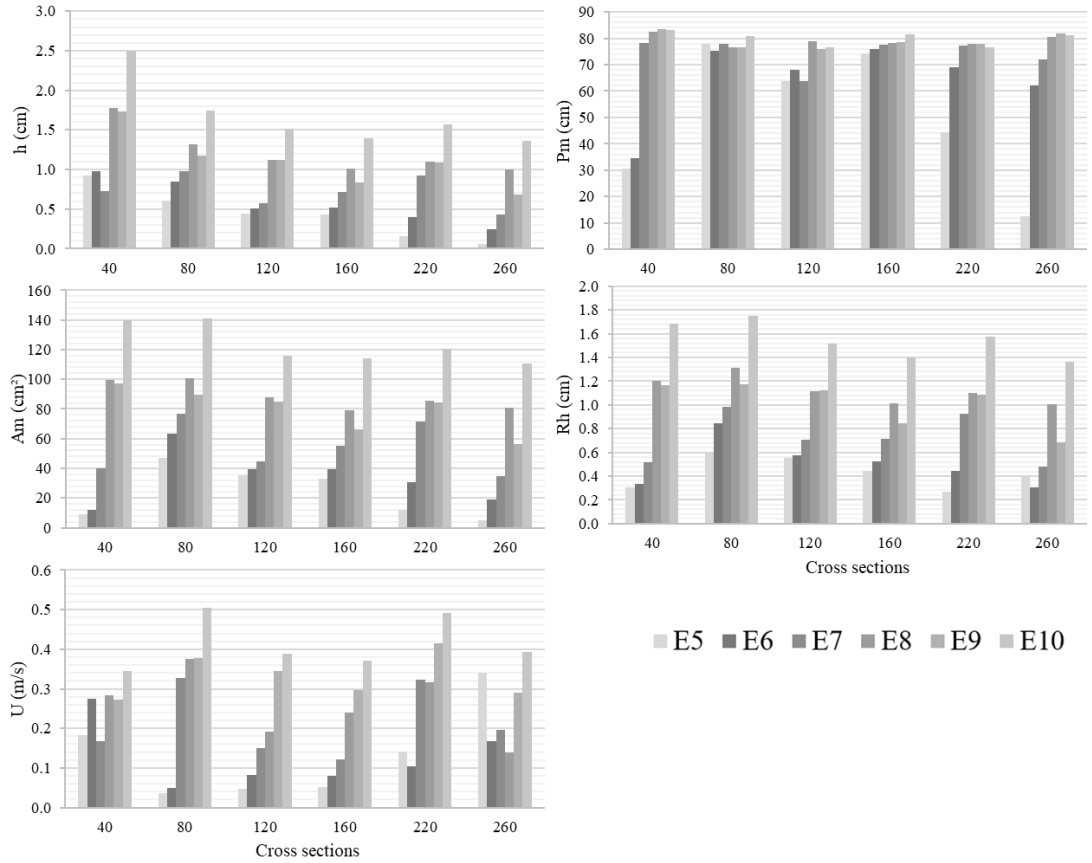


Figure 4-10 - Behavior of a) water depth (h), b) wetted perimeter (Pm); c) wetted area (Am), d) hydraulic radius (Rh), and e) velocity (U) along the cross-sections – Phase II

4.3.2.3 Bed roughness analysis

An analysis of Figure 4-11 reveals a slight increase in the Oscillation Factor (FO) and the standard deviation of the bed elevation in sections ST-160 and ST-260. In these two sections, surface roughening was observed over the course of the experiments, caused by the exposure of larger grains and the definition of the thalweg, which became more pronounced as the experiments progressed. In ST-40, once again, the downstream

boundary condition may have influenced the higher values observed. In contrast, ST-80, ST-120, and ST-220 exhibited more stable values throughout.

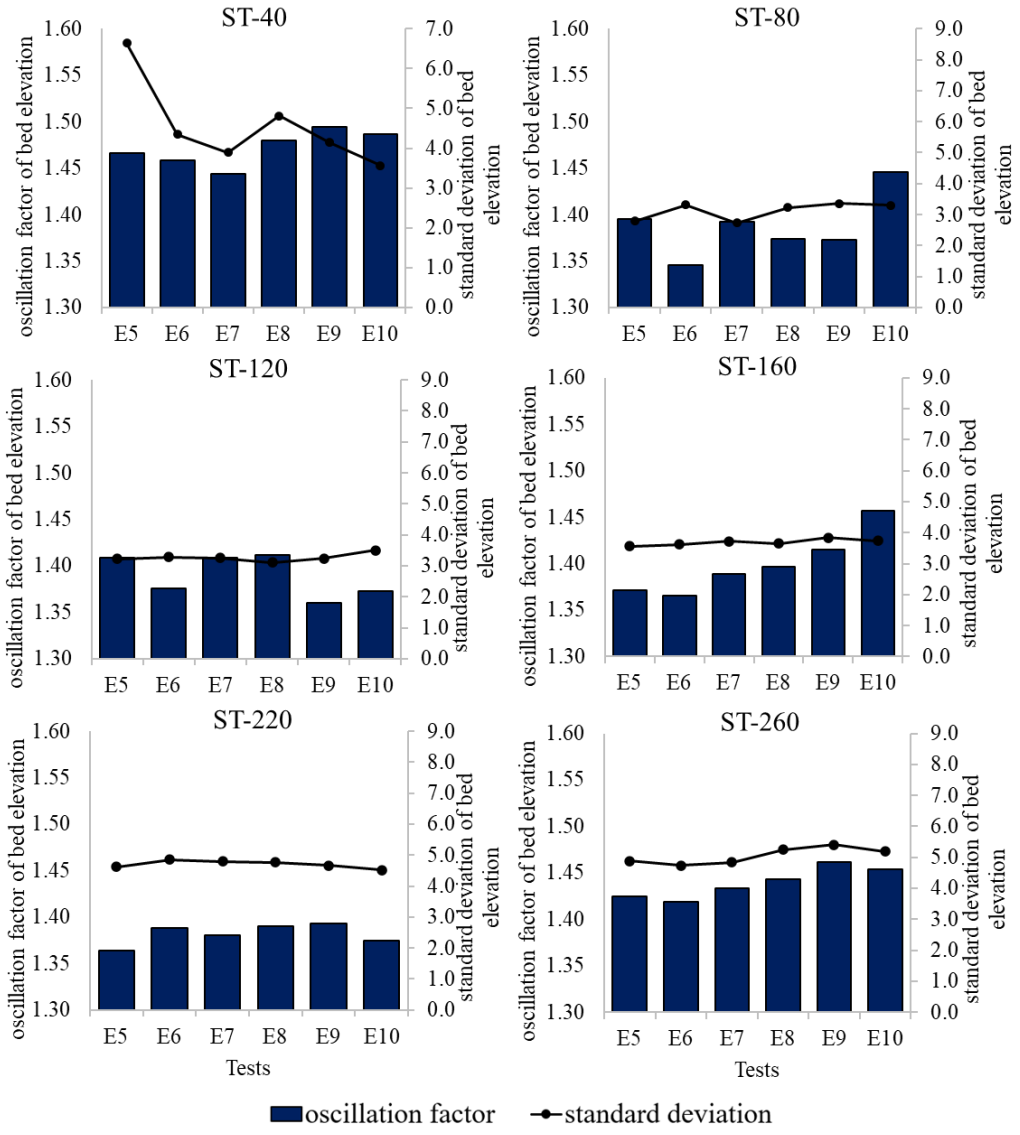


Figure 4-11 - Oscillation factor and standard deviation of bed elevation variations - Phase II

Regarding n values sections ST-120 and ST-160 exhibited similar behavior (Figure 4-12). However, ST-40 exhibited a distinct pattern due to upstream channel conditions, which altered the flow and caused slight localized erosion at the interface where the bed material changed. The same factor may have influenced the behavior of the variables at ST-220 and ST-260, as these locations may have been affected by downstream channel conditions.

The highest values of n were recorded at ST-80 during E5 and E6, with values of 0.09 and 0.08, respectively. In contrast, the lowest value of n was observed at ST-260 during E5 (0.007).

The behavior of the f showed considerable variation. The highest f values occurred at ST-80 during E5 and E6, reaching 3.47 and 2.44, respectively. These values are significantly higher than those at other locations and may be associated with the greater water depth observed at this section compared to upstream and downstream locations.

On the other hand, the lowest f value was also recorded at ST-260 during E5. This outcome was expected, as discharge in E5 was low and the flow at ST-260 was concentrated in the main thalweg of the section.

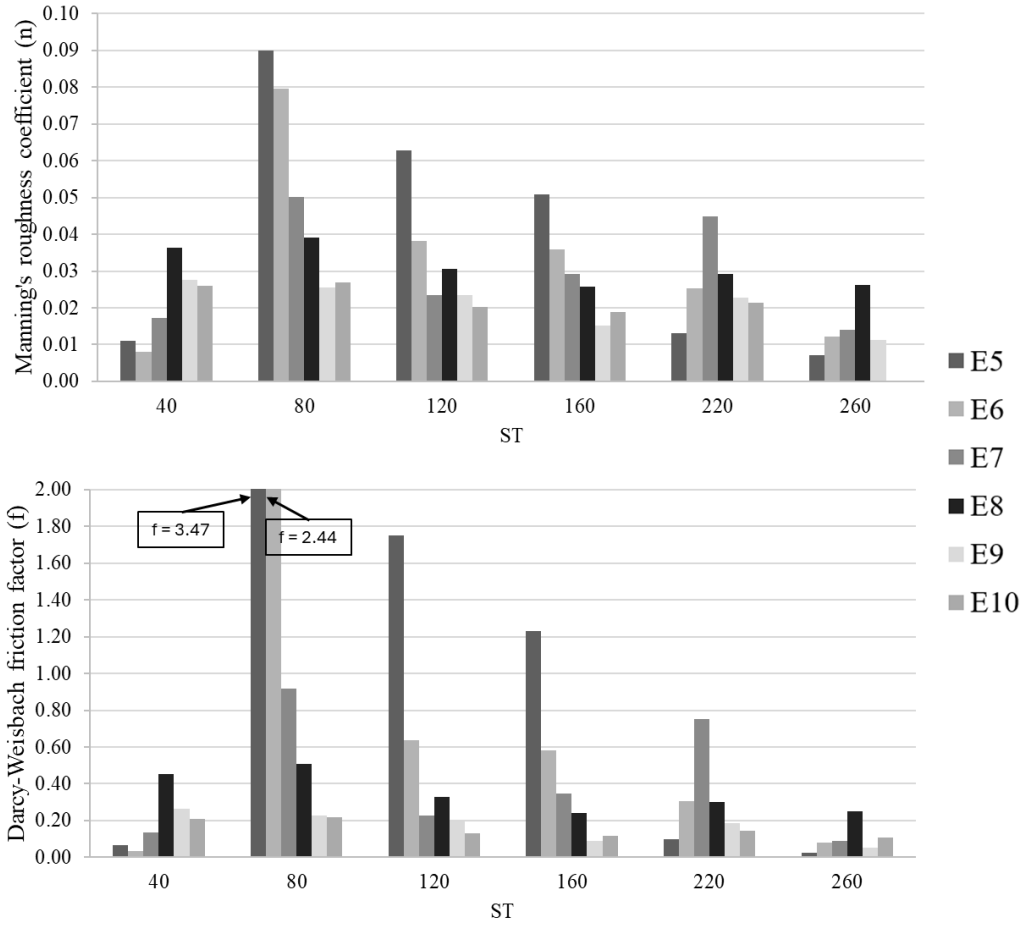


Figure 4-12 - Behavior of Manning's roughness coefficient (n) and Darcy-Weisbach friction factor (f) – Phase II

4.3.3 Flow resistance parameters

4.3.3.1 Bed roughness variation

To analyze flow resistance, we first quantified variations in bed roughness. As described in Section 2.5, bed deformations were calculated based on their relative cumulative frequency.

The resulting distributions are shown in Figure 4-13. From these distributions, the values corresponding to the 90th, 84th, 50th, 16th, and 10th percentiles of |zi − za| were calculated. In this study, these thresholds were adopted as bed roughness coefficients (R), referred to respectively as R90, R84, R50, R16, and R10. Based on this analysis, Figure 14 presents the R84 and R50 coefficients, corresponding to the 84th and 50th percentiles, respectively.

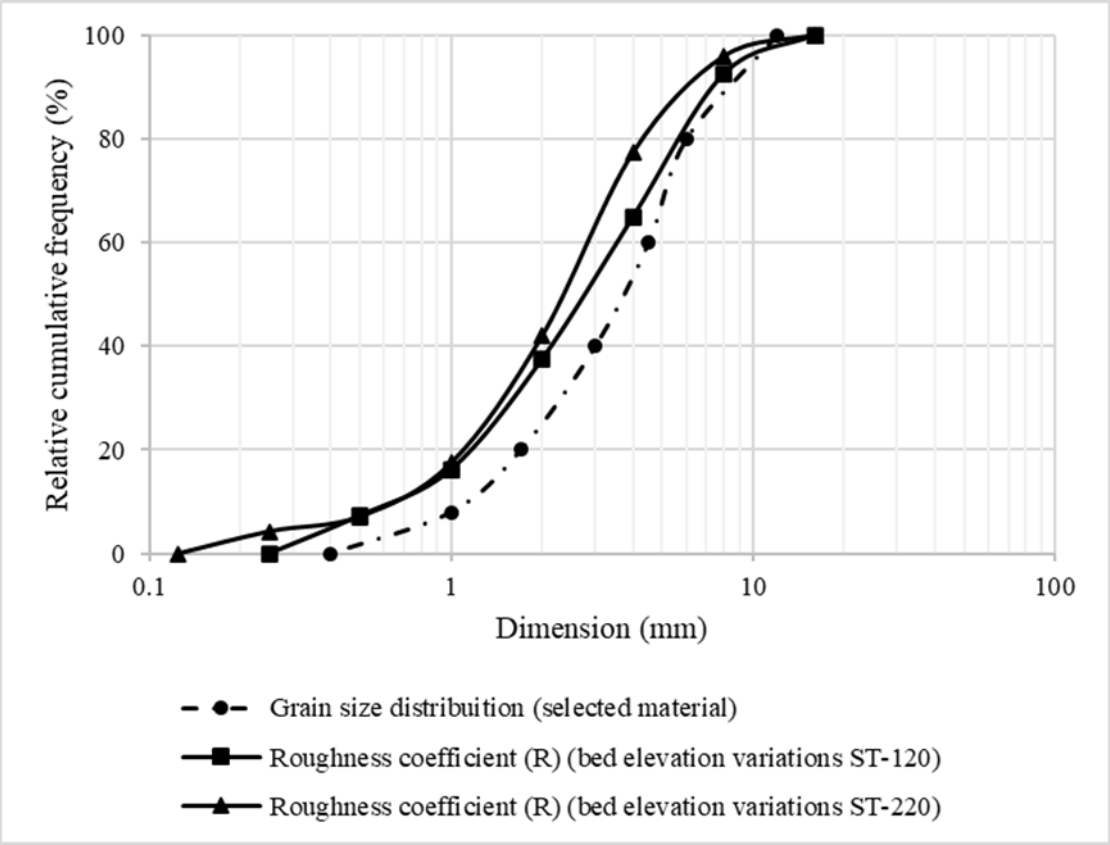


Figure 4-13 - Comparison between the initial sediment distribution (selected material) and the distribution of bed elevation fluctuations (here referred to as roughness coefficient - R) for ST-120 and ST-220

The variation in roughness values: arithmetic absolute (eq 10), root mean square (eq 11), R84 and R50 coefficients between the tests and between sections in each test was notable from Phase I to Phase II, particularly in ST-80 and ST-220, as shown in Figure 4-14. The

coefficients are plotted together to allow a comparative evaluation of their ability to describe bed roughness. The R84 values were more sensitive to bed variation than R50, as the latter represents the cumulative frequency of bed elevation fluctuations at 50%.

In ST-80, the effect of discharge on the roughness values in Phase II cannot be disregarded, since Q was lower compared to Phase I. A similar pattern was also observed in ST-120 and ST-160, although in a more subtle manner. In contrast, in ST-220 and ST-260, the opposite trend was observed: roughness variation was lower in Phase I and higher (with an increasing trend) in Phase II. This behavior may be related to the deposition of the injected sediments during the tests in Phase I. The injected sediments settled in the channel, filling the existing voids and forming armoring on the channel bed, which consequently reduced the roughness variation values. In Phase II, with no further sediment being injected, only transport of existing sediment occurred. As the discharge (Q) increased in each successive test of Phase II, the flow had more energy to carry sediment, leading to the washing out of finer sediments (previously deposited in Phase I), leaving only larger and heavier grains behind. These coarser grains projected prominently from the bed surface, increasing the channel roughness in these sections.

It is important to note that in gravel-bed rivers, where measuring hydraulic variables presents practical limitations, flow resistance is often estimated solely based on a vertical roughness scale, such as grain diameter (Ferguson, 2007). However, as pointed out by Adams (2020), the relationship between grain diameter and flow resistance is not held in natural channels for two main reasons: (1) grain diameter does not account for larger, often more dissipative roughness elements, and (2) it does not consider the horizontal spacing of those elements, which systematically influences flow.

In recent years, the increased availability of high-resolution topographic data has led to the adoption of the standard deviation (σz) of bed elevation as a roughness metric for gravel-bed rivers, as this metric captures information about larger-scale bed structures (Chen et al., 2020). Accordingly, the data shown in Figure 4-14 were organized by section to track the evolution of bed modifications along the channel and to represent bed roughness under different discharge conditions.

It is observed that in sections ST-80, ST-120, and ST-140, roughness values were higher in Phase I. These sections are located in the central portion of the channel, away from the

influence of upstream and downstream boundary conditions, which affect ST-40, ST-220, and ST-260.

This behavior is expected, as this stage is characterized by grain rearrangement and ongoing pore space filling. Additionally, the grains are not yet aligned with the flow or gravity; they have merely been "placed" in the channel. In Phase II, this accommodation process has already occurred, and due to the small discharges, that transport finer sediments, armoring of the bed occurs, contributing to a reduction in bed roughness.

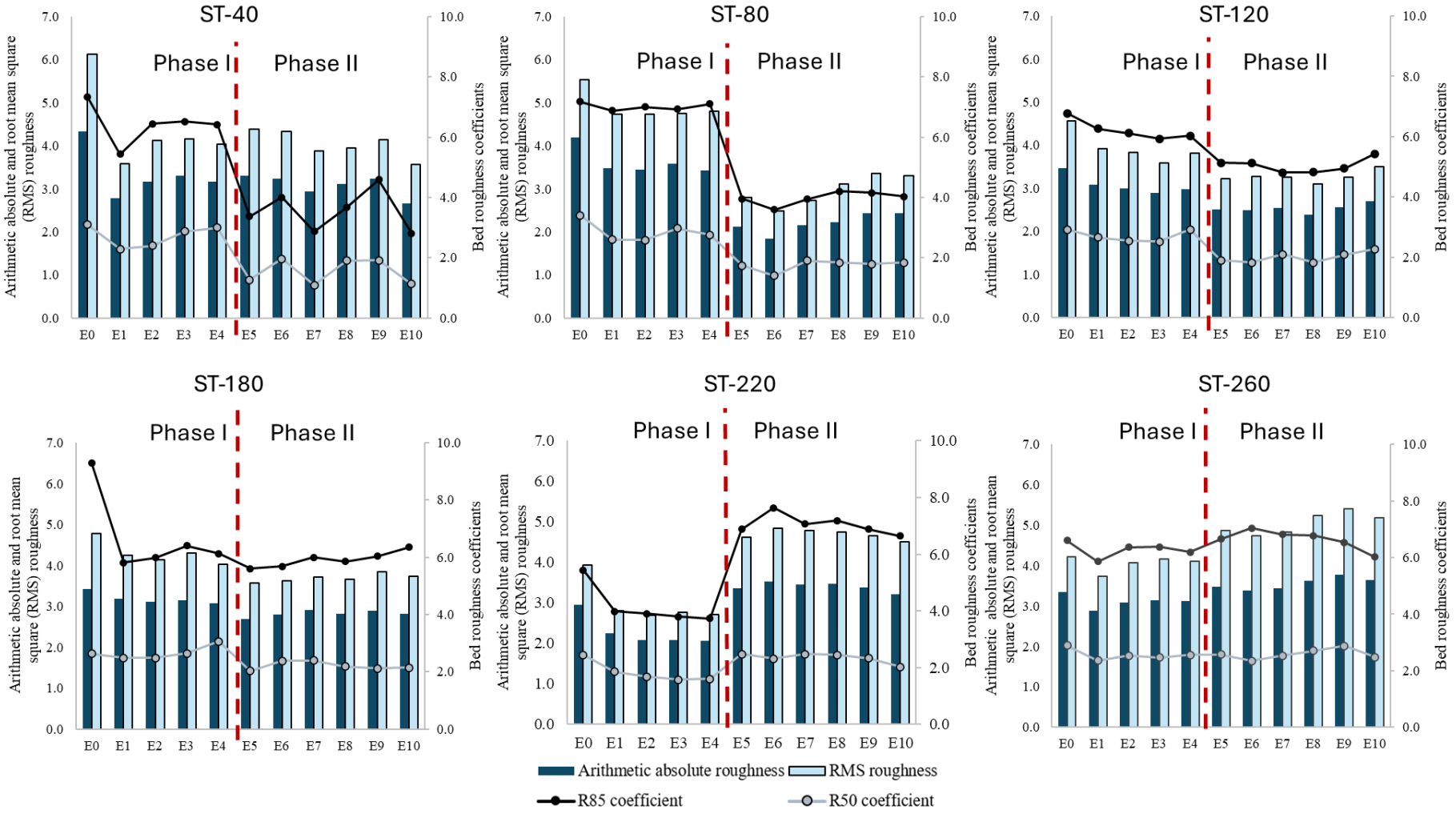


Figure 4-14 - Roughness values: arithmetic absolute, root mean square and bed roughness coefficients R_{84} and R_{50} obtained after each test

4.3.3.2 Flow resistance variables

As previously highlighted, Phase I corresponds to a bed adjustment stage during which the sediment particles reorganize and are subjected for the first time to the action of flow, seeking a new state of equilibrium. Only after this initial phase is it possible to evaluate other flow characteristics that more accurately represent the dynamics of natural environments. In this context, the Manning's roughness coefficient (n) and the Darcy–Weisbach friction factor (f) were analyzed to understand how the bed reorganized after Phase I and how such reconfiguration influenced the flow conditions.

As shown in Figure 4-15, hydraulic radius (Rh) values increased consistently from test E5 to E10, accompanying the increase in discharge. In contrast, n appeared to be influenced by upstream and downstream boundary conditions. Sections ST-40, ST-220, and ST-260 show lower n values in tests E5, E6, and E7 (except for ST-220), which may be attributed to the flow being concentrated primarily along the thalweg due to the low discharge. In the remaining tests (E8 to E10), n values decreased as discharge increased—an expected behavior observed in sections ST-80, ST-120, and ST-160, which are centrally located within the channel and less affected by inlet and outlet constraints.

These results suggest that flow resistance, as expressed by n, decreases with increasing discharge. However, qualitative observations during the experiments indicated the opposite trend: as the discharge increased, the bed surface appeared rougher and devoid of fine particles, since no additional sediment was supplied to the channel during Phase II. This apparent contradiction may be associated with the high sensitivity of the Manning coefficient to discharge, which can overshadow the influence of bed surface characteristics in its estimation.

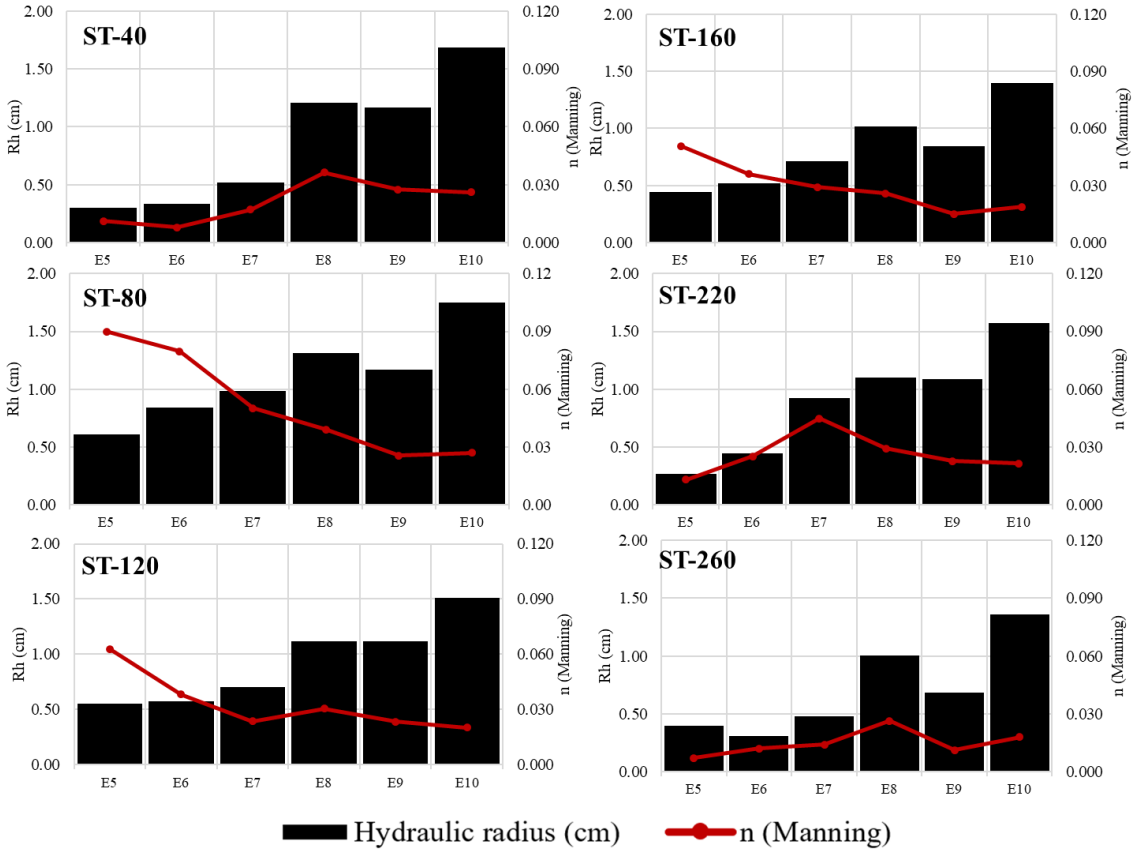


Figure 4-15 - Hydraulic radius and Manning's n over experiments for different sections

A similar trend is observed for the Darcy–Weisbach friction factor (f), as shown in Figure 4-16. Sections ST-80, ST-120, and ST-160 are less affected by upstream and downstream boundary conditions. In these sections, f decreases as mean flow velocity (U) increases. This indicates that, although flow velocities were lower in tests E5 and E6, the flow encountered greater resistance due to bed roughness and friction. As U increases and occupies a larger cross-sectional area, the influence of f on flow velocity becomes less significant.

The highest f values were recorded in ST-80—3.47 in E5 (with U = 0.05 m/s) and 2.44 in E6 (U = 0.07 m/s). Conversely, the highest velocity recorded was 0.48 m/s in ST-260 during E5. In this section, the flow rate was low (10 L/min) and entirely confined within the initial channel, which may explain the elevated f value. Excluding this point, the highest velocities were observed in E9 and E10 at ST-260 (0.46 and 0.45 m/s, respectively), where f values were correspondingly lower: 0.05 and 0.11.

It is important to emphasize that the direct influence of bed roughness on flow resistance coefficients cannot be isolated, as discharge—or more precisely, flow velocity—exerts a

dominant control over the computed values. Therefore, a more detailed analysis of the associated variables is required to accurately assess the role of bed morphology in modulating flow resistance, which will be explored in the following section.

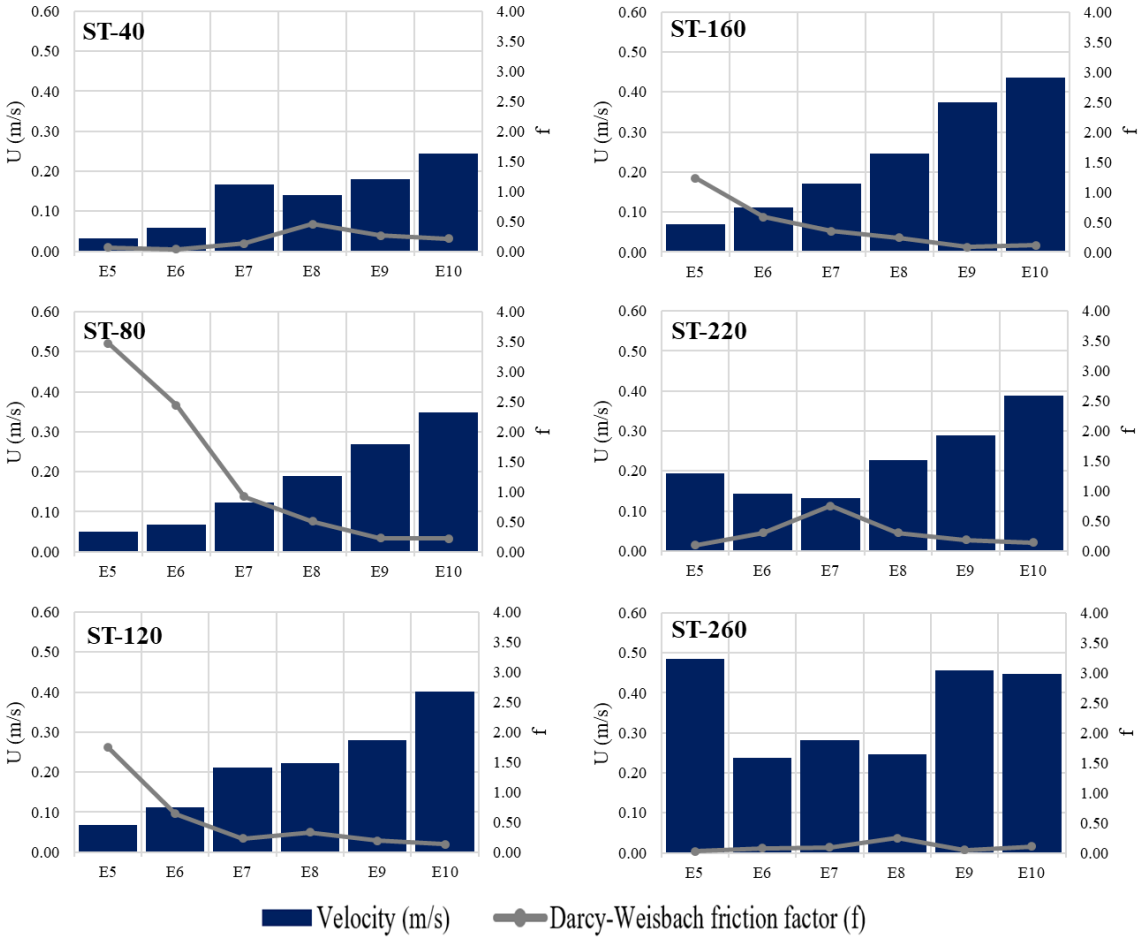


Figure 4-16 - Flow velocity and Darcy-Weisbach friction factor: flow resistance equations

Comparison between the experimental data and widely used flow resistance equations for gravel-bed rivers (the equations are listed in Table 4-3) reveals a general tendency of these models to underestimate the measured values (Figure 4-17). The data can be interpreted as follows:

- Large roughness scale: $h/D_{84} \lesssim 1.5h$. In this range, most of the data lie above the predictions of Recking et al. (2008) and Rickenmann & Recking (2011), indicating that these formulas tend to underestimate flow resistance when the sediment grains are relatively large compared to the flow depth.

- Intermediate roughness scale: $1.5 \lesssim h/D_{84}$. In this range, the experimental data start to align better with some equations, particularly those of Nikora et al. (2004) and Ferguson (2007).
- Small roughness scale: $h/D_{84} \gtrsim 3.5$. Here, the flow depth is relatively large compared to the sediment size, and the different equations tend to converge, showing reduced scatter.

Table 4-3 - Flow resistance equations

Autor	Equation	Nº
Hey (1979)	$\sqrt{\frac{8}{f}} = \frac{u}{u_*} = 5.37 + 5.82 \log\left(\frac{h}{3.5\ D_{84}}\right)$	12
Nikora et al. (2004)	$\sqrt{\frac{8}{f}} = \frac{u}{u_*} = 2.15\left(\frac{h}{D_{84}}\right)$	13
Ferguson (2007))	$\sqrt{\frac{8}{f}} = \frac{u}{u_*} = \frac{7.76\ 8 * 2.28\ \left(\frac{h}{D_{84}}\right)}{(7.76 + 2.28\left(\frac{h}{D_{84}}\right)^{\left(\frac{5}{3}\right)})^{0.5}}$	14
Recking et al. (2008)	$\sqrt{\frac{8}{f}} = \frac{u}{u_*} = -1 + 9{,}5 \log\frac{h}{D_{84}}$	15
Rickenmann e Recking (2011)	$\sqrt{\frac{8}{f}} = \frac{u}{u_*} = \frac{4{,}416\left(\frac{h}{D_{84}}\right)^{1{,}904}}{\left(1 + \left(\frac{h}{1{,}283 D_{84}}\right)^{1{,}618}\right)^{1{,}083}}$	16

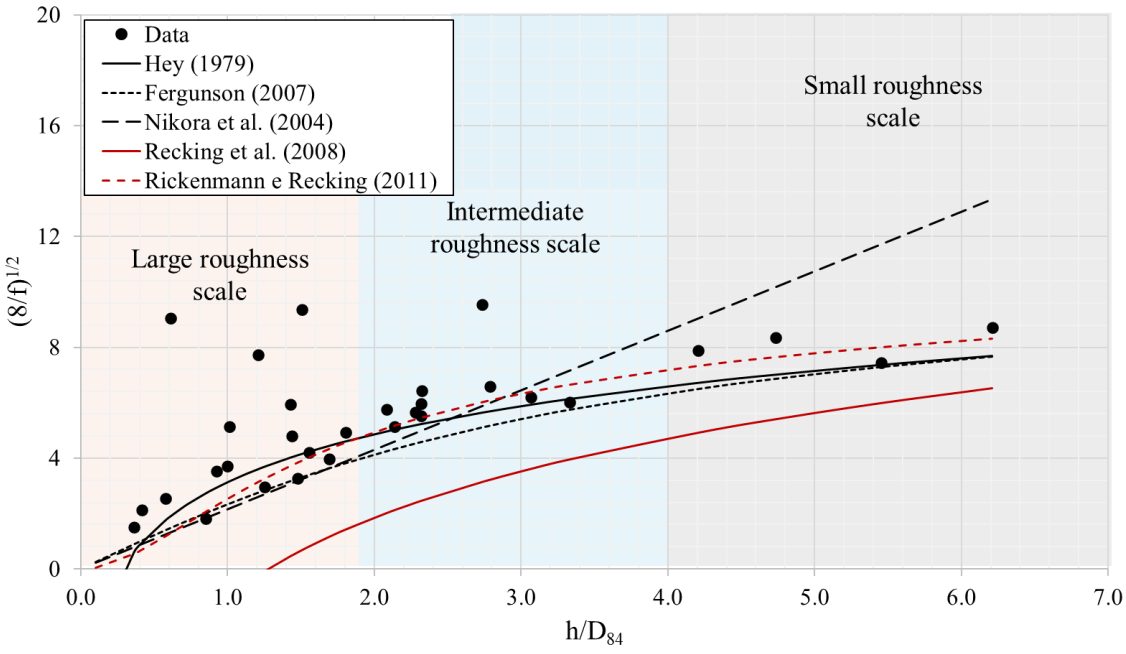


Figure 4-17 - Relationship between $(8/f)^{1/2}$ and h/D_{84} for different equations

The experimental data exhibit considerable variability at low relative submergence levels ($h/D_{84}<2$), with (8/f)1/2 values ranging from approximately 2 to over 12. This high dispersion suggests a strong influence of local roughness conditions and discharge magnitude on the values of h/D_{84}. In large roughness regimes, the flow tends to be more heterogeneous, with localized accelerations and recirculation between boulders and cobbles. This can lead to increased spatial variability in velocity, particularly near the bed, which is reflected in more dispersed velocity profiles, as observed in numerical modeling studies (e.g., Liu et al., 2017).

Nevertheless, the data show a clear overall trend of decreasing flow resistance with increasing relative submergence, which aligns with the predictions of most models. Among the evaluated equations, Hey's (1979) formulation best captures the general trend of the data, particularly within the intermediate range of submergence ($2< h/D_{84}<4$), especially because larger bedforms do not yet fully dominate the flow. The equation by Nikora et al. (2004) underestimates flow resistance at low submergence (high relative roughness), though it performs reasonably well in the mid-range. In contrast, Ferguson's (2007) model tends to overestimate resistance at high submergence (small roughness scale) and underestimate it in other regimes. Other equations (Recking, 2009; Rickenmann; Recking, 2011a), generally underestimate the experimental values across the full range of submergence.

Overall, classical models fail to adequately reproduce flow resistance in shallow flow regimes characterized by large relative roughness, where local bed conditions exert a dominant control. Variations in bed morphology and sediment properties—such as gravel size, armouring, and irregular microtopography—appear to play a crucial role in increasing hydraulic resistance, an effect that is not sufficiently accounted for by the tested formulations.

4.3.4 Sediment transport analysis

Table 4-4 summarizes the characteristics of the sediments transported during the experiments. It is observed that the material transported in E1—during the first 5 hours—showed the smallest grain diameters. This is because this interval represents the time required for all the injected sediment to reach the outlet of the channel, either by deposition or transport. In E2, the arrival of sediment at the channel outlet begins and is

maintained at a linear delivery rate, with cumulative transport continuing steadily through E4 (end of Phase II).

From E5 onward (Phase II), due to the reduced inflow, no sediment transport was observed. Gradually, with the increase in discharge, transport resumes—becoming effective only in E9 and E10, that is, starting from a flow rate of 104 L/min As highlighted in the Materials and Methods section, the material injected into the channel has a smaller grain size than the channel bed. In general, the particle diameters decreased from experiment E1 to E9, except for E10, which exhibited a slight increase. This behavior may be attributed to the characteristics of the bed sediment combined with the increased discharge applied in this test. Figure 4-18 presents the grain size distribution of both the injected and the transported material.

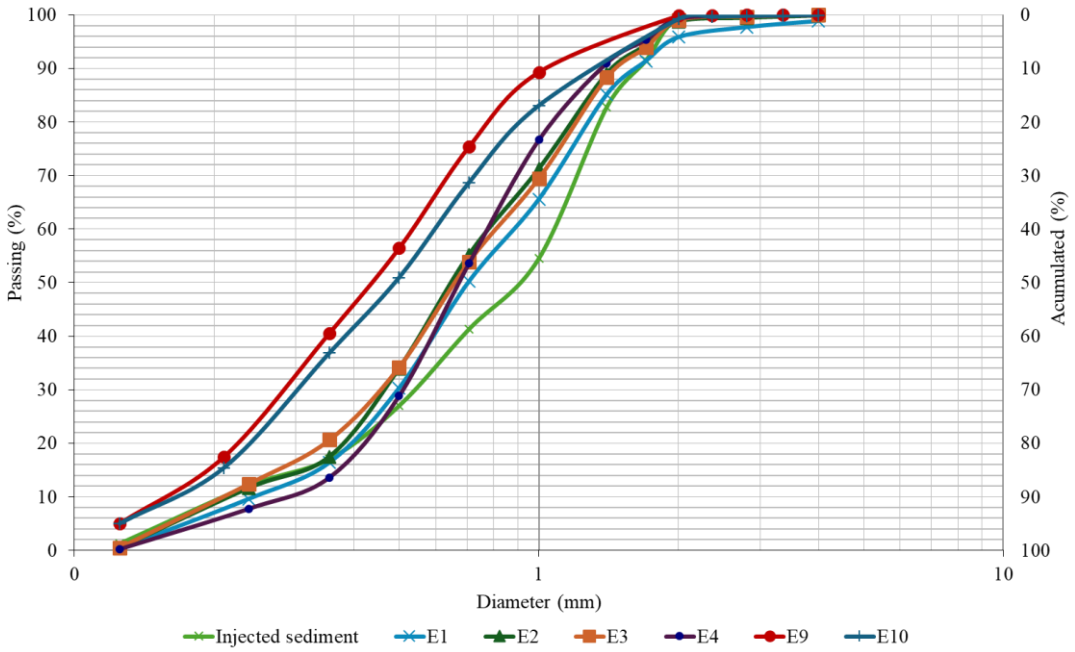


Figure 4-18 - Grain size distribution of the injected and transported sediment

Table 4-4 - Sediment transport characteristics

Part	Test	Q (L/min)	Q_s inlet acumulado (Kg)	D_{10s} (mm)	D_{16s} (mm)	D_{50s} (mm)	D_{84s} (mm)	D_{90s} (mm)	Q_s inlet (g)	Q_s outlet (kg)	Q_s outlet acumulada (kg)	Q_s deposited (kg)
I	E1	366.0	12.6	0.244	0.347	0.705	1.376	1.633	12.6	6.69	6.69	5.91
	E2	366.0	25.2	0.221	0.324	0.656	1.287	1.456	12.6	11.63	18.32	0.97
	E3	366.0	37.8	0.214	0.292	0.666	1.49	1.491	12.6	10.85	29.17	1.75
	E4	366.0	50.4	0.282	0.377	0.677	1.205	1.372	12.6	10.32	39.49	2.28
II	E5	10.2	0.00	-	-	-	-	-	0.00	0.00	39.49	-
	E6	19.2	0.00	-	-	-	-	-	0.00	0.00	39.49	-
	E7	42.6	0.00	-	-	-	-	-	0.00	0.00	39.49	-
	E8	83.6	0.00	-	-	-	-	-	0.00	0.00	39.49	-
	E9	104.0	0.00	0.159	0.200	0.441	0.888	1.064	0.00	0.11	39.60	-0.11*
	E10	204.5	0.00	0.166	0.214	0.490	1.059	1.430	0.00	0.32	39.92	-0.32*

*negative value means erosion

To verify the critical shear stress for the initiation of particle motion, the equations presented in Table 4-5 were used. However, since the sediment is of mixed grain size, particles of different sizes interact uniquely with the flow, leading to selective entrainment, which complicates the calculation of bedload transport rates. This selective entrainment is referred to as the hiding–exposure effect, which describes the process by which smaller grains are sheltered from the flow by larger, more exposed grains. The hiding of particles in sediment mixtures results in an increase in the critical shear stress required to mobilize finer particles, whereas the exposure of larger grains reduces the critical shear stress needed to initiate their motion (Einstein, 1950).

Table 4-5 - Equations used to calculate critical stress

Reference	Equation	Nº
Egiazaroff (1965)	$\theta_{r,i} = \theta_{c,50}\left[\frac{\log(19)}{\log(19\frac{D_i}{D_{50}})}\right]^2$	17
Ashida and Michiue (1973)	$\theta_{r,i} = \theta_{c,50}0.85\left(\frac{D_i}{D_{50}}\right)^{-1}$ for $\frac{D_i}{D_{50}} < 0.4$ $\theta_{r,i} = \theta_{c,50}\left[\frac{\log(19)}{\log(19\frac{D_i}{D_{50}})}\right]^2$ for $\frac{D_i}{D_{50}} > 0.4$	18
(Parker et al. (1982)	$\theta_{r,i} = \theta_{c,50}\left(\frac{D_i}{D_{50}}\right)^{-0.982}$	19
Wilcock and Crowe (2003)	$\theta_{r,i} = \theta_{c,50}\left(\frac{D_i}{D_{50}}\right)^{-\Upsilon}$ for $\Upsilon = 1 - \frac{0.67}{1+e^{(1.5-\frac{Di}{D_{50}})}}$	20

By applying the equations (Figure 4-19), we verify that the formula of Egiazaroff (1965) is shown to be representative only for $0.4 < D_i/D_{50} < 1$, and it overpredicts $\theta_{cr,i}/\theta_{c,50}$ by up to a factor of 13 for $D_i/D_{50} = 0.07$, below which the formula is not valid. The formula of Ashida and Michiue (1973) is more accurate in that it overpredicts values of $\theta_{cr,i}/\theta_{c,50}$ by a factor of 2 – 4 for $D_i/D_{50} < 0.2$ and it is valid below $D_i/D_{50} = 0.07$. As this formula is an adaptation of Egiazaroff's (1965) formula, it too overpredicts $\theta_{cr,i}/\theta_{c,50}$ for $D_i/D_{50} > 1$. The formula of (Wilcock and Crowe, 2003) is the most accurate for $D_i/D_{50} < 1$, however, overpredicts $\theta_{cr,i}/\theta_{c,50}$ for $D_i/D_{50} > 1$.

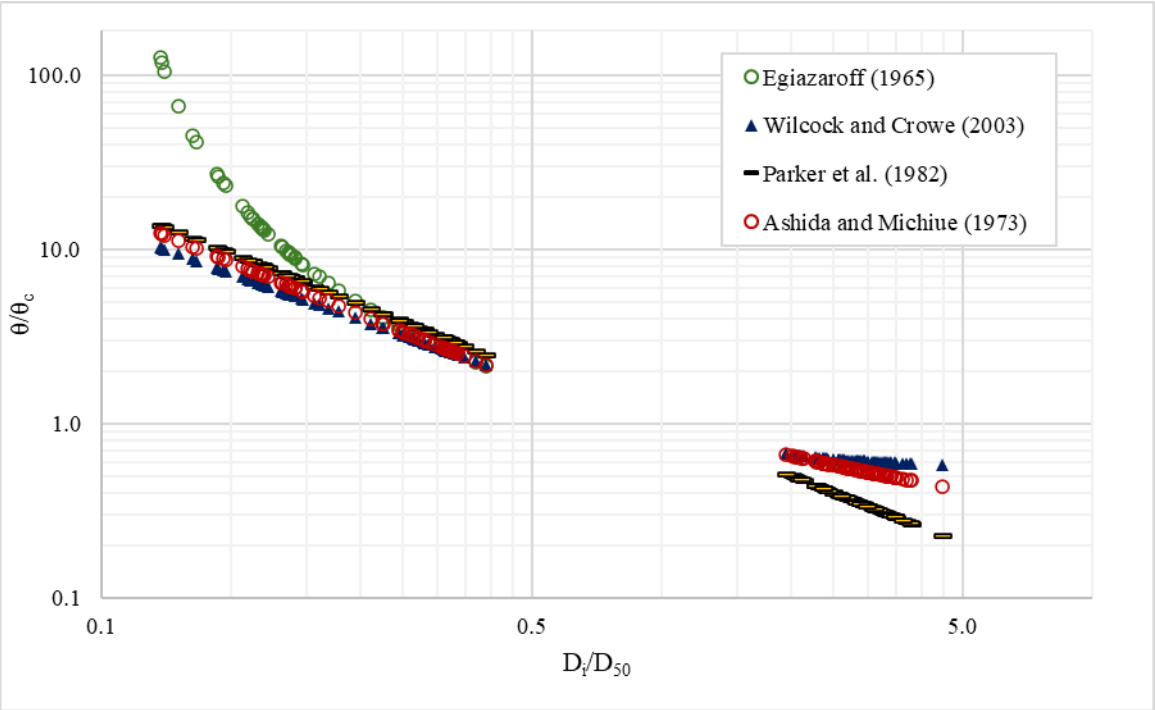


Figure 4-19 - Relationship between θcr,i/θc,50 and Di/D50 for different equations from the literature

In order to compare with the critical shear stress for the initiation of bed material motion—here established based on the calculated coefficients where R_{10} corresponds to D_{10} (the grain size at 10% cumulative occurrence) of the channel bed, and R_{16}, R_{50}, R_{84}, and R_{90} correspond to D_{16}, D_{50}, D_{84}, and D_{90}, respectively—the data for each grain size class were plotted against the boundary shear stress (determined by flow depth).

Based on Figure 4-20, it can be observed that sediment transport recorded during Phase II experiments is explained by the fact that the critical shear stress is lower than the boundary shear stress. For D_{10} particles (represented here by R_{10}), the majority have a critical shear stress (τ_c) lower than the boundary shear stress (τ_b). For D_{16}, this behavior is slightly different: τc is higher than τ_b; however, particles of this size were still observed in transport (as shown in Table 5). In this case, it is important to note that the equations used (Table 6) account for the hiding effect, as the sediment mixture is not uniform in size.

For D_{84} and D_{90}, a few particles exhibit τ_c values lower than τ_b, which is consistent with the sediment characteristics presented in Table 5, and some studies highlight that this behavior is common. For instance, Komar and Li (1988) and Venditti et al. (2010) discuss

how hiding–exposure mechanisms enhance the mobility of coarse grains while restricting that of finer ones. This may be related to the fact that the τc of D_{16} is greater than τb.

Specifically, experiments with sediments of varying sizes show that in graded beds, fine fractions require higher shear stresses to initiate motion, whereas coarse fractions, being more exposed, require lower stress. Kirchner et al. (1990) demonstrate that critical shear stress shows considerable variability within the same bed, and that finer fractions exhibit substantially higher median critical stress values. Initial transport is governed by the most exposed or erodible particles, rather than by the average properties of the sediment mixture.

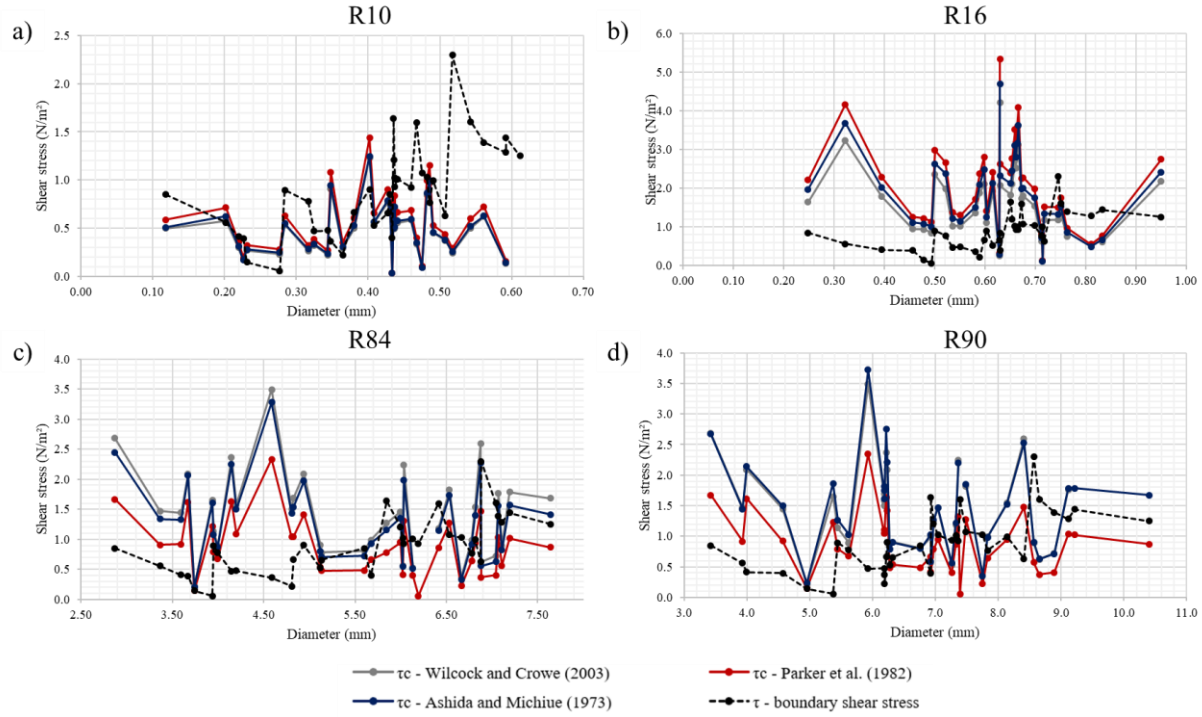


Figure 4-20 - Boundary shear stress and critical shear stress for a) R10, b) R16, c) R84, and d) R90

When analyzing the results obtained, several key aspects emerge, including natural sorting of transported sediments, bed armouring and transport thresholds, the relationship with critical discharge for sediment mobilization, and steady sediment delivery. The fact that the material transported to the downstream end of the channel was finer than the sediment initially injected is consistent with findings widely reported in the literature, particularly in studies on sediment sorting and selective transport (Gomez, 1991; Parker,

1990). Flow tends to mobilize the finer and lighter particles first, while coarser particles remain deposited, leading to a natural granulometric classification process.

The absence of sediment transport observed during tests E5 to E8 reinforces the concept of a threshold of motion, as discussed by Montgomery and Buffington (1997). The literature indicates that in channels with mixed-size bed material, an initial deposition phase is followed by the development of an armoured layer—a surface veneer of coarser grains that shields the finer material underneath—thereby significantly reducing transport until a critical discharge is exceeded.

The resumption of sediment transport in E9 and E10 (above 105 L/min) aligns with the critical discharge or critical shear stress theory, originally proposed by Shields (1936) and later refined by researchers such as Wilcock and Crowe (2003). This indicates that a minimum threshold of hydraulic energy to mobilize the coarser, armoured sediments on the channel bed is 105L/min;

The near-linear sediment delivery rate observed between E2 and E4 corresponds to behavior typically described in transient or supply-limited transport regimes, as outlined by Hassan et al. (2005). This pattern occurs when the sediment supply is steady and the transport capacity of the flow matches the sediment input.

4.3.5 Relationship between characteristic variables

To explore the flow behavior in relation to the channel bed characteristics, velocity and Manning's n data were analyzed for phase II (Figure 4-21). A power-law relationship fits well, with $R^2 = 0.83$. This relationship indicates that the lower the velocity (0.04 m/s), the higher the Manning's coefficient (n = 0.09), which is associated with the bed roughness.

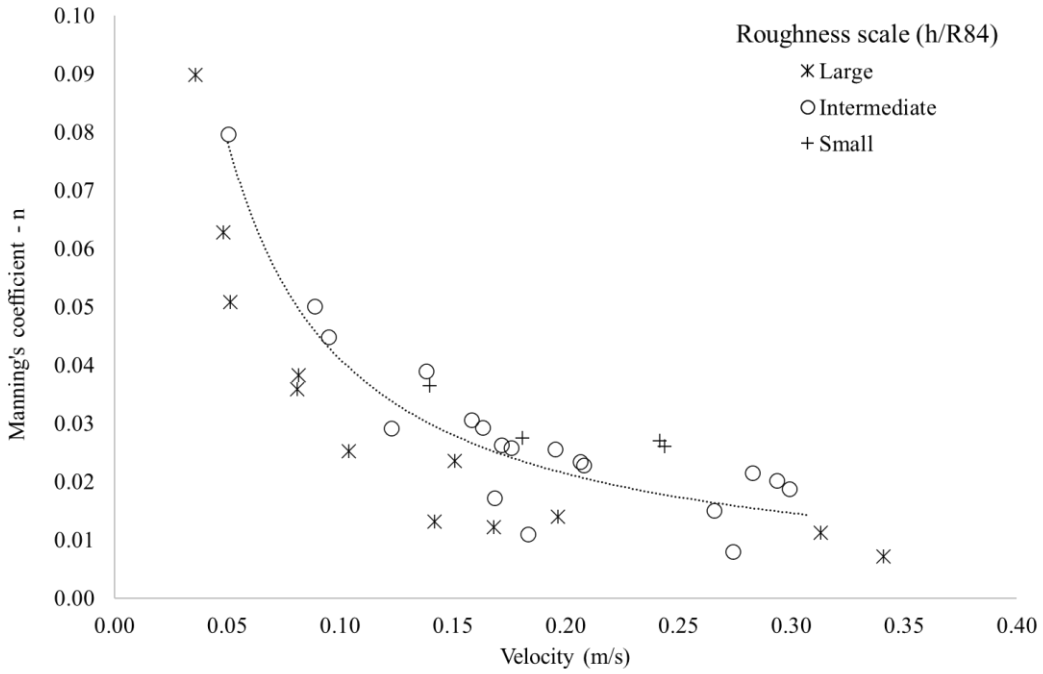


Figure 4-21 - Relationship between velocity and Manning's n for each cross-section in phase II data

Figure 4-22 compares velocity with the Darcy-Weisbach friction factor the data fit yields $R^2 = 0.94$. This behavior is similar to the relationship between velocity and Manning's n but shows a stronger correlation. Comparative studies, such as those by Ferguson (2007) and Yen (2002), indicate that the Darcy-Weisbach friction factor is more sensitive to variations in velocity and channel scale than Manning's coefficient, especially when bed morphology is heterogeneous. It again confirms that bed roughness is higher for lower flow rates (usually associated with lower velocities)

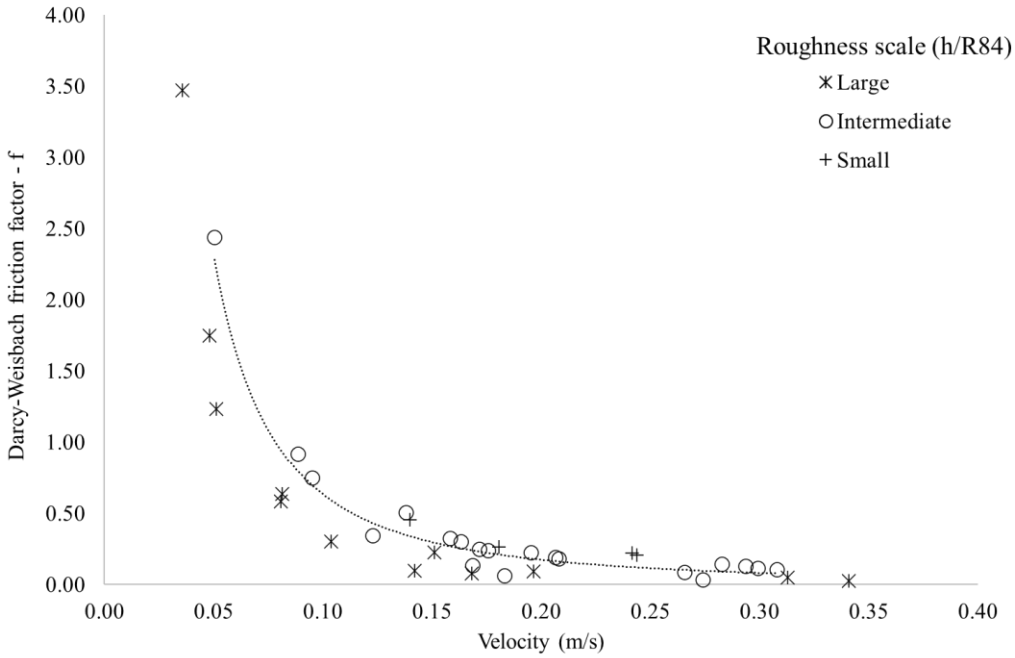


Figure 4-22 - Relationship between velocity and Darcy-Weisbach friction factor for phase II data

In general, in rough-bed channels (such as gravel-bed rivers), the inverse relationship between velocity and flow resistance coefficients—such as *f* (Darcy-Weisbach) and *n* (Manning)—typically arises from two main factors, both of which were observed in this study: (1) Relative submergence effect: at low discharges (and consequently low velocities), the relative depth is smaller, and the relative roughness (e.g., Rh/D84 or Rh/σ) is higher, increasing flow resistance (Ferguson, 2007); and (2) Bed armouring and stability: under low-energy regimes, the bed tends to be more stable and rough, with prominent structures (i.e., coarse grains) exerting greater interference in the flow boundary layer (Bathurst, 1985).

4.4 CONCLUSIONS

The evolution of geometric parameters, such as P_m, R_h, and A_m, observed during Phase I tests, highlights the importance of a preliminary bed stabilization stage in physical modeling. In this stage, the natural adjustment of bed material and the gradual filling of interstitial spaces by finer sediments demonstrated that the initial bed configuration plays a decisive role in shaping the channel's morphological evolution and hydraulic response. Neglecting this process can lead to misinterpretations regarding sediment transport, bed roughness, and flow distribution along the channel.

The stabilization trend of hydraulic parameters observed throughout Phase I suggests that a regime close to equilibrium between sediment transport and deposition can be achieved - an essential condition for physical models to accurately represent the behavior of natural rivers. This initial stabilization stage not only improves experimental control but also enhances the reproducibility of the results, increasing the reliability of the subsequent analyses.

In Phase II, the results showed that flow resistance decreases as relative submergence increases, which is consistent with established findings in the literature. However, under low-flow conditions - and therefore reduced flow depths - hydraulic roughness was significantly higher, revealing the strong influence of bed microtopography and armoring on flow dynamics.

Comparisons with empirical equations available in the literature indicate that these models systematically underestimate hydraulic resistance under conditions of high relative roughness, as observed in the present experiments. This discrepancy may stem from the fact that many of these equations were developed based on data from specific geographic contexts. For instance, although alpine rivers may share similar bed material characteristics with Brazilian rivers, they typically exhibit different channel slopes. Additionally, Brazil's rainfall-dominated hydrological regime contrasts with the snowmelt-driven flows commonly found in temperate or alpine environments, where gravel-bed river dynamics are frequently studied.

Another relevant observation concerns the significant influence of boundary conditions. Cross-sections located near the upstream and downstream ends of the flume displayed distorted velocity and roughness measurements due to edge effects. These variations must be taken into account in both experimental design and data interpretation to ensure that conclusions reflect actual hydraulic behavior rather than localized artifacts.

Moreover, flow resistance could not be attributed solely to bed roughness. Factors such as discharge, flow depth, cross-sectional location, and local bed characteristics influenced the observed outcomes. Classical equations underestimated these effects, especially under low-submergence conditions, limiting their applicability in complex fluvial systems.

The experiments also demonstrated selective sediment transport, the formation of armoring layers, and the existence of a critical discharge threshold necessary to initiate significant sediment movement. This understanding, resulting from the pioneering use of

a reduced-scale physical model of a natural gravel-bed river, provides a solid foundation for further studies and technical applications in the field of fluvial engineering in Brazilian mountainous rivers, offering valuable insights for hydraulic modeling and sediment management.

4.5 FUTURE SCOPE

Based on the results presented in this study, estimating bed roughness, flow resistance rates, and consequently quantifying sediment transport in gravel-bed rivers remains a major challenge. The development of mathematical models grounded in the data obtained here, as well as their comparison with results reported by other authors, are still necessary steps. Furthermore, integrating these data with information collected from the prototype for which this physical model was designed will enable a deeper understanding of water and sediment dynamics in these fluvial systems, representing a significant advance in the study of gravel-bed rivers in Brazil.

Another key aspect concerns the definition of channel stability models for gravel-bed rivers, which still faces important challenges. Studies such as Ali et al. (2021) and Ali & Dey (2021) investigated the formation, instability, and transition of bedform patterns in rivers, though not specifically in gravel-bed contexts. In contrast, for gravel-bed channels, Hey & Thorne (1986) had already demonstrated the dominant role of bankfull discharge in controlling channel geometry, while also highlighting that bedload transport exerts a decisive influence, particularly on channel slope; that riparian vegetation is a crucial control factor on channel width and flow velocity; and that the size of bed material strongly affects channel depth, velocity, and slope.

More recently, Rachelly et al. (2022), through experiments and two-dimensional simulations in gravel-bed channels, emphasized that the success of river restoration—especially regarding the reactivation of lateral connectivity and the enhancement of habitat heterogeneity—depends strongly on sediment balance, and not solely on the removal of bank protections or confinement structures.

In line with these studies, the data presented here still offer considerable potential for further investigation. In this regard, the characterization of bed roughness in relation to water and sediment transport, conducted here through physical modeling, represents an initial step toward defining parameters applicable to hydrodynamic modeling, especially

regarding models for flow resistance and sediment transport in gravel-bed rivers, which may later be refined and employed in different contexts such as channel stability assessments, river renaturalization processes, and flood evaluations.

4.6 REFERENCES

ADAMS, D. L. Toward bed state morphodynamics in gravel-bed rivers. **Progress in Physical Geography**, [s. l.], v. 44, n. 5, p. 700–726, 2020.

ALI, S. Z.; DEY, S. Impact of phenomenological theory of turbulence on pragmatic approach to fluvial hydraulics. **Physics of Fluids**, [s. l.], v. 30, n. 4, 2018.

ALI, S. Z.; DEY, S. Interfacial instability of sand patterns induced by turbulent shear flow. **International Journal of Sediment Research**, [s. l.], v. 36, n. 4, p. 449–456, 2021.

ALI, S. Z.; DEY, S. Origin of the scaling laws of sediment transport. **Proceedings of the Royal Society A: Mathematical, Physical and Engineering Sciences**, [s. l.], v. 473, n. 2197, 2017.

ALI, S. Z.; DEY, S.; MAHATO, R. K. Mega riverbed-patterns: linear and weakly nonlinear perspectives. **Proceedings of the Royal Society A**, [s. l.], v. 477, n. 2252, 2021.

ANCEY, C. Bedload transport: a walk between randomness and determinism. Part 1. The state of the art. **Journal of Hydraulic Research**, [s. l.], v. 58, n. 1, p. 1–17, 2020.

ASHIDA, K., MICHIUE, M., 1973. Studies on bed-load transport rate in open channel flows. IN. SEDIMENT TRANSPORTATION 1.

BATHURST, J. C. Flow resistance estimation in mountain rivers. 1985.

BOGATIN, E., DEGROOT, D., HURAY, P.G., SHLEPNEV, Y. Which one is better? Comparing options to describe frequency dependent losses. In: **DesignCon 2013, 1. Where Chipheads Connect**, pp. 469–494. 2013

BUFFINGTON, J.M., MONTGOMERY, D.R. Effects of hydraulic roughness on surface textures of gravel-bed rivers. **Water Res. Res.** 35 (11), 3507–3521. 1999

CHEN, X. et al. Rough Correlations: Meta-Analysis of Roughness Measures in Gravel Bed Rivers. **Water Resources Research**, [s. l.], v. 56, n. 8, 2020.

CHURCH, M.; FERGUSON, R. I. Morphodynamics: Rivers beyond steady state. **Water Resources Research**, [s. l.], v. 51, n. 4, p. 1883–1897, 2015.

CHURCH, M.; HASSAN, M. A. The fluvial grain-size gap: Experimental confirmation of hydraulic origin. **Earth Surface Processes and Landforms**, [s. l.], v. 48, n. 8, p. 1502–1511, 2023.

CHURCH, M.; HASSAN, M. A.; WOLCOTT, J. F. Stabilizing self-organized structures in gravel-bed stream channels: Field and experimental observations. **Water Resources Research**, [s. l.], v. 34, n. 11, p. 3169–3179, 1998.

COMITI, F., MAO, L. Recent advances in the dynamics of steep channels. **Gravel-bed rivers: Processes, tools, environments**, pp. 351–377. 2012.

DEY, S.; ALI, S. Z. Advances in modeling of bed particle entrainment sheared by turbulent flow. **Physics of Fluids**, [s. l.], v. 30, n. 6, 2018.

DEY, S.; ALI, S. Z. Turbulent friction in canonical flows: state of the science and future outlook. **Journal of Hydraulic Engineering**, [s. l.], v. 150, n. 6, 04024044, 2024.

DIETRICH, W. E., et al. Sediment supply and the development of the coarse surface layer in gravel-bedded rivers. **Nature**, [s. l.], v. 340, p. 215–217, 1989.

DIETRICH, W.E., NELSON, P.A., YAGER, E., VENDITTI, J.G., LAMB, M.P., COLLINS, L., Sediment patches, sediment supply, and channel morphology. **River Coastal Estuarine Morphodynam**ic. 1, 79–90. 2005.

DINGLE, E.H., VENDITTI, J.G., Experiments on Gravel-Sand Transitions: Behavior of the Grain Size Gap Material. **J. Geophys. Res.: Earth Surf**. 128 (11), e2023JF007117. 2023.

EGIAZAROFF, I.V. Calculation of nonuniform sediment concentrations. **J. Hydraul. Div.** 91 (4), 225–247. 1965.

EINSTEIN, H.A. The bed-load function for sediment transportation in open channel flows, 1026. **US Government Printing Office**. 1950.

FERGUSON, R. Flow resistance equations for gravel- and boulder-bed streams. **Water Resources Research**, [s. l.], v. 43, n. 5, p. 1–12, 2007.

FERGUSON, R. I. et al. Predicting flow resistance in rough-bed rivers from topographic roughness: Review and open questions. **Earth Surface Processes and Landforms**, [s. l.], 2024.

GILBERT, J.; WILCOX, A. C. Estimating Grain Stress and Distinguishing Between Mobility and Transportability Improves Bedload Transport Estimates in Coarse-Bedded Mountain Rivers. **Journal of Geophysical Research: Earth Surface**, [s. l.], v. 129, n. 8, 2024.

GILBERT, G.K. The transportation of debris by running water (No. 86). **US Government Printing Office**. 1914.

GOMEZ, B. Bedload transport. **Earth-Science Reviews**, [s. l.: s. n.], 1991.

HASSAN, M. A., CHURCH, M., LISLE, T. E., BRARDINONI, F., BENDA, L., & GRANT, G. E. (2005). Sediment transport and channel morphology of small, forested streams 1. **Journal of the American Water Resources Association,** *41*(4), 853-876. 2005.

HEY, R. D.; THORNE, C. R. Stable channels with mobile gravel beds. **Journal of Hydraulic Engineering**, [s. l.], v. 112, n. 8, p. 671–689, 1986.

HEY, R.D. Flow resistance in gravel-bed rivers. **J. Hydraul. Div.** 105 (4), 365–379. 1979.

ISEYA, F., IKEDA, H. Pulsations in bedload transport rates induced by a longitudinal sediment sorting: A flume study using sand and gravel mixtures. **Geografiska Annaler: Series A, Phys. Geogr.** 69 (21), 15–27. 1987.

JACKSON, W.L., BESCHTA, R.L. Influences of increased sand delivery on the morphology of sand and gravel channels 1. **JAWRA J. Am. Water Res. Ass**. 20 (4), 527–533. 1984

KASAI, M., MARUTANI, T., BRIERLEY, G. Channel bed adjustments following major aggradation in a steep headwater setting: findings from Oyabu Creek, Kyushu,Japan. **Geomorphology** 62 (3–4), 199–215. 2004.

KIRCHNER, J. W. et al. The variability of critical shear stress, friction angle, and grain protrusion in water-worked sediments. **Sedimentology**, [s. l.], v. 37, n. 4, p. 647–672, 1990.

KOMAR, P. D.; LI, Z. Applications of grain-pivoting and sliding analyses to selective entrapment of gravel and to flow-competence evaluations. **Sedimentology**, [s. l.], v. 35, n. 4, p. 681–695, 1988.

LAMB, M. P.; BRUN, F.; FULLER, B. M. Hydrodynamics of steep streams with planar coarse-grained beds: Turbulence, flow resistance, and implications for sediment transport. **Water Resources Research**, 53(3), 2240–2263, 2017.

LIU, Y.; STOESSER, T.; FANG, H.; PAPANICOLAOU, A.; TSAKIRIS, A. G. Turbulent flow over an array of boulders placed on a rough, permeable bed. **Computers & Fluids**, [s. l.], v. 158, p. 120–132, 2017.

LLENA, M.; VERICAT, D.; MARTINEZ-CASASNOVAS, J. A.; SMITH, M. W. Geomorphic adjustments to multi-scale disturbances in a mountain river: A century of observations. **Catena**, 192, 104584, 2020.

LISLE, T.E., CHURCH, M. Sediment transport-storage relations for degrading, gravel bed channels. **Water Res. Res.** 38 (11), 1. 2002.

LISLE, T.E., HILTON, S. The volume of fine sediment in pools: An index of sediment supply in gravel-bed streams. **JAWRA J. Am. Water Res. Assoc.** 28 (2), 371–383. 1992.

LISLE, T.E., IKEDA, H., ISEYA, F. Formation of stationary alternate bars in a steep channel with mixed-size sediment: A flume experiment. **Earth Surf. Process. Landforms** 16 (5), 463–469. 1991.

LISLE, T.E., NELSON, J.M., PITLICK, J., MADEJ, M.A., BARKETT, B.L. Variability of bed mobility in natural, gravel-bed channels and adjustments to sediment load at local and reach scales. **Water Res. Res.** 36 (12), 3743–3755. 2000.

LISLE, T.E. Sediment transport and resulting deposition in spawning gravels, north coastal California. **Water Res. Res.** 25 (6), 1303–1319. 1989.

LISLE, T. E. Particle size variations between bed load and bed material in natural gravel bed channels. **Water Resources Research**, [s. l.: s. n.], 1995.

MAZUMDER, B. S.; GHOSHAL, K.; DALAL, D. C. Influence of bed roughness on sediment suspension: experimental and theoretical studies. **Journal of Hydraulic Research**, [s. l.], v. 43, n. 3, p. 245–257, 2005.

MENEZES, D.; BORGES, A. L. de O. Exploring morphological equilibrium and flow resistance in gravel-bed rivers: insights from channel-scale experimental analysis. **Revista Brasileira de Recursos Hídricos**, [s. l.], v. 30, 2025.

MENEZES, D. Hydrosedimentological characterization of a section of the Forqueta River, Maquiné, RS (Master's thesis). Graduate Program in Water Resources and Environmental Sanitation, Federal University of Rio Grande do Sul, Porto Alegre, Brazil, 2021.

MONTGOMERY, D. R.; BUFFINGTON, J. M. Channel-reach morphology in mountain drainage basins. **Bulletin of the Geological Society of America**, [s. l.], v. 109, n. 5, p. 596–611, 1997.

NICOSIA, A.; CAROLLO, F. G.; FERRO, V. Evaluating the influence of boulder arrangement on flow resistance in gravel-bed channels. **Journal of Hydrology**, [s. l.], p. 129610, 2023.

NIKORA, V. I.; GORING, D. G.; BIGGS, B. J. F. On gravel-bed roughness characterization. **Water Resources Research**, [s. l.], v. 34, n. 3, p. 517–527, 1998.

PADHI, E. et al. Hydrodynamics of water-worked and screeded gravel beds: A comparative study. **Physics of Fluids**, [s. l.], v. 30, n. 8, 2018.

PARKER, G. Relation permettant le calcul du charriage dans les rivieres a graviers, a partir de la composition de surface. **Journal of Hydraulic Research**, [s. l.], v. 28, n. 4, p. 417–436, 1990.

PARKER, G.; KLINGEMAN, P. C. On why gravel bed streams are paved. **Water Resources Research**, [s. l.], v. 18, n. 5, p. 1409–1423, 1982.

POWELL, D. M. Flow resistance in gravel-bed rivers: Progress in research. **Earth-Science Reviews**, 136, 301–338, 2014.

RACHELLY, C.; VETSCH, D. F.; BOES, R. M.; WEITBRECHT, V. Sediment supply control on morphodynamic processes in gravel-bed river widenings. **Earth Surface Processes and Landforms**, [s. l.], v. 47, n. 15, p. 3415–3434, 2022.

RECKING, A. et al. Feedback between bed load transport and flow resistance in gravel and cobble bed rivers. **Water Resources Research**, [s. l.], v. 44, n. 5, 2008.

RECKING, A. Theoretical development on the effects of changing flow hydraulics on incipient bed load motion. **Water Resources Research**, [s. l.], v. 45, n. 4, 2009.

RICKENMANN, D.; RECKING, A. Evaluation of flow resistance in gravel-bed rivers through a large field data set. **Water Resources Research**, [s. l.], v. 47, n. 7, 2011.

SENGUPTA, S. Grain-size distribution of suspended load in relation to bed materials and flow velocity. **Sedimentology**, [s. l.], v. 26, n. 1, p. 63–82, 1979.

SHIELDS, A. Application of similarity principles and turbulence research to bed-load movement. [s. l.], 1936.

SHOCKLING, M. A.; ALLEN, J. J.; SMITS, A. J. Roughness effects in turbulent pipe flow. **Journal of Fluid Mechanics**, [s. l.], v. 564, p. 267–285, 2006.

VENDITTI, J. G. et al. Effect of sediment pulse grain size on sediment transport rates and bed mobility in gravel bed rivers. **Journal of Geophysical Research: Earth Surface**, *115*(F3). 2010.

WEICHERT, R.B., BEZZOLA, G.R. Bed morphology and generation of step-pool channels. **Earth Surf. Process. Landforms** 33 (11), 1678–1692. 2008.

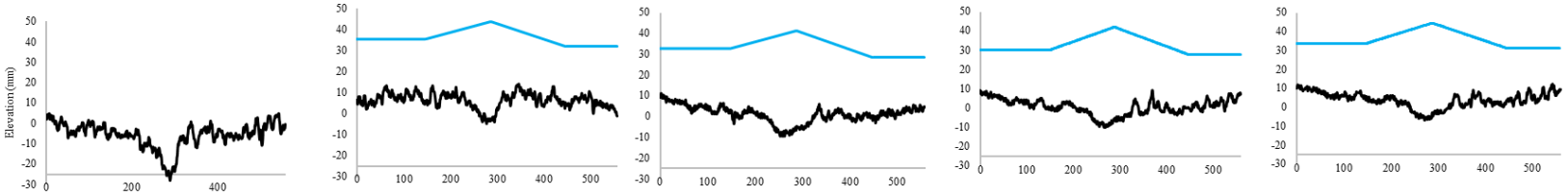
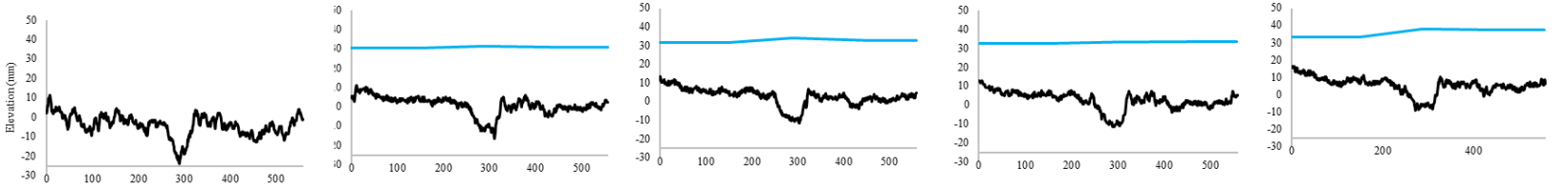
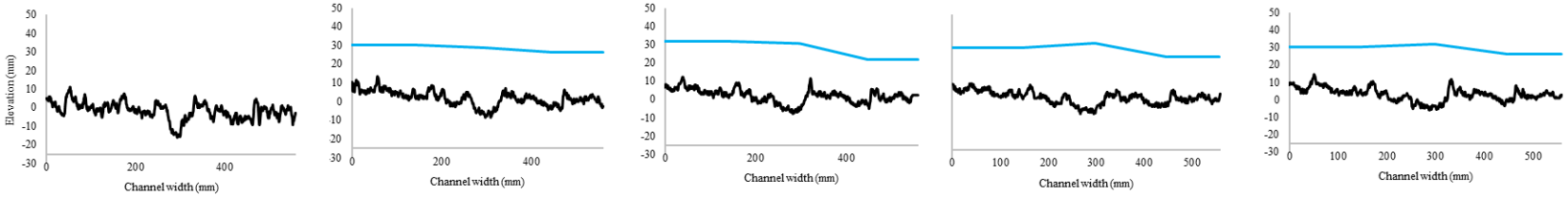
WILCOCK, P.R. Toward a practical method for estimating sediment-transport rates in gravel-bed rivers. **Earth Surf. Process. Landforms** 26 (13), 1395–1408. 2001.

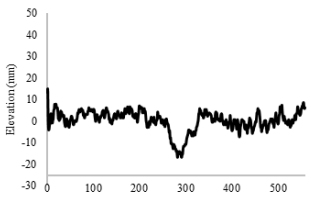
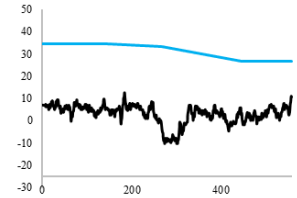
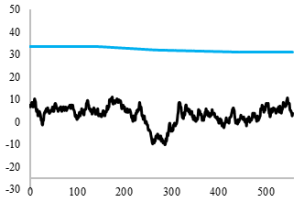
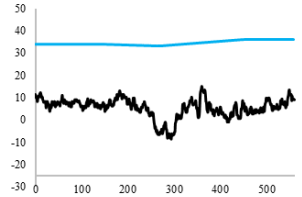
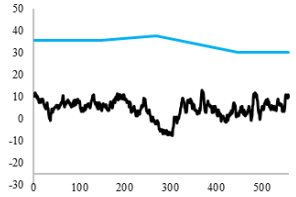
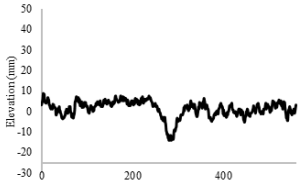
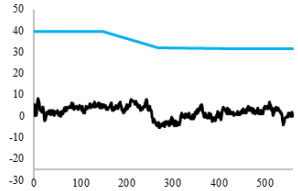
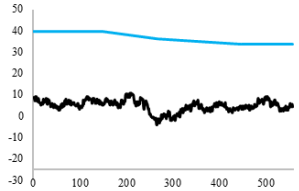
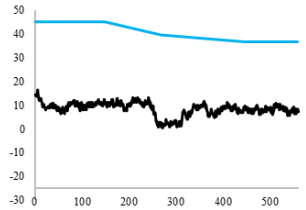
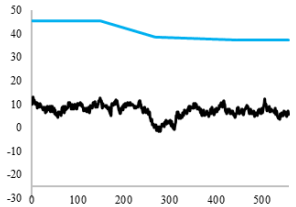
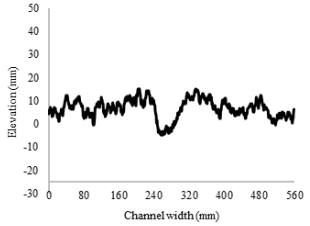
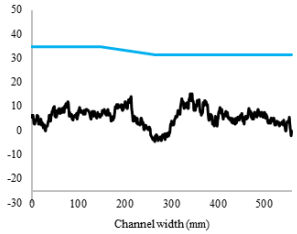
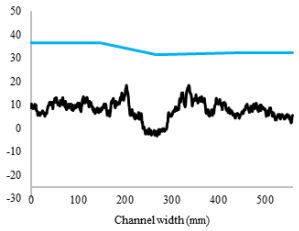
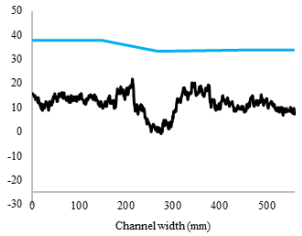
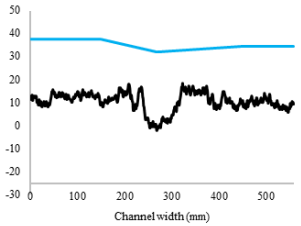
WILCOCK, P. R.; ASCE, M.; CROWE, J. C. Surface-based Transport Model for Mixed-Size Sediment. [s. l.], v. 129, n. February, p. 120–128, 2003.

YEN, B. C.; ASCE, F. Open Channel Flow Resistance. **Journal of hydraulic engineering,** *128*(1), 20-39. 2002

4.1 APPENDIX A

Cross-section of the tests performed in Phase I

Cross section	Inicial bed	E1	E2	E3	E4
ST - 40					
ST - 80					
ST - 120					

Cross section	Inicial bed	E1	E2	E3	E4
ST - 160					
ST - 220					
ST - 260					

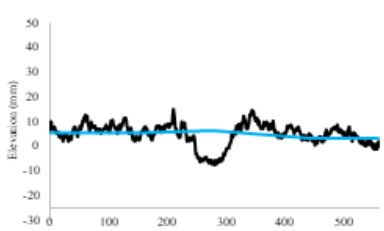
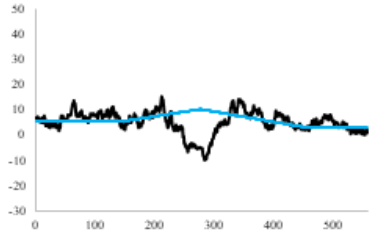
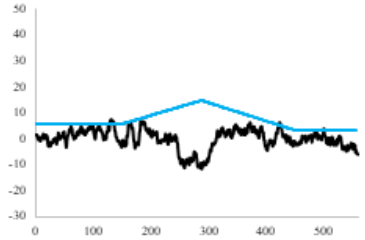
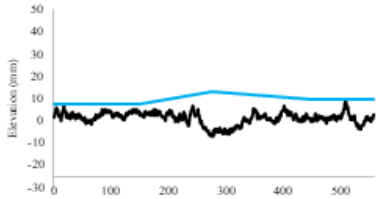
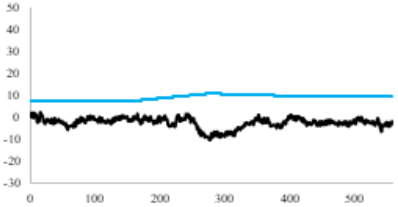
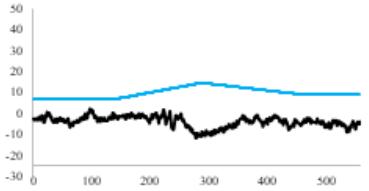
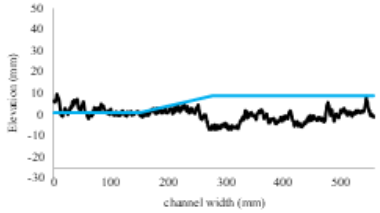
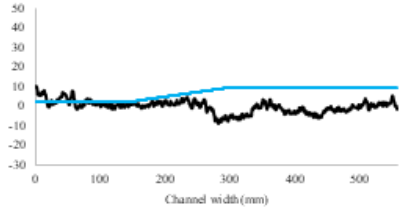
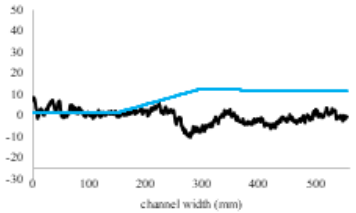
4.2 APPENDIX B

Tests	ST	Area (cm²)	Perimeter (cm)	Average depth (cm)	Hydraulic radius (cm)	Discharge (L/min)	Velocity (m/s)	n (Manning)	Boundary shear stress (N/m²)	Shields number	Reynolds number	Froude number	Darcy-Weisbach friction factor	R10 (mm)	R16 (mm)	R50 (mm)	R84 (mm)	R90 (mm)	Relative submergence (Rh/R84)
E1	40	169.48	86.54	3.03	1.96	366	0.36	0.02	2.78	0.025	5381	0.66	0.11	0.4	0.64	3.1	7.32	8.84	0.027
E1	80	168.7	77.72	3.01	2.17	366	0.36	0.021	2.77	0.025	5991	0.67	0.12	0.63	0.94	3.41	7.17	7.89	0.03
E1	120	149.62	79.76	2.67	1.88	366	0.41	0.017	2.46	0.022	5838	0.8	0.08	0.65	0.99	2.92	6.77	7.64	0.028
E1	160	158.03	85.03	2.82	1.86	366	0.39	0.018	2.59	0.023	5476	0.73	0.09	0.36	0.49	2.63	9.3	7.43	0.02
E1	220	182.95	77.37	3.27	2.36	366	0.33	0.024	3	0.027	6019	0.59	0.16	0.64	0.93	2.45	5.44	6.73	0.043
E1	260	151.32	81.85	2.7	1.85	366	0.4	0.017	2.48	0.022	5689	0.78	0.08	0.63	0.92	2.89	6.6	7.55	0.028
E2	40	181.35	78.55	3.24	2.31	366	0.34	0.023	2.98	0.027	5928	0.6	0.15	0.54	0.8	2.29	5.44	6.73	0.042
E2	80	167.2	78.65	2.99	2.13	366	0.36	0.02	2.74	0.025	5920	0.67	0.12	0.67	0.93	2.6	6.88	8.36	0.031
E2	120	146.83	79.31	2.62	1.85	366	0.42	0.016	2.41	0.022	5871	0.82	0.08	0.37	0.59	2.65	6.26	7.18	0.03
E2	160	160.57	79.93	2.87	2.01	366	0.38	0.019	2.63	0.024	5825	0.72	0.1	0.57	0.83	2.48	5.82	7.33	0.035
E2	220	176.7	77.85	3.16	2.27	366	0.35	0.022	2.9	0.026	5981	0.62	0.14	0.55	0.69	1.86	3.99	5.48	0.057
E2	260	143.8	82.16	2.57	1.75	366	0.42	0.015	2.36	0.021	5668	0.85	0.07	0.48	0.68	2.35	5.86	7.01	0.03
E3	40	177.2	78.04	3.16	2.27	366	0.34	0.023	2.91	0.026	5967	0.62	0.14	0.37	0.51	2.4	6.44	7.5	0.035
E3	80	171.28	76.58	3.06	2.24	366	0.36	0.022	2.81	0.025	6081	0.65	0.13	0.42	0.66	2.58	7.01	8.31	0.032
E3	120	148.87	78.38	2.66	1.9	366	0.41	0.017	2.44	0.022	5941	0.8	0.08	0.51	0.68	2.54	6.11	7.08	0.031

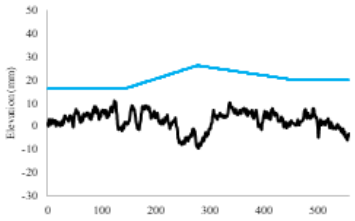
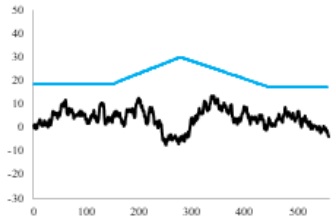
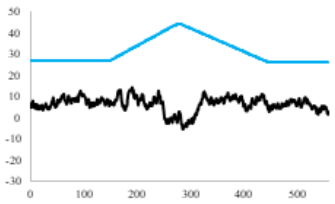
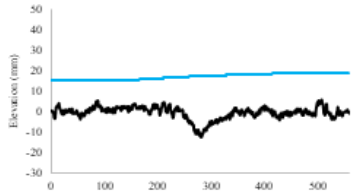
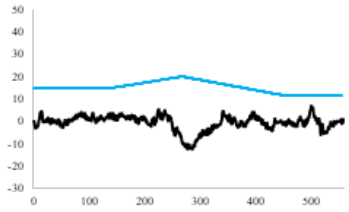
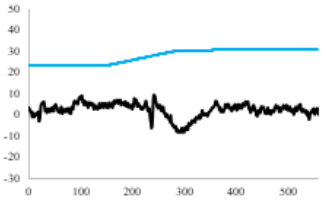
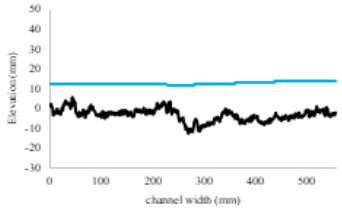
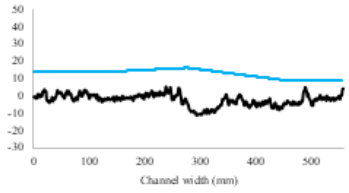
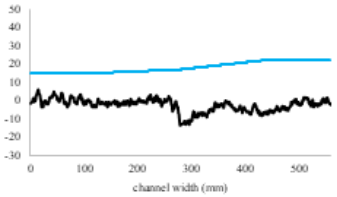
Tests	ST	Area (cm^2)	Perimeter (cm)	Average depth (cm)	Hydraulic radius (cm)	Discharge (L/min)	Velocity (m/s)	n (Manning)	Boundary shear stress (N/m^2)	Shields number	Reynolds number	Froude number	Darcy-Weisbach friction factor	R10 (mm)	R16 (mm)	R50 (mm)	R84 (mm)	R90 (mm)	Relative submergence (Rh/R84)
E3	160	161.4	82.06	2.88	1.97	366	0.38	0.019	2.65	0.024	5675	0.71	0.1	0.64	0.86	2.49	5.98	7.29	0.033
E3	220	180.07	81.34	3.22	2.21	366	0.34	0.023	2.95	0.027	5725	0.6	0.14	0.31	0.44	1.69	3.9	5.32	0.057
E3	260	132.24	81.61	2.36	1.62	366	0.46	0.013	2.17	0.019	5706	0.96	0.06	0.43	0.71	2.53	6.36	7.91	0.025
E4	40	177.41	79.43	3.17	2.23	366	0.34	0.022	2.91	0.026	5862	0.62	0.14	0.57	0.79	2.87	6.52	7.48	0.034
E4	80	171.17	81.16	3.06	2.11	366	0.36	0.021	2.81	0.025	5738	0.65	0.12	0.7	1.21	2.97	6.93	8.04	0.03
E4	120	147.9	77.65	2.64	1.9	366	0.41	0.017	2.43	0.022	5996	0.81	0.08	0.46	0.77	2.52	5.93	6.79	0.032
E4	160	164.99	82.76	2.95	1.99	366	0.37	0.019	2.71	0.024	5626	0.69	0.11	0.38	0.56	2.5	6.22	7.59	0.032
E4	220	186.36	78.36	3.33	2.38	366	0.33	0.024	3.06	0.027	5942	0.57	0.16	0.33	0.45	1.58	3.81	5.11	0.062
E4	260	136.67	82.35	2.44	1.66	366	0.45	0.014	2.24	0.02	5654	0.91	0.06	0.41	0.7	2.47	6.38	7.66	0.026

4.3 APPENDIX C

Cross-section of the tests performed in Phase II (E5 to E7 / ST-40 to ST-120)

Cross section	E5	E6	E7
ST - 40			
ST - 80			
ST - 120			

16 Cross-section of the tests performed in Phase II (E8 to E10 / ST-40 to ST-120)

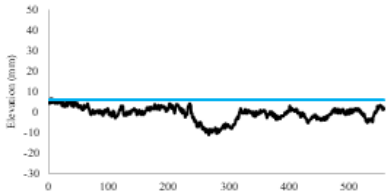
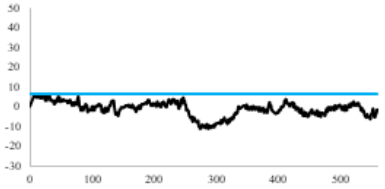
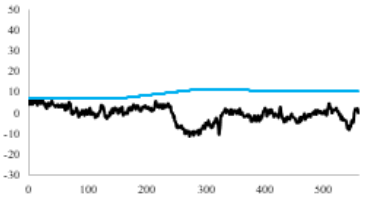
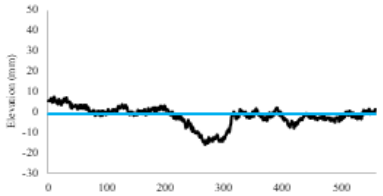
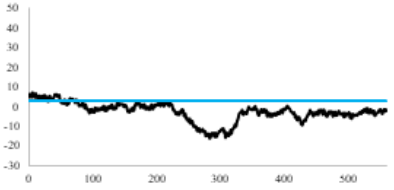
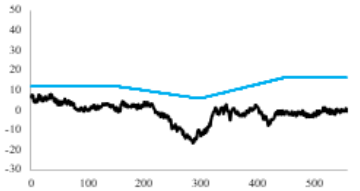
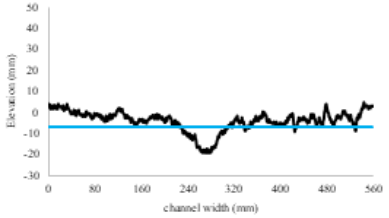
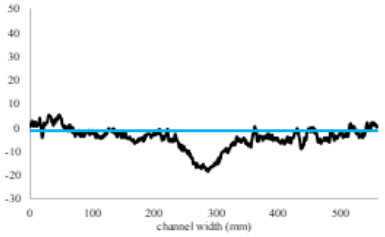
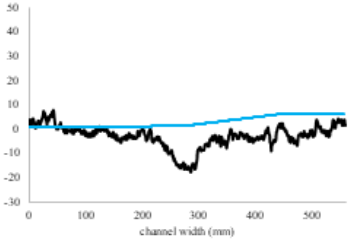
Cross section	E8	E9	E10
ST - 40			
ST - 80			
ST - 120			

17

18

19

20 Cross-section of the tests performed in Phase II (E5 to E7 / ST-160 to ST-260)

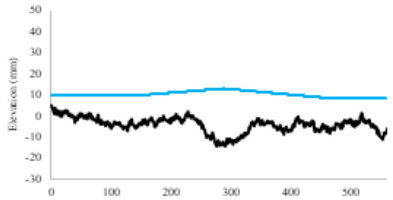
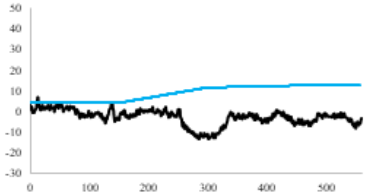
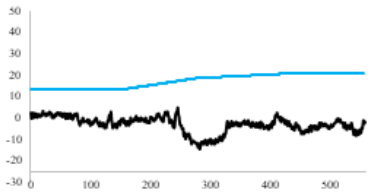
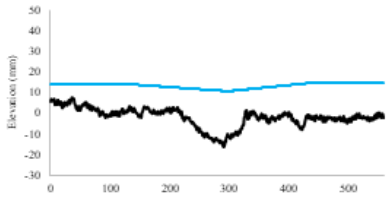
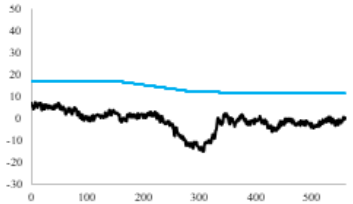
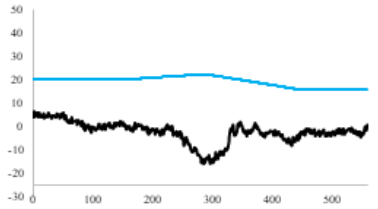
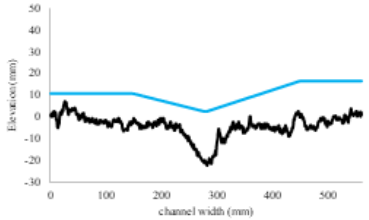
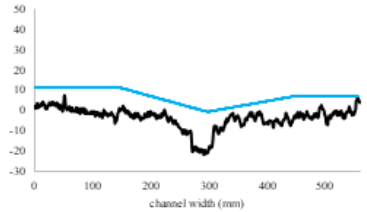
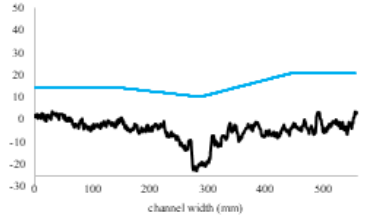
Cross section	E5	E6	E7
ST - 160			
ST - 220			
ST - 260			

21

22

23

24 Cross-section of the tests performed in Phase II (E8 to E10 / ST-160 to ST-260)

Cross section	E8	E9	E10
ST - 160			
ST - 220			
ST - 260			

25

26

27

4.4 APPENDIX D

Tests	ST	Area (cm²)	Perimeter (cm)	Average depth (cm)	Hydraulic radius (cm)	Discharge (L/min)	Velocity (m/s)	n (Manning)	Boundary shear stress (N/m²)	Shields number	Reynolds number	Froude number	Darcy-Weisbach friction factor	Relative submergence (Rh/D84inicial)	R10 (mm)	R16 (mm)	R50 (mm)	R84 (mm)	R90 (mm)	raiz (8/f)	FO	σ	Rh/R84	Rh/OF	Rh/σ	Roughness scale (h/R84)
E5	40	9.24	30.61	0.92	0.3	10	0.03	0.011	0.85	0.008	422	0.61	0.07	0.44	0.54	0.75	3	6.42	7.32	11.01	1.47	6.63	0.47	2.06	0.45	Intermediate
E5	80	47.27	77.98	0.61	0.61	10	0.05	0.09	0.56	0.005	166	0.15	3.47	0.88	0.28	0.54	2.76	7.1	8.57	1.52	1.39	2.79	0.85	4.35	2.17	Large
E5	120	35.17	63.71	0.45	0.55	10	0.07	0.063	0.41	0.004	203	0.23	1.75	0.8	0.52	0.71	2.92	6.02	6.93	2.14	1.41	3.22	0.92	3.92	1.71	Large
E5	160	32.92	74.23	0.43	0.44	10	0.07	0.051	0.39	0.004	174	0.25	1.23	0.64	0.61	0.83	3.06	6.13	7.26	2.55	1.37	3.56	0.72	3.23	1.24	Large
E5	220	11.92	44.37	0.16	0.27	10	0.19	0.013	0.14	0.001	291	1.15	0.1	0.39	0.48	0.63	1.61	3.74	4.95	9.04	1.36	4.62	0.72	1.97	0.58	Large
E5	260	4.97	12.43	0.06	0.4	10	0.48	0.007	0.06	0.001	1040	4.36	0.03	0.58	0.43	0.71	2.56	6.19	7.39	17.79	1.42	4.88	0.65	2.8	0.82	Large
E6	40	11.69	34.66	0.97	0.34	19	0.06	0.008	0.89	0.008	706	0.89	0.03	0.49	0.28	0.4	1.27	3.37	3.93	15.58	1.46	4.34	1	2.31	0.78	Intermediate
E6	80	63.53	75.21	0.84	0.84	19	0.07	0.08	0.78	0.007	325	0.18	2.44	1.23	0.44	0.58	1.73	3.95	5.44	1.81	1.35	3.32	2.14	6.28	2.55	Intermediate
E6	120	39.29	68.06	0.51	0.58	19	0.11	0.038	0.47	0.004	359	0.36	0.64	0.84	0.36	0.48	1.89	5.13	6.27	3.54	1.38	3.29	1.12	4.2	1.76	Large
E6	160	39.55	75.93	0.52	0.52	19	0.11	0.036	0.48	0.004	322	0.36	0.58	0.76	0.32	0.46	2.03	5.6	6.76	3.7	1.37	3.63	0.93	3.81	1.44	Large
E6	220	30.82	68.94	0.4	0.45	19	0.14	0.025	0.36	0.003	355	0.53	0.3	0.65	0.59	0.76	2.48	6.88	8.66	5.13	1.39	4.85	0.65	3.22	0.92	Large
E6	260	19.05	62.23	0.24	0.31	19	0.24	0.012	0.22	0.002	393	1.1	0.08	0.44	0.59	0.81	2.57	6.66	7.75	10.03	1.42	4.74	0.46	2.16	0.65	Large
E7	40	40.26	78.09	0.72	0.52	41	0.17	0.017	0.66	0.006	663	0.63	0.13	0.75	0.33	0.55	1.97	4	5.62	7.74	1.44	3.89	1.29	3.57	1.32	Intermediate
E7	80	76.49	77.73	0.98	0.98	41	0.12	0.05	0.9	0.008	666	0.29	0.92	1.43	0.2	0.25	1.4	3.6	4.57	2.95	1.39	2.74	2.74	7.07	3.6	Intermediate
E7	120	44.92	63.78	0.57	0.7	41	0.21	0.024	0.52	0.005	812	0.64	0.23	1.02	0.23	0.6	1.82	5.12	6.32	5.94	1.41	3.26	1.38	5	2.16	Large

Tests	ST	Area (cm²)	Perimeter (cm)	Average depth (cm)	Hydraulic radius (cm)	Discharge (L/min)	Velocity (m/s)	n (Manning)	Boundary shear stress (N/m²)	Shields number	Reynolds number	Froude number	Darcy-Weisbach friction factor	Relative submergence (Rh/D84inicial)	R10 (mm)	R16 (mm)	R50 (mm)	R84 (mm)	R90 (mm)	raiz (8/f)	FO	σ	Rh/R84	Rh/OF	Rh/σ	Roughness scale (h/R84)
E7	160	55.26	77.61	0.71	0.71	41	0.17	0.029	0.65	0.006	667	0.46	0.35	1.03	0.51	0.75	2.37	5.68	6.92	4.8	1.39	3.72	1.25	5.13	1.91	Intermediate
E7	220	71.33	77.17	0.92	0.92	41	0.13	0.045	0.85	0.008	671	0.32	0.75	1.34	0.38	0.52	2.32	7.64	10.4	3.26	1.38	4.8	1.21	6.7	1.93	Intermediate
E7	260	34.5	71.94	0.43	0.48	41	0.28	0.014	0.4	0.004	720	0.96	0.09	0.7	0.34	0.49	2.34	7.04	8.89	9.37	1.43	4.83	0.68	3.35	0.99	Large
E8	40	99.6	82.59	1.78	1.21	84	0.14	0.036	1.64	0.015	1287	0.33	0.45	1.75	0.12	0.32	1.09	2.87	3.42	4.2	1.48	4.81	4.2	8.15	2.51	Small
E8	80	100.8	76.67	1.31	1.31	84	0.19	0.039	1.21	0.011	1387	0.39	0.51	1.91	0.44	0.62	1.9	3.94	5.37	3.97	1.37	3.22	3.34	9.57	4.08	Intermediate
E8	120	88.03	78.91	1.12	1.12	84	0.22	0.031	1.03	0.009	1347	0.48	0.33	1.62	0.46	0.68	2.09	4.81	6.19	4.94	1.41	3.11	2.32	7.9	3.59	Intermediate
E8	160	79.2	78.09	1.01	1.01	84	0.25	0.026	0.93	0.008	1361	0.56	0.24	1.47	0.44	0.67	2.39	6	7.04	5.76	1.4	3.65	1.69	7.26	2.78	Intermediate
E8	220	85.33	77.71	1.1	1.1	84	0.23	0.029	1.01	0.009	1368	0.5	0.3	1.59	0.44	0.65	2.47	7.07	9.12	5.14	1.39	4.76	1.55	7.9	2.31	Intermediate
E8	260	81.11	80.66	1.01	1.01	84	0.25	0.026	0.92	0.008	1318	0.55	0.25	1.46	0.23	0.65	2.52	6.81	8.14	5.65	1.44	5.24	1.48	6.97	1.92	Intermediate
E9	40	97.16	83.42	1.74	1.16	105	0.18	0.028	1.6	0.014	1607	0.44	0.26	1.69	0.35	0.5	1.9	3.67	3.99	5.53	1.49	4.15	3.17	7.79	2.81	Small
E9	80	89.86	76.66	1.17	1.17	105	0.27	0.026	1.08	0.01	1749	0.58	0.23	1.7	0.43	0.59	1.84	4.2	6.19	5.95	1.37	3.36	2.79	8.54	3.49	Intermediate
E9	120	85.04	76.01	1.12	1.12	105	0.28	0.023	1.03	0.009	1764	0.62	0.19	1.62	0.41	0.63	1.82	4.82	6.18	6.44	1.36	3.24	2.32	8.23	3.45	Intermediate
E9	160	66.09	78.41	0.84	0.84	105	0.38	0.015	0.77	0.007	1710	0.93	0.09	1.22	0.49	0.7	2.19	5.85	6.97	9.55	1.41	3.85	1.44	5.96	2.19	Intermediate
E9	220	84.45	77.75	1.08	1.09	105	0.29	0.023	1	0.009	1724	0.64	0.18	1.58	0.22	0.6	2.45	7.19	9.21	6.58	1.39	4.66	1.51	7.8	2.33	Intermediate
E9	260	56.1	81.71	0.69	0.69	105	0.46	0.011	0.63	0.006	1641	1.21	0.05	1	0.47	0.72	2.7	6.78	7.83	12.46	1.46	5.4	1.01	4.7	1.27	Large
E10	40	139.79	82.98	2.5	1.68	205	0.24	0.026	2.3	0.021	3136	0.49	0.21	2.45	0.4	0.63	1.91	4.59	5.93	6.2	1.49	3.57	3.67	11.33	4.72	Small
E10	80	141.06	80.7	1.75	1.75	205	0.35	0.027	1.6	0.014	3224	0.58	0.22	2.54	0.49	0.66	1.79	4.15	6.22	6.03	1.45	3.3	4.21	12.09	5.29	Small
E10	120	116.11	76.72	1.51	1.51	205	0.4	0.02	1.39	0.012	3392	0.76	0.13	2.2	0.48	0.66	2.08	4.94	6.23	7.87	1.37	3.5	3.06	11.03	4.32	Intermediate

Tests	ST	Area (cm²)	Perimeter (cm)	Average depth (cm)	Hydraulic radius (cm)	Discharge (L/min)	Velocity (m/s)	n (Manning)	Boundary shear stress (N/m²)	Shields number	Reynolds number	Froude number	Darcy-Weisbach friction factor	Relative submergence (Rh/D84inicial)	R10 (mm)	R16 (mm)	R50 (mm)	R84 (mm)	R90 (mm)	raiz (8/f)	FO	σ	Rh/R84	Rh/OF	Rh/σ	Roughness scale (h/R84)
E10	160	113.92	81.46	1.4	1.4	205	0.44	0.019	1.29	0.012	3194	0.81	0.11	2.03	0.44	0.66	2.12	6.04	7.37	8.35	1.46	3.74	2.32	9.6	3.74	Intermediate
E10	220	120.54	76.69	1.57	1.57	205	0.39	0.021	1.44	0.013	3393	0.72	0.14	2.28	0.43	0.67	2.33	6.88	8.41	7.44	1.37	4.51	2.29	11.44	3.48	Intermediate
E10	260	110.68	81.29	1.36	1.36	205	0.45	0	1.25	0.011	3201	0.84	0.11	1.98	0.56	0.95	2.88	6.53	7.48	8.71	1.45	5.19	2.08	9.36	2.63	Intermediate

6. CONCLUSÕES E PERSPECTIVAS

Com o propósito de sintetizar e destacar as principais contribuições desta tese, este capítulo foi estruturado em três partes: (i) generalizações decorrentes dos resultados obtidos; (ii) principais considerações e interpretações dos achados; e (iii) recomendações para pesquisas futuras. Essa organização visa evidenciar de forma clara como a estrutura metodológica desenvolvida e os procedimentos experimentais adotados podem fornecer suporte para o avanço do conhecimento sobre a dinâmica do escoamento e do transporte de sedimentos em canais com leito de granulometria extensa.

Além disso, busca-se demonstrar como os resultados aqui alcançados podem ser aplicados em problemas de engenharia hidráulica, contribuindo para o aprimoramento de modelos físicos e conceituais e servindo de base para investigações futuras que ampliem a compreensão dos processos hidrossedimentológicos em rios similares ao desse estudo.

6.1 GENERALIZAÇÕES

Ao avaliar as condições hidrodinâmicas e as características do material constituinte do leito, é possível estabelecer diversas relações empíricas ou semiempíricas (modelos) que auxiliam na compreensão dos processos interdependentes entre essas variáveis, além de permitir a estimativa de parâmetros cuja obtenção em campo é frequentemente complexa. Nesse contexto, a formulação de um modelo que relacione a tensão de cisalhamento de fundo (τ) com a razão entre a profundidade da lâmina d'água e o coeficiente de rugosidade (h/ks) possibilita a aplicação dessa relação em situações nas quais não foi possível determinar experimentalmente o valor de *ks*, por exemplo.

Dessa forma, aplicou-se aos dados apresentados no Artigo II a equação proposta no Artigo III (Equação 22), considerando $ks = 3{,}16 \cdot D_{84}$, conforme ilustrado na Figura 5-15. Cabe destacar que os dados utilizados no Artigo II não derivam de medições de perfis de velocidade, tampouco apresentam medições espacializadas do nível d'água. Nesse caso, a profundidade média (*h*) foi obtida pela razão entre a área útil de escoamento e a largura útil do escoamento, enquanto a velocidade média da seção foi estimada pela equação da continuidade ($U = Q/A$). Isso implica que os dados do Artigo III possuem maior nível de detalhamento, uma vez que representam a distribuição espacial das velocidades e dos níveis d'água em cada ponto das seções analisadas.

Os resultados apresentados na Figura 6-1evidenciam uma superestimativa dos valores de τ, em virtude das diferenças da relação h/ks. Essa diferença pode estar associada à limitação mencionada anteriormente, isto é, ao fato de que os dados médios empregados no Artigo II não refletem as medições pontuais obtidas no Artigo III. O uso de medições pontuais de velocidade permite um detalhamento mais preciso do comportamento hidrodinâmico espacializado, diferindo significativamente dos valores médios de seção obtidos no canal experimental.

Além disso, foram plotados os dados obtidos por Menezes (2021), considerando a correção do *ks* determinada no Artigo III, e observou-se que esses pontos se sobrepõem aos dados medidos a partir dos perfis de velocidade, no entanto, apresentam uma menor variabilidade dos dados. Esse resultado indica que as medições realizadas com base em perfis de velocidade podem representar o comportamento hidrodinâmico observado em campo.

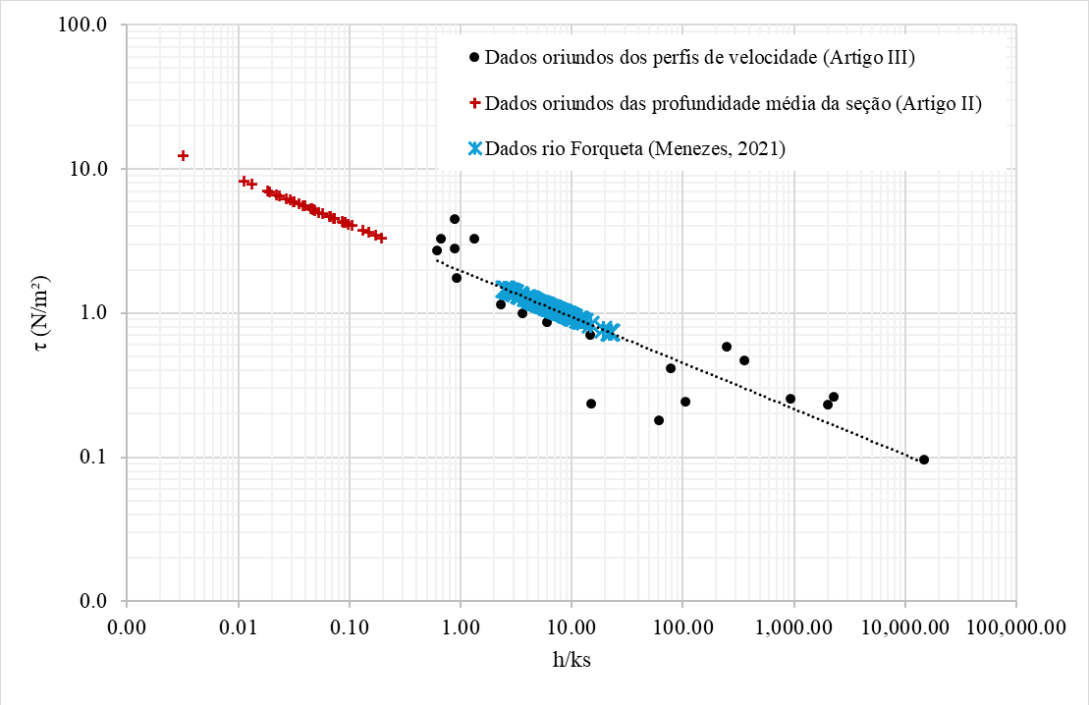


Figura 6-1 – Relação entre τxh/ks para os dados do artigo III e artigo II.

Acrescenta-se a essas generalizações, o cálculo da declividade local do fundo do canal. Em rios situados em ambientes montanhosos, é comum a ocorrência de diferentes formas morfológicas — tais como *step-pool*, *plane-bed*, *cascade*, entre outras — que exercem influência direta na determinação da declividade média de um trecho ou de todo o canal. Nesse contexto, a partir da estimativa da tensão de cisalhamento de fundo (τ), torna-se

possível determinar a declividade local ($I_{local} = J$) por meio da aplicação da Equação 23, expressa como:

$$J = \frac{\tau}{\Upsilon h} \qquad 23$$

Na Figura 6-2 é apresentado o comportamento da relação entre τ e I_{local} para os dados do Artigo III, bem como a aplicação dessa relação aos dados do Artigo II e aos dados de campo. Os resultados apresentaram diferenças significativas, principalmente em virtude da reduzida variabilidade dos valores de τ quando aplicados aos dados de campo. Além disso, observou-se que, embora os dados do Artigo II apresentem valores subestimados de τ, o comportamento de I_{local} obtido mostrou-se próximo ao dos dados apresentados no Artigo III.

Ao comparar os valores de declividade local obtidos pela Equação 23 com a declividade média do canal, observa-se que, para os dados do Artigo III, os valores correspondem, em média, a 34% da declividade do canal (0,00937 m/m). Por outro lado, para os dados do Artigo II, essa correspondência é de aproximadamente 84,9%. Essa diferença, por si só, evidencia o quanto o nível de detalhamento das medições influencia os valores estimados, ressaltando a importância de se incluir medições pontuais para uma representação mais realista e precisa da inclinação local do fundo do canal.

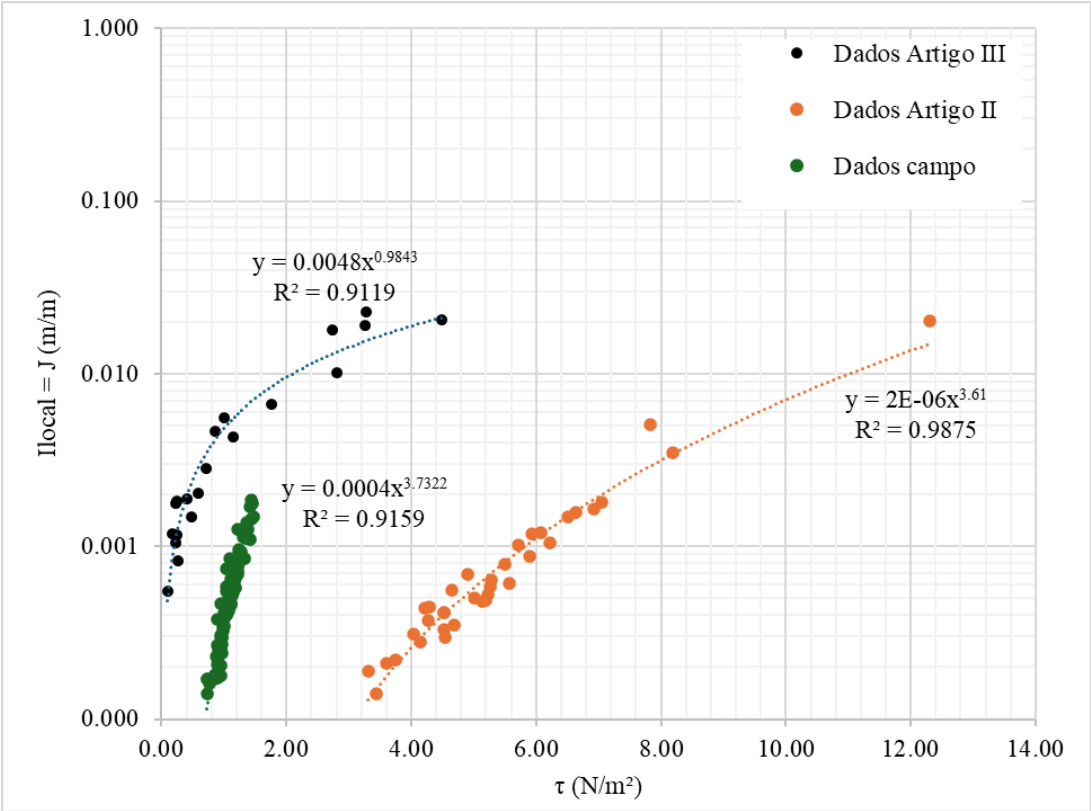


Figura 6-2 - Relação entre τ e I_{local}=J para os dados do artigo III, artigo II e dados de campo

Outra generalização possível a partir dos dados obtidos nesta tese refere-se à determinação de parâmetros de resistência ao escoamento, como o fator de atrito de Darcy–Weisbach (*f*). A formulação de um modelo baseado em dados experimentais contribui para o entendimento do comportamento do escoamento frente a diferentes condições de rugosidade, especialmente em rios com leitos de granulometria extensa.

Nesse contexto, é comum na literatura estabelecer uma relação entre h/D_{84} e $\sqrt{(8/f)}$, uma vez que esses parâmetros representam, respectivamente, a rugosidade relativa do fundo do canal e a resistência ao escoamento. Na Figura 6-3 é apresentado o modelo desenvolvido a partir dos dados relatados no Artigo III, aplicado aos dados do Artigo II e aos dados de campo. O modelo resultante é expresso na equação a seguir e apresentou um coeficiente de determinação (R^2) relativamente baixo (0,044), o que se deve à reduzida variabilidade observada nos dados analisados.

$$\sqrt{\frac{8}{f}} = 6{,}8989\left(\frac{h}{D_{84}}\right)^{0{,}4198} \qquad 24$$

Embora o valor de R^2 obtido tenha sido relativamente baixo, o comportamento observado mostra-se coerente com o apresentado por equações consagradas na literatura, conforme discutido no item 5.3.3 do Artigo III, especialmente as formulações propostas por Rickenmann e Recking (2011), Ferguson (2007) e Hey (1979). Contudo, todas essas equações tendem a subestimar os valores medidos neste estudo. Esse resultado reforça a importância do desenvolvimento e da calibração de relações locais entre rugosidade e resistência ao escoamento, de modo a representar com maior fidelidade as condições hidráulicas específicas de cada ambiente.

De maneira geral, os dados medidos tanto em canal experimental (nos Artigos II e III) quanto no rio natural apresentaram comportamento semelhante. A aplicação da equação proposta, entretanto, encontra-se limitada ao conjunto de dados disponíveis no Artigo III — o ideal seria a realização de testes sob diferentes condições de vazão e com distintas características granulométricas do leito.

Além disso, cabe destacar que este trabalho não adotou um único diâmetro representativo nos ensaios; ao contrário, empregou-se uma granulometria extensa, de forma a reproduzir, de maneira mais realista, as condições observadas em rios naturais. Embora tal abordagem dificulte a comparação direta com as equações clássicas da literatura, ela proporciona resultados mais representativos e condizentes com a realidade física analisada neste estudo.

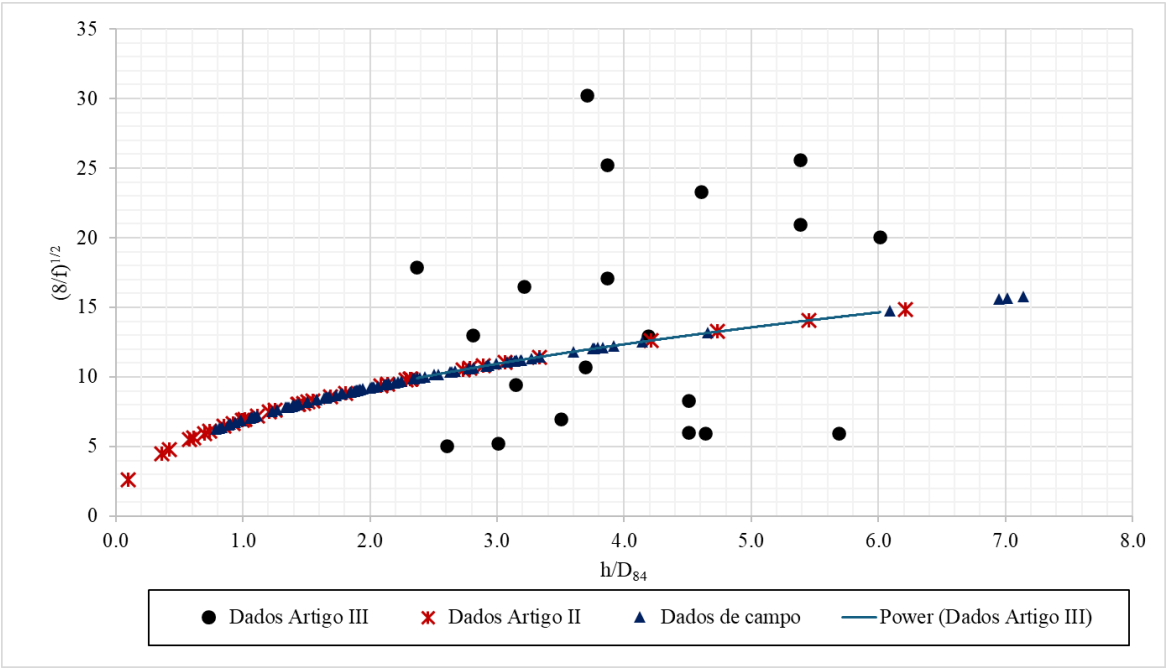


Figura 6-3 - Relação entre h/D_{84} e $(8/f)^{1/2}$

6.2 PRINCIPAIS CONSIDERAÇÕES

Conforme destacado, esta tese teve como objetivo principal investigar a influência da rugosidade de fundo na dinâmica do escoamento e do transporte de sedimentos em rios de leito cascalhoso, por meio de uma abordagem integrada envolvendo a modelagem física inspirada em um rio natural. A partir do desenvolvimento subsequencial desta tese, foi possível avançar na compreensão dos processos físicos que governam a resistência ao escoamento, a organização morfológica do leito e a mobilização de sedimentos em ambientes fluviais com granulometria extensa.

A concepção e execução de um modelo físico reduzido representativo de um rio natural brasileiro constituíram uma das principais contribuições deste trabalho. O aparato experimental, desenvolvido com base em dados de campo, permitiu reproduzir padrões de escoamento e sedimentação observados em sistemas reais, oferecendo uma alternativa controlada para quantificar variáveis que, em campo, demandariam maior tempo, recursos e esforço logístico. Essa infraestrutura experimental viabilizou o controle de condições hidráulicas, a medição de perfis de velocidade e a caracterização de parâmetros morfológicos e sedimentológicos com elevado grau de precisão.

No primeiro artigo, foi realizada a fase preliminar de experimentos com o objetivo de desenvolver um leito móvel capaz de reproduzir a morfologia e o comportamento hidráulico de um rio natural, alcançando conformações geométricas e trajetórias de fluxo compatíveis com aquelas observadas em campo. Os resultados demonstraram que a distribuição dos sedimentos e o preenchimento de vazios intergranulares por partículas finas influenciaram significativamente a resistência ao escoamento e os parâmetros de rugosidade (n, f e C). O aumento do diâmetro médio dos grãos móveis resultou em maior resistência hidráulica, enquanto a redução da vazão produziu elevação de ks e intensificação dos efeitos de deposição. Esses resultados forneceram uma base física e conceitual sólida para os experimentos subsequentes, validando a metodologia adotada e confirmando a relevância de modelos físicos para a investigação de processos fluviais complexos.

O segundo artigo abordou de forma aprofundada a caracterização da rugosidade de fundo e da resistência hidráulica em um canal experimental estabilizado inspirado em um rio natural (escala 1:20), destacando a importância de uma etapa de equilíbrio

morfológico anterior à realização dos ensaios. Verificou-se que, durante essa fase, o ajuste natural do material de fundo e o preenchimento gradual dos espaços intersticiais por sedimentos finos influenciaram diretamente a resposta hidráulica, reforçando a necessidade de se considerar a condição de equilíbrio entre o transporte e a deposição de sedimentos em modelos físicos representativos. Os resultados mostraram que a resistência ao escoamento diminui com o aumento da submergência relativa, enquanto condições de baixa vazão e submergência reduzida resultaram em valores elevados de rugosidade hidráulica, associados ao desenvolvimento de microtopografia e camadas de *armoring*. Além disso, as equações empíricas tradicionais se mostraram insuficientes para reproduzir adequadamente os resultados obtidos, indicando a necessidade de formulações específicas para rios de leito cascalhoso em regiões tropicais.

O terceiro artigo explorou os efeitos hidrodinâmicos da rugosidade sobre os perfis de velocidade, avaliando experimentalmente a relação entre os parâmetros de resistência ao fluxo. Os resultados confirmaram que o coeficiente de rugosidade (ks) não é constante, mas dependente das condições de escoamento e do grau de submergência relativa. Em baixos valores de h/D_{84} (rugosidade em grande escala), observou-se predominância da resistência de forma (*form drag*). A análise também revelou o comportamento dual de ks, que aumenta em condições rasas e estabiliza em regimes mais profundos, enfatizando o papel determinante da submergência relativa no controle da resistência hidráulica.

De forma integrada, os três estudos mostraram que a rugosidade de fundo exerce papel central na organização do escoamento e no transporte de sedimentos, e que o comportamento hidráulico em rios de leito cascalhoso é condicionado por interações multiescalares entre topografia de fundo, granulometria e submergência. A partir das análises realizadas, foi possível definir parâmetros representativos de resistência ao escoamento para rios de leito de cascalho, como o estudado nessa tese.

Por conseguinte, esta tese contribui de forma inédita para o entendimento dos processos hidrossedimentológicos em rios de granulometria extensa no Brasil, oferecendo um arcabouço experimental e conceitual capaz de subsidiar aplicações práticas em projetos de engenharia hidráulica, manejo de áreas inundáveis, renaturalização de rios e modelagem de escoamentos naturais. De modo geral, esta tese consolidou uma base experimental robusta e um conjunto de evidências que fortalecem a integração entre

observações empíricas, modelagem física e formulações teóricas, reforçando a importância de abordagens combinadas para o estudo de sistemas fluviais complexos.

6.3 RECOMENDAÇÕES PARA TRABALHOS FUTUROS

Embora os resultados obtidos tenham proporcionado avanços relevantes, diversos aspectos ainda podem ser aprofundados em pesquisas futuras. As principais recomendações incluem:

- Simular diferentes condições de contorno e regimes de escoamento, variando a vazão, a declividade e o aporte de sedimentos, de modo a compreender a resposta morfológica e hidráulica em um espectro mais amplo de cenários representativos;
- Comparar os resultados experimentais com simulações numéricas em softwares hidrodinâmicos e morfodinâmicos, permitindo avaliar a aplicabilidade de equações empíricas e ajustar parâmetros calibráveis com base em dados físicos;
- Expandir a base de dados experimental, incluindo medições tridimensionais de velocidade, tensão de cisalhamento e topografia de fundo com sensores de alta resolução (como perfiladores acústicos e scanners a laser), a fim de reduzir incertezas associadas às medições pontuais;
- Investigar a estabilidade de canais de leito cascalhoso sob diferentes regimes hidrológicos, incorporando aspectos de vegetação ripária, conectividade lateral e heterogeneidade de habitats, de forma a apoiar iniciativas de restauração e gestão fluvial;
- Desenvolver modelos matemáticos específicos para rios brasileiros de montanha, calibrados com base nos resultados experimentais obtidos nesta pesquisa e comparados com dados provenientes de protótipos naturais.

A continuidade dessas investigações permitirá refinar modelos de resistência ao escoamento e de transporte de sedimentos, aumentar a previsibilidade dos comportamentos hidrodinâmicos em rios naturais e subsidiar o planejamento e a gestão sustentável de sistemas fluviais no contexto brasileiro. Essas recomendações reforçam a importância de uma abordagem multidisciplinar e integrada no estudo de sistemas

fluviais, essencial para compreender os processos que controlam a evolução morfológica dos rios e subsidiar estratégias de gestão e conservação de recursos hídricos mais eficientes e sustentáveis.

7. REFERÊNCIAS

ABERLE, J.; SMART, G. M. The influence of roughness structure on flow resistance on steep slopes. **Journal of Hydraulic Research**, v. 41, n. 3, p. 259–269, 2003.

ANCEY, C. Bedload transport: a walk between randomness and determinism. Part 1. The state of the art. **Journal of Hydraulic Research**, v. 58, n. 1, p. 1–17, 2020.

BATHURST, J. C. Critical conditions for particle motion in coarse bed materials of nonuniform size distribution. **Geomorphology**, v. 197, p. 170–184, 2013.

BATHURST, J. C. **Flow resistance estimation in mountain rivers**. [*S. l.: s. n.*], 1985.

BOGATIN, E. *et al*. Which one is better? Comparing options to describe frequency dependent losses. 2013.

BRENNA, A.; SURIAN, N.; MAO, L. Response of A Gravel - Bed River To Dam Closure: Insights From Sediment Transport Processes And Channel Morphodynamics. **Earth Surface Processes and Landforms**, v. 45, n. 3, p. 756–770, 2020.

BRIDGE, J. S.; DOMINIC, D. F. Bed load grain velocities and sediment transport rates. **Water Resources Research**, v. 20, n. 4, p. 476-490, 1984.

BUFFIN-BÉLANGER, T. *et al.* A casting procedure for reproducing coarse-grained sedimentary surfaces. **Earth Surface Processes and Landforms**, v. 28, n. 7, p. 787–796, 2003.

CANOVARO, F.; PARIS, E.; SOLARI, L. Effects of macro-scale bed roughness geometry on flow resistance. **Water Resources Research**, v. 43, n. 10, 2007.

CHEN, X. *et al.* Rough Correlations: Meta-Analysis of Roughness Measures in Gravel Bed Rivers. **Water Resources Research**, v. 56, n. 8, 2020.

CHURCH, M.; FERGUSON, R. I. Morphodynamics: Rivers beyond steady state. **Water Resources Research**, v. 51, n. 4, p. 1883–1897, 2015.

CHURCH, M.; HASSAN, M. A.; WOLCOTT, J. F. Stabilizing self-organized structures in gravel-bed stream channels: Field and experimental observations. **Water Resources Research**, v. 34, n. 11, p. 3169–3179, 1998.

CHURCH M. Geomorphic Thresholds in Riverine Landscape. **Freshwater Biology**, v. 47, p. 541–557, 2002a.

COMITI, F.; MAO, L. **Recent Advances in the Dynamics of Steep Channels**. [*S. l.: s. n.*], 2012.

COOPER, J. R. *et al.* Influence of relative submergence on spatial variance and form-induced stress of gravel-bed flows. **Water Resources Research**, v. 49, n. 9, p. 5765–5777, 2013.

CURRAN, J. H.; WOHL, E. E. Large woody debris and flow resistance in step-pool channels, Cascade Range, Washington. **Geomorphology**, v. 51, n. 1-3, p. 141-157, 2003.

DAVID, G. C. L. *et al.* Comparative analysis of bed resistance partitioning in high-gradient streams. **Water Resources Research**, v. 47, n. 7, 2011.

DIETRICH, W. E., *et al.* Sediment supply and the development of the coarse surface layer in gravel-bedded rivers. **Nature**, v. 340, p. 215–217, 1989.

DU BOYS, M. P. Le Rhône et les rivières à lit affouillable. **Annales des Ponts et Chaussées,** Série 5, Tome 18, 141–195. 1879.

EGIAZAROFF, I. V. Calculation of nonuniform sediment concentrations. **Journal of the Hydraulics Division**, v. 91, n. 4, p. 225-247, 1965.

ENGELUND, F.; FREDSØE, J. A sediment transport model for straight alluvial channels. **Hydrology Research**, v. 7, n. 5, p. 293-306, 1976.

FERGUSON, R. Flow resistance equations for gravel- and boulder-bed streams. **Water Resources Research**, v. 43, n. 5, p. 1–12, 2007.

FERNANDEZ LUQUE, R.; VAN BEEK, R. Erosion and transport of bed-load sediment. **Journal of Hydraulic Research/De Recherches Hydrauliques**, v. 14, n. 2 (1976), p. 127–144, 1976.

FERRARO, D.; COSCARELLA, F.; GAUDIO, R. Scales of turbulence in open-channel flows with low relative submergence. **Physics of Fluids**, v. 31, n. 12, 2019.

FERRO, V. Assessing flow resistance in gravel bed channels by dimensional analysis and self-similarity. **Catena**, v. 169, p. 119–127, 2018.

GHILARDI, T.; FRANCA, M. J.; SCHLEISS, A. J. Bed load fluctuations in a steep channel. **Water Resources Research**, v. 50, n. 8, p. 6557–6576, 2014.

GOMEZ, B. **Bedload transportEarth-Science Reviews**. v. 31, n. 2, p. 89-132, 1991.

HARDY, R. J. *et al.* Coherent flow structures in a depth-limited flow over a gravel surface: The influence of surface roughness. **Journal of Geophysical Research: Earth Surface**, v. 115, n. 3, 2010.

HASCHENBURGER, J. K.; WILCOCK, P. R. Partial transport in a natural gravel bed channel. **Water Resources Research**, v. 39, n. 1, p. 1–9, 2003.

HEY, Richard D. Flow resistance in gravel-bed rivers. **Journal of the Hydraulics Division**, v. 105, n. 4, p. 365-379, 1979.

HEYMAN, J. *et al.* Statistics of bedload transport over steep slopes: Separation of time scales and collective motion. **Geophysical Research Letters**, v. 40, n. 1, p. 128–133, 2013.

LAMB, M. P.; DIETRICH, W. E.; VENDITTI, J. G. Is the critical shields stress for incipient sediment motion dependent on channel-bed slope?. **Journal of Geophysical Research: Earth Surface**, v. 113, n. 2, p. 1–20, 2008a.

LENZI, M. A.; D'AGOSTINO, V.; BILLI, P. Bedload transport in the instrumented catchment of the Rio Cordon. Part I: Analysis of bedload records, conditions and threshold of bedload entrainment. **Catena**, v. 36, n. 3, p. 171–190, 1999.

LENZI, M. A.; MAO, L.; COMITI, F. Effective discharge for sediment transport in a mountain river: Computational approaches and geomorphic effectiveness. **Journal of Hydrology**, v. 326, n. 1–4, p. 257–276, 2006.

LENZI, M. A.; MAO, L.; COMITI, F. Magnitude-frequency analysis of bed load data in an Alpine boulder bed stream. **Water Resources Research**, v. 40, n. 7, p. 1–12, 2004.

LISLE, T. E. Particle size variations between bed load and bed material in natural gravel bed channels. **Water Resources Research**, v. 31, n. 4, p. 1107-1118, 1995.

LÓPEZ, R. *et al.* Bed-material entrainment in a mountain river affected by hydropeaking. **Science of the Total Environment**, v. 856, 2023.

MANICA, R. Geração de correntes de turbidez de alta densidade: condicionantes hidráulicos e deposicionais. **Tese de Doutorado. PPG Recursos Hídricos e Saneamento Ambiental**. UFRGS. 2009.

MAO, L. *et al.* Bed material transport estimate in large gravel-bed rivers using the virtual velocity approach. **Earth Surface Processes and Landforms**, v. 42, n. 4, p. 595–611, 2017.

MAO, L. *et al.* Controls Over Particle Motion and Resting Times of Coarse Bed Load Transport in a Glacier-Fed Mountain Stream. **Journal of Geophysical Research: Earth Surface**, v. 125, n. 4, p. 1–15, 2020.

MAO, L.; LENZI, M. A. Sediment of mobility and bedload transport conditions in an alpine stream. **Hydrological Processes**, v. 21, n. 14, p. 1882–1891, 2007.

MASTELLER, C. C.; FINNEGAN, N. J. Interplay between grain protrusion and sediment entrainment in an experimental flume. **Journal of Geophysical Research: Earth Surface**, v. 122, n. 1, p. 274–289, 2017.

MENEZES, D. *et al.* Avaliação do transporte de sedimentos de fundo por meio da pintura de sedimentos grosseiros em rio pedregoso. XXIV Simpósio Brasileiro de Recursos Hídricos (Belo Horizonte). **Anais. ABRHidro.** 2021

MENEZES, D. Caracterização hidrossedimentológica de trecho do rio Forqueta, Maquiné/RS. **Dissertação de Mestrado. PPG Recursos Hídricos e Saneamento Ambiental**. UFRGS. 2021.

MENEZES, D.; KOBIYAMA, M. Sediment size and shape observation in a mountain river, southern Brazil. In: **EGU General Assembly Conference Abstracts**. 2021.

MENEZES, D.; KOBIYAMA, M.; MICHEL, G. Análise da composição da vazão na bacia hidrográfica do rio Forqueta (Maquiné/RS), Sul do Brasil. **Revista de Gestão de Água da América Latina**, v. 19, n. 1, p. 11–0, 2022.

MENEZES, D.; KOBIYAMA, M. Hydrosedimentological characterization of a reach in the Forqueta River catchment, south Brazil. **Journal of South American Earth Sciences**, p. 104430, 2023.

MEYER-PETER, E; MÜLLER, R. Formulas for bed-load transport. In: **IAHSR 2nd meeting, Stockholm**. IAHR, 1948.

MONSALVE, A.; YAGER, E. M.; SCHMEECKLE, M. W. Effects of Bed Forms and Large Protruding Grains on Near-Bed Flow Hydraulics in Low Relative Submergence Conditions. **Journal of Geophysical Research: Earth Surface**, v. 122, n. 10, p. 1845–1866, 2017.

MONTGOMERY, D. R.; BUFFINGTON, J. M. Channel-reach morphology in mountain drainage basins. **Bulletin of the Geological Society of America**, v. 109, n. 5, p. 596–611, 1997.

NELSON, A.; DUBÉ, K. Channel response to an extreme flood and sediment pulse in a mixed bedrock and gravel-bed river. **Earth Surface Processes and Landforms**, v. 41, n. 2, p. 178–195, 2016.

NIKORA, V. *et al*. Spatially averaged open-channel flow over rough bed. **Journal of Hydraulic engineering**, v. 127, n. 2, p. 123-133, 2001.

PAPANICOLAOU, A. N.; TSAKIRIS, A. G.; KRAMER, C. M. Effects of relative submergence on flow and sediment patterns around clasts. **River Flow 2010**, p. 793-799, 2010.

PAPANICOLAOU, A. N.; BDOUR, A.; WICKLEIN, E. One-dimensional hydrodynamic/sediment transport model applicable to steep mountain streams. **Journal of Hydraulic Research**, v. 42, n. 4, p. 357–375, 2004.

PAPANICOLAOU, A. N.; KRAMER, C. The role of relative submergence on cluster microtopography and bedload predictions in mountain streams. In: **Proc. Int. Symp "River, Coastal and Estuarine Morphodynamics**. p. 4-7. 2006.

PAQUIER, A. *et al.* Quantifier le transport solide dans un petit bassin versant et les évolutions morphologiques d'un bief de rivière. 2008.

PARKER, G.; DHAMOTHARAN, S.; STEFAN, H. Model experiments on mobile, paved gravel bed streams. **Water Resources Research**, v. 18, n. 5, p. 1395-1408, 1982.

PARKER, G. Relation permettant le calcul du charriage dans les rivieres a graviers, a partir de la composition de surface. **Journal of Hydraulic Research**, v. 28, n. 4, p. 417–436, 1990.

PARKER, C.; CLIFFORD, N. J.; THORNE, C. R. Understanding the influence of slope on the threshold of coarse grain motion: Revisiting critical stream power. **Geomorphology**, v. 126, n. 1–2, p. 51–65, 2011.

PELLEGRINI, G. *et al.* The morphological evolution of a step–pool stream after an exceptional flood and subsequent ordinary flow conditions. **Water (Switzerland)**, v. 13, n. 24, 2021.

PITLICK, J. *et al.* Earth Surface Processes and Landforms Earth Surf. **Earth Surf. Process. Landforms**, v. 33, p. 1192–1209, 2008.

POLVI, L. E. Morphodynamics of Boulder-Bed Semi-Alluvial Streams in Northern Fennoscandia: A Flume Experiment to Determine Sediment Self-Organization. **Water Resources Research**, v. 57, n. 3, 2021.

RACHELLY, C. *et al.* Morphological Response of Channelized, Sinuous Gravel-Bed Rivers to Sediment Replenishment. **Water Resources Research**, v. 57, n. 6, 2021.

RAINATO, R.; MAO, L.; PICCO, L. Near-bankfull floods in an Alpine stream: Effects on the sediment mobility and bedload magnitude. **International Journal of Sediment Research**, v. 33, n. 1, p. 27–34, 2018.

RECKING, A. *et al.* Feedback between bed load transport and flow resistance in gravel and cobble bed rivers. **Water Resources Research**, v. 44, n. 5, 2008.

RECKING, A. *et al.* Quantifying the Morphological Print of Bedload Transport. **Earth Surface Processes and Landforms**, v. 41, n. 6, p. 809–822, 2016.

RECKING, A. Theoretical development on the effects of changing flow hydraulics on incipient bed load motion. **Water Resources Research**, v. 45, n. 4, 2009.

RECKING, A.; VÁZQUEZ TARRÍO, D.; PITON, G. The contribution of grain sorting to the dynamics of the bedload active layer. **Earth Surface Processes and Landforms**, 2022.

RENNER, L. C., KLABUNDE, E., KANAZAWA, D. S., & HARTMANN, L. A. Geologia dos primeiros derrames de lavas do grupo Serra Geral no rifte Fronteira Oeste, extremo sul do Brasil–guia de campo. **Estudios Geologicos-Madrid,** *34*(2), 27-49. 2024.

RICKENMANN, D. Comparison of bed load transport in torrents and gravel bed streams. **Water Resources Research**, v. 37, n. 12, p. 3295–3305, 2001.

RICKENMANN, D. Hyperconcentrated flow and sediment transport at steep slopes. **Journal of hydraulic engineering**, v. 117, n. 11, p. 1419-1439, 1991.

RICKENMANN, D. Sediment transport in swiss torrents. **Earth Surface Processes and Landforms**, v. 22, n. 10, p. 937–951, 1997.

RICKENMANN, D.; RECKING, A. Evaluation of flow resistance in gravel-bed rivers through a large field data set. **Water Resources Research**, v. 47, n. 7, 2011a.

SMART, G. M.; JAEGGI, M. N. R. Sedimenttransport in steilen Gerinnen ('Sediment transport in steep channels'). **Mitt. VAW Zürich**, v. 64, 1983.

SCHEINGROSS, J. S. *et al.* Influence of bed patchiness, slope, grain hiding, and form drag on gravel mobilization in very steep streams. **Journal of Geophysical Research: Earth Surface**, v. 118, n. 2, p. 982–1001, 2013.

SHIELDS, A. Application of similarity principles and turbulence research to bed-load movement. 1936.

SCHMEECKLE, M. W.; NELSON, J. M.; SHREVE, R. L. Forces on stationary particles in near-bed turbulent flows. **Journal of Geophysical Research: Earth Surface**, v. 112, n. 2, 2007.

SCHNEIDER, J. M., *et al.* Scaling relationships between bed load volumes,transport distances, and stream power in steep mountain channels. **Journal of Geophysical Research: Earth Surface**, v. 119, n. 3, p. 533-549, 2014.

SHAMLOO, H.; RAJARATNAM, N.; KATOPODIS, C. Hydraulics of simple habitat structures. **Journal of Hydraulic Research**, v. 39, n. 4, p. 351–366, 2001.

SMITH, H. E., *et al*. Controls of local grain size distribution, bed structure, and flow conditions on sediment mobility. **Earth Surface Processes and Landforms**, 2023.

SIMONS, D. B.; ŞENTÜRK, F. Sediment transport technology: water and sediment dynamics. **Water Resources Publication**, 1992.

SOUTHARD, J. An Introduction to Fluid Motions. Sediment Transport, and Current-Generated Sedimentary Structures**. Massachusetts Institute of Technology**, 2006.

SPILLER, S. M.; RÜTHER, N.; BAUMANN, B. Form-induced stress in non-uniform steady and unsteady open channel flow over a static rough bed. **International Journal of Sediment Research**, v. 30, n. 4, p. 297–305, 2015.

STRICKLER, A. Beitrage zur frage der geschwindigkeitsformel und der rauhigkeitszahlen fur strome, kanale und geschlossene leitungen. **Mitteilungen des Eidgenössischen Amtes für Wasserwirtschaft**, v. 16. 1923.

THANOS, A N., *et al*. Investigating the role of clasts on the movement of sand in gravel bed rivers. **Journal of Hydraulic Engineering**, v. 137, n. 9, p. 871-883, 2011.

THOMPSON, R. N., GIBSON, S. A., MITCHELL, J. G., DICKIN, A. P., LEONARDOS, O. H., BROD, J. A., & GREENWOOD, J. C. Migrating cretaceous–eocene magmatismin the serra do mar alkaline province, SE Brazil: melts from the deflected trindade mantle plume?. **Journal of Petrology**, 39(8), 1493-1526. 1998.

TSAKIRIS, A. G. *et al.* Influence of collective boulder array on the surrounding time-averaged and turbulent flow fields. **Journal of Mountain Science**, v. 11, n. 6, p. 1420–1428, 2014.

VÁZQUEZ-TARRÍO, D.; MENÉNDEZ-DUARTE, R. Bedload transport rates for coarse-bed streams in an Atlantic region (Narcea River, NW Iberian Peninsula). **Geomorphology**. v. 217, p. 1–14, 2014.

WANG, Xianye *et al.* Effects of Bed Load Movement on Mean Flow Characteristics in Mobile Gravel Beds. **Water Resources Management**, v. 25, n. 11, p. 2781–2795, 2011.

WILCOCK, P. R.; ASCE, M.; CROWE, J. C. Surface-based Transport Model for Mixed-Size Sediment. **Journal of hydraulic engineering**, v. 129, n. 2, p. 120-128, 2003.

WILCOCK, P. R.; KENWORTHY, S. T. A two-fraction model for the transport of sand/gravel mixtures. **Water Resources Research**, v. 38, n. 10, p. 12-1-12–12, 2002.

WILCOCK, P. R.; MCARDELL, B. W. Partial transport of a sand/gravel sediment. **Water Resources Research**, v. 33, n. 1, p. 235–245, 1997.

WILCOX, A. C.; WOHL, E. E. Flow resistance dynamics in step-pool stream channels: 1. Large woody debris and controls on total resistance. **Water Resources Research**, v. 42, n. 5, p. 1–16, 2006.

WONG, M.; PARKER, G. Reanalysis and Correction of Bed-Load Relation of Meyer-Peter and Müller Using Their Own Database. **Journal of Hydraulic Engineering**, v. 132, 2006.

YAGER, E. M. *et al.* Prediction of sediment transport in step-pool channels. **Water Resources Research**, v. 48, n. 1, p. 1–20, 2012a.

YAGER, E. M. *et al.* Sediment supply, grain protrusion, and bedload transport in mountain streams. **Geophysical Research Letters**, v. 39, n. 10, p. 1–5, 2012b.

YAGER, E. M.; KIRCHNER, J. W.; DIETRICH, W. E. Calculating bed load transport in steep boulder bed channels. **Water Resources Research**, v. 43, n. 7, p. 1–24, 2007.

8. APÊNDICE A

8.1 ÁREA DE ESTUDO (PROTÓTIPO)

O curso d'água que serviu como inspiração para o desenvolvimento desta tese foi o rio Forqueta, localizado na região Sul do Brasil, na área da Serra Geral. Trata-se de um rio de características montanhosas, previamente investigado e caracterizado no trabalho de mestrado de Menezes (2021). Nesta seção, são apresentadas apenas as principais características do sistema fluvial, com o objetivo de fornecer o contexto necessário à compreensão dos resultados obtidos neste estudo.

8.2 LOCALIZAÇÃO

O trecho analisado por Menezes (2021) está inserido na bacia hidrográfica do rio Forqueta, com área aproximada de 46 km² (Figura 8-1), a qual constitui uma sub-bacia da bacia do rio Maquiné, que possui cerca de 510 km². Essa bacia localiza-se na porção nordeste do estado do Rio Grande do Sul, abrangendo parte do setor leste do município de Maquiné. O rio Forqueta apresenta leito predominantemente pedregoso e abriga uma queda d'água de relevância cênica, que se configura como um dos atrativos turísticos da região.

A bacia hidrográfica é recoberta principalmente por formações de Floresta Ombrófila Densa e Floresta Ombrófila Mista, além de áreas associadas aos Campos de Cima da Serra (Rocha, 2013; Castro et al., 2019). A nascente do rio Forqueta situa-se em área protegida, parte inserida na Reserva Biológica da Serra Geral (REBIO) e parte na Área de Proteção Ambiental (APA) Rota do Sol (MMA, 2020). Adicionalmente, a bacia encontra-se próxima a outras Unidades de Conservação, compondo um importante corredor ecológico associado ao bioma Mata Atlântica no sul do Brasil.

A diferença altimétrica entre a nascente e o exutório do rio é de aproximadamente 746 m. Essa condição geomorfológica confere elevada energia ao escoamento superficial, especialmente durante eventos de precipitação intensa, favorecendo processos erosivos no vale e o transporte significativo de sedimentos. Do ponto de vista do relevo, a paisagem regional é marcada pela presença de planícies restritas intercaladas com vertentes e escarpas bem definidas ao longo do vale fluvial.

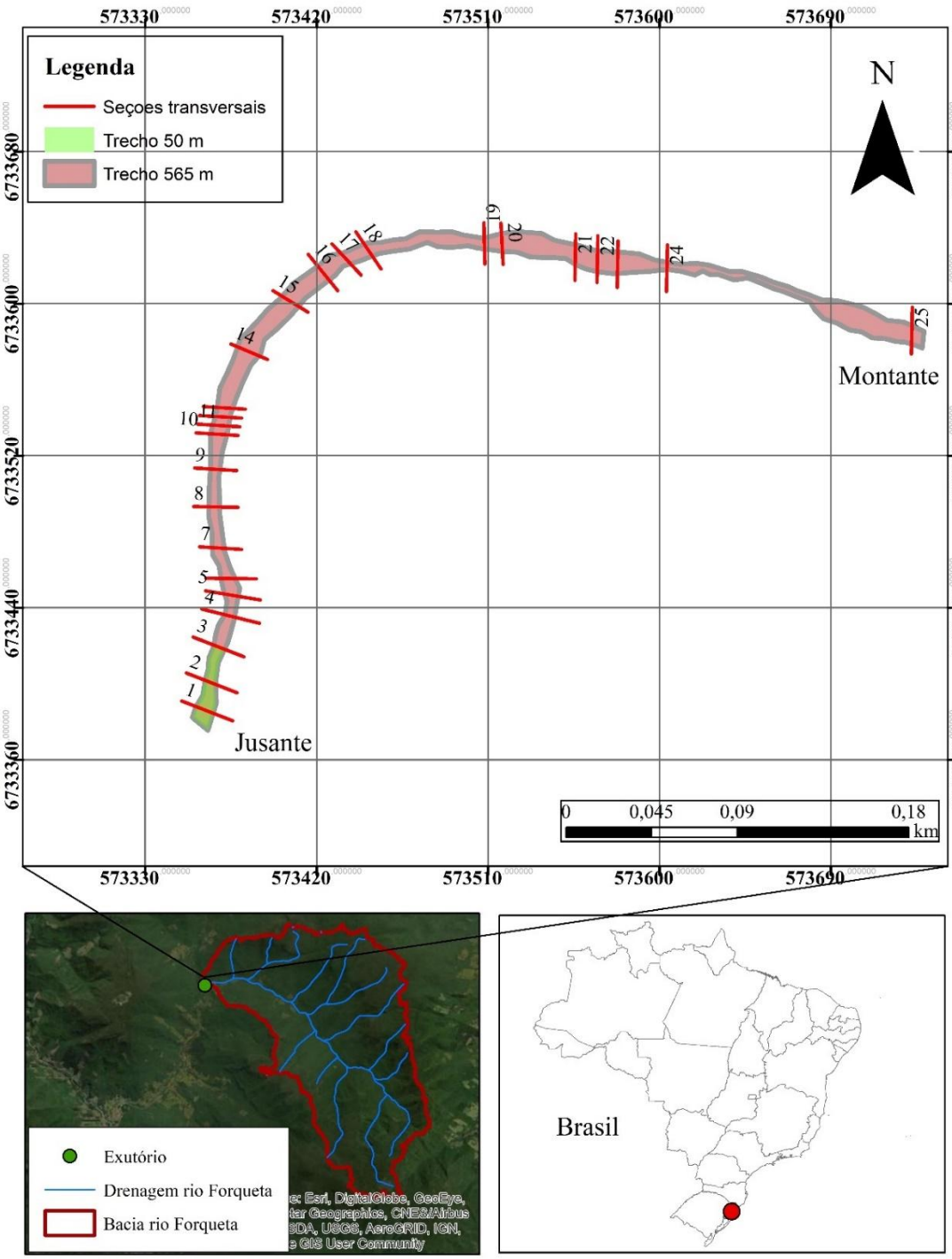


Figura 8-1 - Localização do trecho do rio Forqueta. Fonte: Menezes (2021).

No que se refere ao arcabouço geológico, a bacia do rio Forqueta é constituída predominantemente por litologias pertencentes à Formação Serra Geral, composta essencialmente por rochas basálticas, com a presença das fácies Gramado e Caxias (Vieiro; Silva, 2010). Essa formação é resultado de sucessivos episódios de derrames

vulcânicos e eventos intrusivos, que originaram uma associação litológica dominada por basaltos e riolitos.

As variações composicionais entre magmas básicos e ácidos condicionam diferenças nos registros estruturais e texturais das rochas após os processos de extrusão e resfriamento. As sequências de rochas básicas, amplamente dominantes em termos de área e volume, são representadas por basaltos, enquanto os produtos de composição ácida correspondem a riolitos, normalmente exibindo tonalidades avermelhadas ou esbranquiçadas quando submetidos a processos de intemperismo. A distribuição desses litotipos ao longo das diferentes unidades da paisagem encontra-se ilustrada na Figura 8-2.

Conforme discutido por Mello e Castro (2019), a presença de derrames de composição ácida exerce forte controle sobre a morfologia do relevo e sobre o padrão de cobertura vegetal. O elevado teor de SiO_2 dessas rochas confere maior resistência aos processos erosivos, resultando na preservação de formas de relevo mais elevadas e escarpadas, além de favorecer a ocorrência de afloramentos rochosos com cobertura vegetal pouco desenvolvida. Em contraste, nas áreas dominadas por rochas basálticas, a maior suscetibilidade ao intemperismo químico favorece a formação de solos mais espessos e evoluídos, permitindo o desenvolvimento de uma vegetação mais densa.

Os solos da bacia apresentam distribuição fortemente condicionada pela posição na paisagem, variando entre as unidades de planalto, depressão e planície. Nas áreas de planalto, predomina o Cambissolo Húmico Alumínico típico (CHa), caracterizado por profundidade moderada e horizonte B incipiente. Nas regiões de encostas e fundos de vale, associadas às depressões do relevo, ocorre o Neossolo Regolítico húmico léptico, classificado como solo raso, com contato lítico situado geralmente entre 50 cm e 100 cm de profundidade.

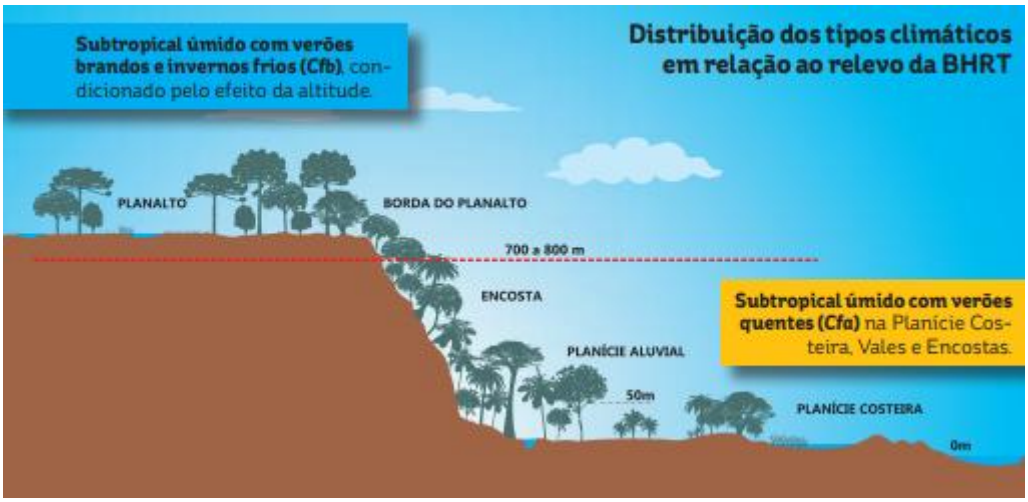


Figura 8-2 - Distribuição climática em relação ao relevo. Fonte: Rocha (2013).

8.3 MONITORAMENTO HIDROSSEDIMENTOLÓGICO

O monitoramento hidrológico do rio Forqueta foi realizado por meio da construção de uma curva-chave (relação cota–vazão), obtida a partir de medições pontuais de descarga líquida associadas ao registro contínuo do nível d'água na seção de controle, realizado por sensor de pressão. Esse procedimento permitiu a obtenção de séries temporais de vazão a partir dos dados de nível monitorados de forma contínua.

Na Figura 8-3 são apresentadas algumas das campanhas de medição realizadas na seção localizada nas proximidades do exutório da bacia. A partir dos valores de vazão e do levantamento batimétrico da seção transversal, foi possível estimar a velocidade média do escoamento, por meio da razão entre a descarga líquida e a área molhada correspondente.



Figura 8-3 - Medição da vazão: (a) em baixo nível d'água; e (b) alto nível d'água. Fonte: Menezes (2021)

A caracterização dos sedimentos de fundo (tamanho e forma) foi realizada por meio do método *Wolman Pebble Count* (zigue-zague no trecho), assim como, foram levantadas 25 seções ao longo do trecho do rio, conforme mostrado na Figura 8-1.

Os sedimentos tiveram seus eixos (*A*, *B* e *C*) medidos por meio de um paquímetro, para eixos menores que 10 cm, e uma suta (Mantax Blue - 950mm), para os maiores (>10 cm). Em seguida, o diâmetro nominal (D_n) (mm) foi calculado para cada sedimento.

$$D_n = (A.B.C)^{\frac{1}{3}}$$

onde *A* é o maior diâmetro (mm); *B* é o diâmetro intermediário (mm); e *C* é o menor diâmetro (mm).

Para a análise granulométrica ao longo das seções transversais, adotou-se como critério a medição da largura da seção (L) e a definição do espaçamento entre pontos de amostragem em função dessa largura: intervalos de 0,5 m para seções com L < 10 m e de 1,0 m para seções com L ≥ 10 m. Em cada ponto, o sedimento superficial do leito foi cuidadosamente removido, tiveram seus três eixos ortogonais medidos e, em seguida, a partícula foi reposicionada em sua posição original, de forma a manter a configuração natural do leito.

Esse procedimento foi aplicado em 25 seções transversais ao longo do trecho estudado. A partir dos dados obtidos, foram determinados os diâmetros característicos de cada seção (D10, D16, D50, D84 e D90). As seções foram estrategicamente posicionadas de modo a representar a variabilidade morfológica do canal. Ao longo dos 565 m analisados, o rio Forqueta apresenta formas de leito típicas de sistemas fluviais de montanha, com predomínio de unidades morfológicas do tipo cascade e step–pool.

O perfil longitudinal do trecho monitorado foi levantado em agosto de 2020 (Figura 8-4), resultando em uma declividade média de 1,54%.

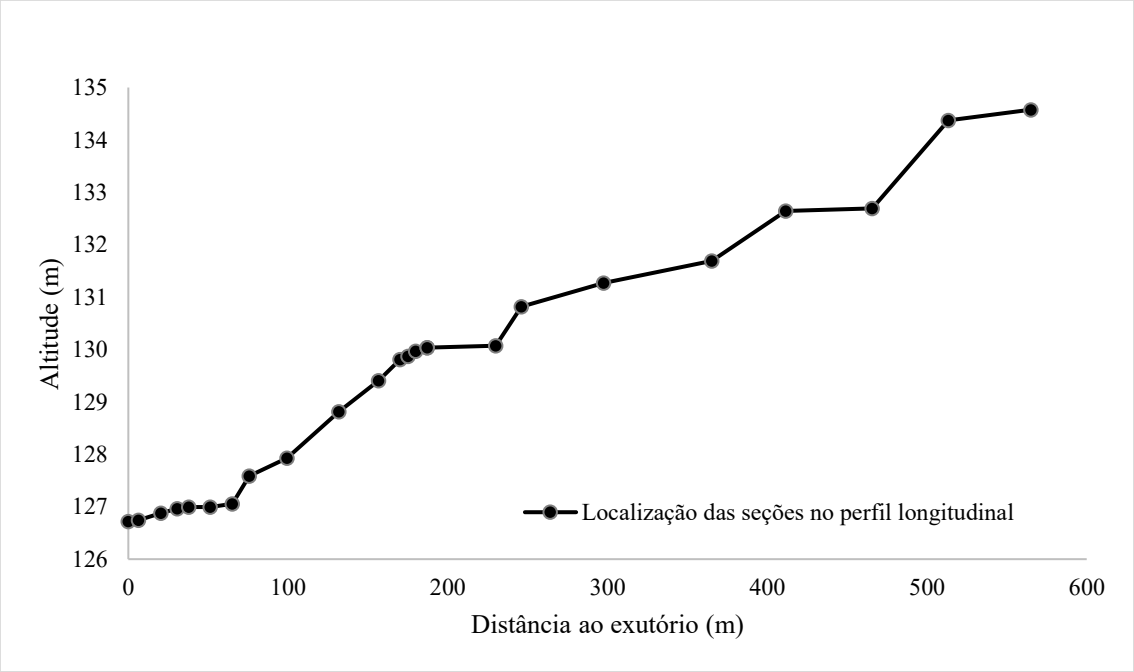


Figura 8-4 - Perfil longitudinal do trecho em estudo do rio Forqueta (565 m). Fonte: Menezes (2021).

Na Figura 8-5 são mostradas algumas seções levantadas e a respectiva classificação morfológica de cada seção com uma fotografia, para representar visualmente a característica do material do leito. Além disso, é mostrado na Tabela 8-1 os dados obtidos para um dos levantamentos realizados por Menezes (2021).

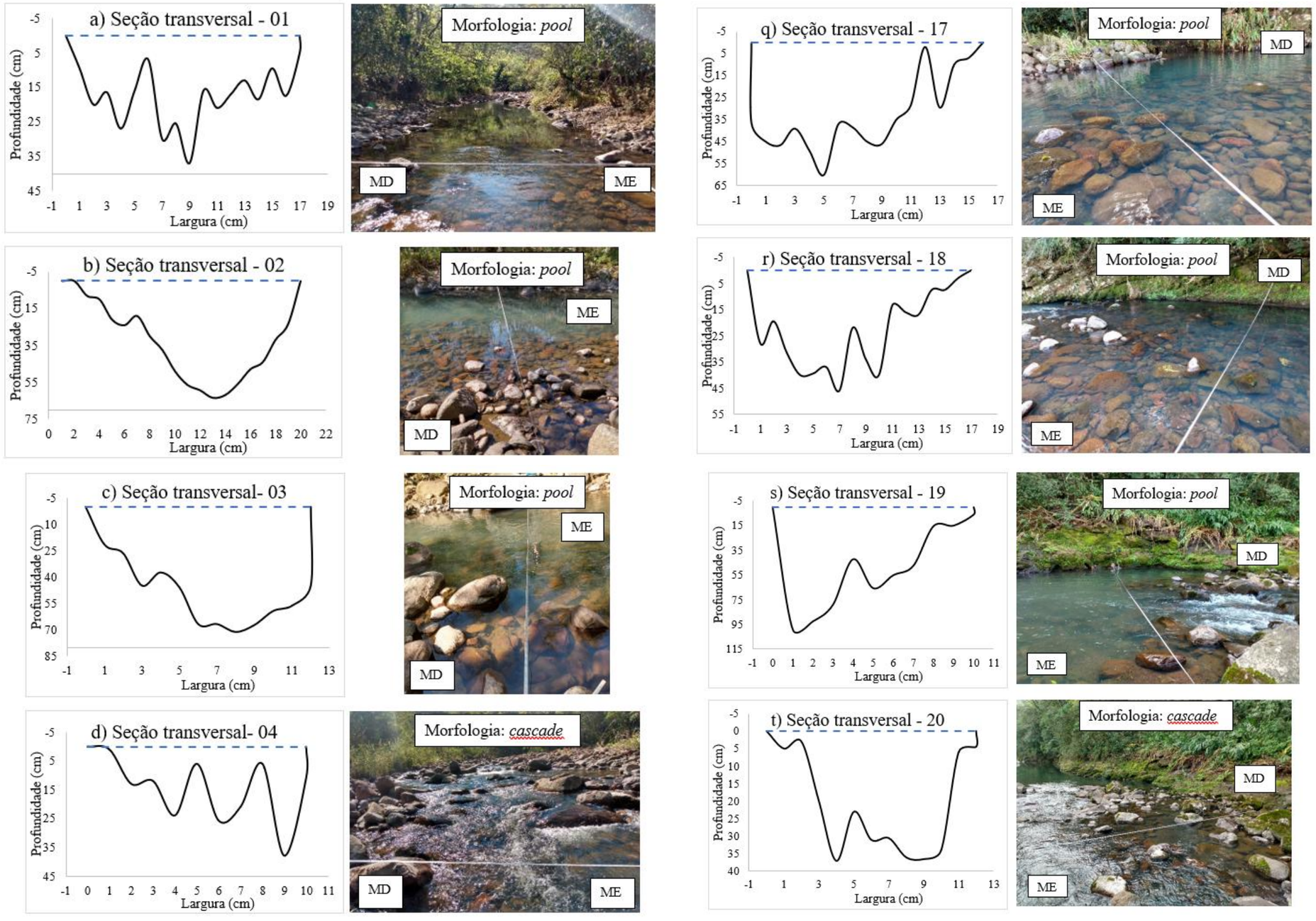


Figura 8-5 - Batimetria de seções do rio Forqueta. Fonte: Menezes (2021)

Tabela 8-1 - Variáveis hidráulicas levantadas na primeira campanha (agosto/2020). Fonte: Menezes (2021).

Seção	Morfologia do canal	Largura (m)	Profundidade média (m)	Profundidade máxima (m)	Perímetro molhado (m)	Raio hidráulico (m)	Área molhada (m²)	Velocidade(m/s)	Vazão (m³/s)	D_{90} (mm)	D_{84} (mm)	D_{50} (mm)	D_{16} (mm)	D_{10} (mm)
1	*Pool*	9,0	0,18	0,37	9,24	0,17	1,59	0,19	0,30	117,76	103,94	54,40	34,82	30,40
2	*Pool*	9,4	0,36	0,64	9,55	0,33	3,18	0,09	0,30	102,40	87,04	50,67	32,53	16,00
3	*Pool*	5,9	0,51	0,72	6,51	0,45	2,95	0,10	0,30	108,80	97,28	53,33	31,36	25,60
4	*Cascade*	10,0	0,16	0,38	10,26	0,15	1,57	0,19	0,30	140,80	113,92	52,00	27,52	23,20
5	*Cascade*	10,0	0,19	0,32	10,07	0,16	1,62	0,19	0,30	126,40	115,84	60,80	36,86	32,64
6	*Cascade*	7,0	0,19	0,39	7,25	0,17	1,21	0,25	0,30	117,33	110,93	74,67	40,96	35,20
7	*Cascade*	8,5	0,21	0,41	8,56	0,19	1,64	0,18	0,30	99,20	81,92	44,00	22,02	18,56
8	*Cascade*	11,8	0,11	0,25	11,95	0,10	1,19	0,25	0,30	172,80	126,72	61,71	41,51	37,94
9	*Cascade*	6,5	0,29	0,46	6,62	0,26	1,71	0,18	0,30	121,60	108,16	54,86	33,10	27,20
10	*Cascade*	13,0	0,12	0,27	13,05	0,10	1,34	0,22	0,30	166,40	122,88	48,00	23,17	20,48
11	*Cascade*	12,6	0,14	0,26	12,63	0,12	1,54	0,20	0,30	123,73	114,77	64,00	27,95	23,47
12	*Cascade*	12,3	0,12	0,39	12,44	0,11	1,39	0,22	0,30	124,16	114,18	61,33	37,76	33,60
13	*Cascade*	11,4	0,21	0,41	11,50	0,21	2,46	0,12	0,30	118,40	112,64	80,00	41,81	34,13
14	*Plane-bed*	10,0	0,19	0,34	10,06	0,18	1,81	0,17	0,30	96,00	76,80	50,29	34,74	32,00
15	*Cascade*	17,8	0,08	0,19	17,89	0,08	1,48	0,20	0,30	116,48	101,89	54,67	37,44	34,40
16	*Cascade*	6,0	0,19	0,43	6,24	0,16	1,03	0,29	0,30	124,16	114,18	61,71	41,51	37,94
17	*Pool*	8,0	0,33	0,60	8,65	0,29	2,48	0,12	0,30	112,46	103,13	58,00	34,88	29,60
18	*Pool*	8,6	0,25	0,46	8,86	0,22	1,96	0,15	0,30	112,46	103,13	57,14	30,51	25,07
19	*Pool*	10,0	0,52	0,99	10,64	0,44	4,69	0,06	0,30	151,47	139,95	72,00	27,52	23,20
20	*Cascade*	12,0	0,22	0,37	12,13	0,22	2,64	0,11	0,30	125,87	118,19	80,00	26,24	22,40
21	*Cascade*	11,0	0,20	0,48	11,26	0,20	2,30	0,13	0,30	140,80	129,28	64,00	37,89	33,28
22	*Cascade*	13,6	0,15	0,40	13,76	0,14	1,94	0,15	0,30	62,40	59,52	43,20	25,60	22,00
23	*Pool*	10,0	0,51	0,78	10,32	0,47	4,83	0,06	0,30	96,00	76,80	44,80	20,80	16,00
24	*Pool*	5,0	0,40	0,87	5,71	0,34	1,95	0,15	0,30	102,40	87,04	48,00	13,12	11,20
25	*Plane-bed*	10,0	0,15	0,40	10,19	0,16	1,60	0,19	0,30	185,60	143,36	60,80	36,86	32,64

8.4 REFERÊNCIAS

MELLO, R. S. P.; CASTRO, D. (org.). 2019. Ciclo das Águas na bacia hidrográfica do rio Tramandaí. Porto Alegre, RS: Sapiens, 135 – 140.

MENEZES, D. Caracterização hidrossedimentológica de trecho do rio Forqueta, Maquiné/RS. **Dissertação de Mestrado. PPG Recursos Hídricos e Saneamento Ambiental**. UFRGS. 2021.

ROCHA, C. M. 2013. Qualidade das águas na BH Rio Tramandaí. Atlas Ambiental da Bacia Hidrográfica do Rio Tramandaí, [s. l.], p. 180.

VIEIRO, A.; SILVA, D. R. A. 2010.Geodiversidade do estado do Rio Grande do Sul.

WOLMAN, M. G. 1954. A method of sampling coarse river-bed material. **Transactions, American Geophysical Union**, [s. l.], v. 35, p. 1–8.